Assessing the ability of filtering unwanted sound pressure peaks via a Meta Cushion during pile driving of a monopile: An analysis using small-scale testing

Saving lives of marine life
during off-shore wind turbines installation

S. Heijnen

Delft University of Technology

Assessing the ability of filtering unwanted sound pressure peaks via a Meta Cushion during pile driving of a monopile: An analysis using small-scale testing

Saving lives of marine life during off-shore wind turbines installation

by

S. Heijnen

Master Thesis

in partial fulfilment of the requirements for the degree of

Master of Science
in Mechanical Engineering

at the Department Maritime and Transport Technology of Faculty Mechanical, Maritime and Materials Engineering of Delft University of Technology
to be defended publicly on Thursday March 16, 2023 at 10:00 AM

Student number:	4234332
MSc track:	Multi-Machine Engineering
Report number:	2023.MME.8781

Thesis committee:	Dr. J. Jovanova,	TU Delft, committee Chair
	A.C. Azevedo Vasconcelos, MSc,	TU Delft, daily supervisor
	Dr. ir. D. Schott,	TU Delft, committee member
	B. Holtzer, MSc,	Huisman Equipment B.V., committee member

Acknowledgement

I would like to take this opportunity to express my heartfelt gratitude to the individuals who have supported me throughout the course of this master thesis.

First and foremost, I would like to thank my daily supervisor Ana Vasconcelos and my supervisor Jovana Jovanova for their invaluable guidance, support, and encouragement throughout the entirety of this thesis. Ana's daily supervision and collaboration were crucial in helping me make substantial progress on the design and execution of the project. Her constructive feedback was always helpful and appreciated, and I am grateful for the time and effort she invested in my work. Jovana's exceptional expertise and experience helped me navigate not only this project but also all the other projects in my second year. Her straight-to-the-point advice was invaluable in guiding me through the various challenges that arose.

I would also like to extend my appreciation to the team at Huisman Equipment B.V. for providing the location for the tests, the weekly meetings, and their helpful advice throughout the entire process. The employees at Huisman Equipment B.V. were always willing to lend their time and expertise to help me improve my research. I would like to specifically thank Aris Niemantsverdriet and Bart Holtzer for their daily support.

I am incredibly grateful to my partner for his unwavering moral support throughout the project and for checking my report for grammatical errors and stylistic coherence, his support was indispensable, and I am incredibly lucky to have him by my side. Last but not least I would like to extend my gratitude to my family for their endless encouragement and support.

I would like to express my deepest appreciation to everyone who has contributed to this research project. Your guidance, support, and encouragement have been instrumental in the achievement of my research goals.

S. Heijnen
Delft, March 2023

Summary

One of the biggest challenges of the century is the fight against global warming. In all sectors people are doing their best to reduce their carbon footprints and their impact on the environment. In the energy sector this is done by making use of renewable energy sources (RES), such as wind turbines, instead of fossil fuels. This transition to RES and the growing demand of energy results in extensive off-shore wind farms containing large wind turbines. During the installation of these wind turbines, the monopile (MP) foundation is driven into the seabed using an impact hammer, which dissipates a high amount of energy into the water in the form of sound pressure waves. The intensity of these sound pressure waves can be expressed in sound levels and is used to quantify the effects of such waves in underwater environment.

These high underwater noise levels have a large impact on its marine life as marine mammals rely on sound waves, particularly low-frequency wave. The noise from pile driving damages their auditory systems and can lead to multiple injuries making them more vulnerable to predators (Popper and Hasting, 2009; Andersson et al., 2017). For this reason, it is crucial to research methods for predicting underwater noise and reducing the noise during off-shore pile driving operations (Jiang et al., 2022; Andersson et al., 2017).

The mitigation techniques currently in use or in development lack the ability to filter the sound pressure peaks at a specific frequency band. For this reason, an elastic meta material-based structure, called Meta Cushion, is designed to reduce low-frequency noise during off-shore impact pile driving. To assess the functionality of the Meta Cushion in reducing low-frequency noise during offshore impact pile driving, a small-scale pile driving test setup was designed and built. The small-scale test aimed to validate the numerical results and to provide a better understanding of the cushion's effectiveness. This test was a joint effort of Delft University of Technology and Huisman Equipment B.V..

The small-scale impact test setup was scaled using scaling laws on the large-scale appliance, and the instrumentation was selected to perform the required measurements to quantify wave propagation. The test setup was built using a test tank with sound-absorbing foam attached to its walls and soil at the bottom to reduce the reflection waves of the tank sides. In the middle of the tank a small-scaled MP was placed on top of a damping plate, to protect the MP and the bottom of the tank. This damping plate was changed during the experiments, because the initial plate caused a large backlash on the MP after impact. On top of the MP, different cushions were placed, and on the MP wall, a set of strain gauges and an accelerometer was attached to measure the behaviour of the MP throughout the tests. In the tank, a hydrophone was placed to measure the sound pressure as a result of the impact force.

The small-scale test setup had three test rounds; the first round assessed the functionality of the meta-material unit cell by testing a modular Meta Cushion made from three different materials: aluminium, acrylic, and nylon, while using a pivot impact hammer; the second and third test rounds were performed on two aluminium non-modular cushions, which were designed and built to withstand the stresses during an impact test with a higher impact force, using a drop weight impact hammer. The FRF-experiments were conducted to extract the actual TL frequency and the attenuation caused by it for each cushion.

The sound pressure measured by the hydrophone was used to calculate the Sound Expsosure Level of a single impact pules ($\mathrm{SEL}_{\mathrm{ss}}$) and the peak Sound Pressure Level ($\mathrm{SPL}_{\mathrm{z,p}}$) in the time domain for all cushions, after which the data was transformed into the frequency domain to show the peak Sound Pressure Level ($\mathrm{SPL}_{\mathrm{peak}}$) for the frequencies in the low-frequency range. The data from the sensors on the MP were also transformed into the Linear Spectrum in to compare the frequency attenuation of Meta Cushion with its Conventional Cushion in the frequency domain.

The modular cushions consisted of four arrays, a top plate, and a clamp to secure the cushion on the MP. Each array for the Meta Cushion contained six meta-material unit cells with resonators attached to the arrays by beams, resulting in a 40 dB TL at a specific frequency. To compare the results of the tests, a Conventional Array with the same axial stiffness was manufactured for each meta array. On the Meta Arrays, an FRF-test (Frequency Response Function-test) was performed to extract the actual transmission loss (TL) frequency and the attenuation caused by it. The aluminium modular Meta Array was designed for an attenuation around a frequency of 2500 Hz. After the array was manufactured, the

TL was detected around 2250 Hz with a value of minus 50 dB. The acrylic array was designed for a TL frequency of 1027 Hz, which was observed at a frequency of 1150 Hz with an attenuation of 40 dB. The nylon array was designed for a TL around a frequency of 592 Hz, which was also the actual frequency determined during the FRF-tests, with an attenuation of 35 dB. The differences in the designed TL frequencies and the actual TL frequencies for the Meta Arrays were caused by the different thickness of the beams attaching the resonators to the arrays.

The non-modular Meta Cushion, designed and built to withstand the stresses caused by a higher impact, consists of 12 Meta Arrays welded together forming a do-decagon, attached to the same clamp as for the modular cushions. The arrays for this cushion were designed for a TL frequency of 350 Hz with an attenuation of 15 dB. The FRF-experiments started showed a TL around a frequency of 220 Hz of 15 dB, after which the array shows TLs and peak values until the frequency of 320 Hz where it reaches a peak value.

The functionality of the modular cushions were tested using a pivot hammer, with each cushion tested ten times. The aluminium modular Meta Cushion showed an attenuation in the SEL_{ss} of 7 dB (re $1\mu Pa^2s$), and an attenuation in the $SPL_{z,p}$ of 6 dB (re $1\mu Pa$), which could be caused by the lower stiffness of the Meta Array. The Meta Cushion shows a TL around the frequency of 2200 Hz, with an attenuation of 10 dB (re $1\mu Pa$). The cushion also showed a TL around a frequency of 1950 Hz with an attenuation of 15 dB, which should be investigated more to find the cause of this TL.

The acrylic modular Meta Cushion showed an attenuation in the SEL_{ss} of 3 dB (re $1\mu Pa^2s$), but no difference in the $SPL_{z,p}$. The sensors on the MP wall detected the TL around the expected frequency, while the SPL in the frequency domain did not show a TL around this frequency, which could be caused by the eigenfrequencies of the tank.

The Nylon Conventional Cushion had a SEL_{ss} of 194 dB (re 1 μPa^2s) and an $SPL_{z,p}$ of 180 dB (re 1 μPa), while the Meta Cushion had a SEL of 191 dB (re 1 μPa^2s) and SPL 173 dB (re 1 μPa). The length of the Meta Cushion had a large offset compared to the other arrays, which caused a larger impact from the impact hammer. The behaviour of this Meta Cushion was the inverse compared to the results from the FRF-tests: The TL was designed for a frequency around 592 Hz, at which the Meta Cushion showed an increase in the SPL and in the pile wall movement detected by the strain gauges and accelerometer; Around a frequency of 760 Hz a TL was visible in the LS from the sensors on the MP.

The non-modular cushion were tested with a higher impact force using the drop weight impact hammer. During this second test round the test setup was assessed, and the MP experienced a backlash from the damping plate, therefore the granular rubber tile was removed. The repeatability of the tests was improved as the deviation in the results for the sensors for both cushions decreased. The hydrophone location showed the best performance at 500 mm from the MP at a depth of 500 mm. The third test round was executed on the same two non-modular cushions to asses the KPIs of the Meta Cushion. The SEL_{ss} and the $SPL_{z,p}$ were the same for both cushions in the time domain. The TL was detected by the strain gauges around the expected frequency of 220 Hz for the non-modular Meta Cushion, which was different from the designed TL frequency of 350 Hz. The thickness of the arrays of this Meta Cushion caused problems during the manufacturing process, which influenced the behaviour of the resonators and therefore the Meta Cushion.During the tests the resonators perish plastic deformation elongating the beams. This plastic deformation caused the resonators to rotate in plane and this could cause changes in the vibrating behaviour.

Only the aluminium modular Meta Cushion showed a noise reduction detected by the hydrophone, but the strain gauges and accelerometer did show TL for the Meta-Cushions.

Nomenclature

Abbreviations

Abbreviation	Definition
BBC	Acoustic Big Bubble Curtain
CAD	Computer-Aided Design
CC	Conventional Cushion
FFT	Fast Fourier Transform
FM	Field Model
FRF-test	Frequency Response Function-test
HSD	Hydro Sound Damper
LB	Laboratory Model
MP	Monopile
MC	Meta Cushion
PTS	Permanent Threshold Shift
PUC	Periodic Unit Cells
RES	Renewable Energy Sources
SBR	Styreen Butadieen Rubber
SEL	Sound Exposure Level expressed in dB re 1 μPa^{2}s in water
SEL_{cum}	Cumulative Sound Exposure Level expressed in dB re 1 μPa^{2}s in water
SEL_{ss}	Sound Exposure Level of a single pulse expressed in dB re 1 μPa^{2}s in water
SPL	Sound Pressure Level expressed in dB re 1 μPa in water and dB re 20 μPa in air
$SPL_{p,p}$	Sound Pressure Level from peak-to-peak value of the sound pressure expresses in dB re 1 μPa in water
SPL_{peak}	Peak Sound Pressure Level expresses in dB re 1 μPa in water
SPL_{RMS}	Sound Pressure Level from the root-mean-square value of the sound pressure expresses in dB re 1 μPa in water
$SPL_{z,p}$	Sound Pressure Level from zero-to-peak value of the sound pressure expresses in dB re 1 μPa in water
TL	Transmission Loss
TTS	Temporary threshold Shift

Symbols

Symbol	Definition	Unit
Ax[k]	Discrete acceleration of the pile wall in the x direction in the time domain	[m/s^2]
Ax[m]	Discrete acceleration of the pile wall in the x direction in the frequency domain	[m/s^2]
AxLS[m]	Linear spectrum for the acceleration of the pile wall in the x direction in the frequency domain	[m/s^2]

Symbol	Definition	Unit
Ay[k]	Discrete acceleration of the pile wall in the y direction in the time domain	[m/s^2]
Ay[m]	Discrete acceleration of the pile wall in the y direction in the frequency domain	[m/s^2]
AyLS[m]	Linear spectrum for the acceleration of the pile wall in the y direction in the frequency domain	[m/s^2]
Az[k]	Discrete acceleration of the pile wall in the z direction in the time domain	[m/s^2]
Az[m]	Discrete acceleration of the pile wall in the z direction in the frequency domain	[m/s^2]
AzLS[m]	Linear spectrum for the acceleration of the pile wall in the z direction in the frequency domain	[m/s^2]
A_F	Cross-section area of the field monopile	[mm^2]
A_L	Cross-section area of the lab monopile	[mm^2]
C_l	Length coefficient	[-]
c_{water}	Speed of sound in water	[m/s]
d_{water}	Water depth	[m] [mm]
D_{MP}	Outside diameter of a monopile	[m] [mm]
DH_{ram}	Drop height of the ram	[mm]
E_{alu}	Young's modulus aluminium	[GPa]
E_{kin}	Kinetic energy	[J]
E_{pot}	Gravitational potential energy	[J]
E_{spring}	Elastic potential energy	[J]
E_{steel}	Young's modulus steel	[GPa]
f[m]	Discrete frequency vector in the frequency domain	[Hz]
F_{hammer}	Hammer force	[kN]
$f_{l,n,m}$	Eigenfrequency of the test tank	[Hz]
f_n	Eigenfrequency of the monopile	[Hz]
f_{Ny}	Nyquist frequency	[Hz]
f_{res}	Frequency resolution	[Hz]
f_s	Sample frequency	[Hz]
g	Gravitational acceleration	[m/s^2]
H(f)	Transfer function in the frequency domain as a function of frequency (f)	[]
h(t)	Transfer function as a function of time (t)	[]
H(f,r,z)	Transfer function in the frequency domain as a function of frequency (f), radial distance from the pile wall (r), and water depth (z)	[]
h(t,r,z)	Transfer function as a function of time (t), radial distance from the pile wall (r), and water depth (z)	[]
H_{tank}	Height of the test tank	[mm] [m]
I_F	Moment of inertia of the field monopile	[mm^4]
I_L	Moment of inertia of the lab monopile	[mm^4]
$k_{cushion}$	Axial stiffness of the cushion	[kN/mm]
k_H	Natural wave number in the direction of the height of the tank	[1/m]
k_L	Natural wave number in the direction of the length of the tank	[1/m]
k_{MP}	Axial stiffness of the monopile	[kN/mm]
k_W	Natural wave number in the direction of the width of the tank	[1/m]
L_F	Length of the field monopile	[mm]
L_L	Length of the lab monopile	[mm]
L_{MP}	Length of the monopile	[mm]

Symbol	Definition	Unit
L_{tank}	Length of the test tank	[mm] [m]
m_{hammer}	mass of the pivot impact hammer	[kg]
m_{ram}	mass of the ram from the drop weigth impact hammer	[kg]
p[k,r,z]	Discrete sound pressure in the time domain as a function of data point (k), radial distance from the pile wall (r), and water depth (z)	[Pa]
P[m,r,z]	Sound pressure in the frequency domain as a function of data point (m), radial distance from the pile wall (r), and water depth (z)	[Pa]
p_{ref}	Reference pressure in water	[Pa^2s] or [μPa]
p_{RMS}	Root-mean-square value of the sound pressure wave	[Pa]
R_F	Radius of the field monopile	[mm]
R_L	Radius of the lab monopile	[mm]
S[k]	Discrete data from the strain gauges on the pile wall in the time domain	[V]
S[m]	Discrete data from the strain gauges on the pile wall in the frequency domain	[V]
s_{hammer}	path traveled by the hammer tip	[m] SE_{ss}
Sound Exposure	[μPa^2s]	
SEL_{ss}	Sound Exposure Level	[dB re 1 μPa^2s]
SPL(t,r,z)	Sound pressure level as a function of time (t), radial distance from the pile wall (r), and water depth (z)	[dB re 1 μPa]
SPL_{peak}[f,r,z]	Peak sound pressure level in the frequency domain as a function of frequency (f), radial distance from the pile wall (r), and water depth (z)	[dB re 1 μPa]
SPS[f,r,z]	Sound pressure spectrum in the frequency domain as a function of frequency (f), radial distance from the pile wall (r), and water depth (z)	[Pa]
StrLS[m]	Linear spectrum from the strain gauges on the pile wall in the frequency domain	[V]
t[k]	Discrete time vector in the time domain	[s]
t_F	Wall thickness of the field monopile	[mm]
t_L	Wall thickness of the lab monopile	[mm]
t_{MP}	Wall thickness of the monopile	[mm]
T_s	Sample period	[s]
u_{ram}	Displacement of the ram during impact	[mm]
v	Velocity	[m/s]
v_{impact}	Impact velocity of the ram	[m/s]
W_F	Modulus of section of the field monopile	[mm^3]
W_L	Modulus of section of the lab monopile	[mm^3]
W_{pivot}	Work done by the pivot hammer	[J]
W_{tank}	Width of the test tank	[mm] [m]
ρ_{alu}	Density of aluminium	[kg/m^3]
ρ_{steel}	Density of steel	[kg/m^3]
μ_{alu}	Poisson's ratio of aluminium	[-]
μ_{steel}	Poisson's ratio of steel	[-]

Contents

List of Figures

List of Tables

1 Introduction

One of the biggest challenges of the 21th century is the fight against global warming. In all sectors people are doing their best to reduce their carbon footprint and their impact on the environment. In the energy sector this is done by making use of renewable energy sources (RES), such as wind turbines, instead of fossil fuels. This transition to RES and the growing demand of energy results in extensive off-shore wind farms containing large wind turbines.

The most common foundation for offshore wind turbines are monopiles (MPs) (Deltares, 2022). A MP is a steel cylindrical tube, which can vary in length from 90 m to 120 m and in diameter from 8 m to 11 m (Nordenham, 2020). The dominant method used to drive the MP into the seabed is impact hammering (Deltares, 2022; Woolfe, 2012). An impact hammer is dropped on top of the MP to generate an axial force, driving the pile downwards into the seabed. The impact also produces a compression wave in the MP and an associated radial displacement motion caused by the effect of Poisson's ratio of the pile material. This radial displacement is the source of high sound pressure waves in its surrounding water (Woolfe, 2012). The intensity of these sound pressure waves can be expressed in sound levels and it is used to quantify the effects of such waves in an underwater environment.

The noise generated during the installation of MPs has caused significant harm to the marine environment. The peak Sound Pressure Levels (SPLs) of these waves can exceed 200 dB (re 1 µPa) within 10 m from the MP. These high underwater noise levels have a large impact on marine life as marine mammals rely on sound waves, particularly low-frequency waves, for communication, navigation, foraging and avoiding predators. The noise from pile driving damages their auditory systems and can lead to multiple injuries such as swim bladder rupture, tissue damage, bruises, hearing loss and changes in migration patterns making them more vulnerable to predators (Popper and Hasting, 2009; Andersson et al., 2017). For this reason, it is crucial to research methods for predicting underwater noise and reducing the noise during off-shore pile driving operations (Jiang et al., 2022; Andersson et al., 2017).

International regulations have been implemented to define maximum noise levels to reduce the impact on marine life around the wind parks. In the Netherlands the Sound Exposure Level of a single pulse (SEL_{ss}), which measures the sound energy received by an organism during a single impact pulse, should not exceed 168 dB (re 1 $\mu Pa^2 s$) measured around 750 m from the MP (Faijer et al., 2020). The restriction on the SEL_{cum}, the cumulative sound that a swimming animal experiences throughout the pile driving process, expressed in dB (re 1 $\mu Pa^2 s$) mostly taken over a period of 24 hours. The Sound Pressure Level (SPL) is a measurement of the intensity of a sound at a specific point in time and should not exceed 185 dB in Belgium waters (re 1 μPa) (Staat, 2018). (The sound close to an air alarm reaches 140 dB in air (re 20 μPa) and is harmful for the human ear. A sound of 180 dB in air (re 20 μPa), caused on a missile launch pad, causes irreversible hearing damage to the human ear, to give some perspective (MediaPower, 2020).)

Table 1.1: Traditional mitigation techniques for offshore impact pile driving and their performance properties (Koschinski and Lüdemann, 2020)

Mitigation technique	Max noise reduction	Best performance frequency	Operational limit
Acoustic Bubble Curtain	15 dB	> 1 kHz	$D_{MP} \leq 8$ m, $d_{water} \leq 25$m
Double Bubble Curtain	18 dB	> 1 kHz	$D_{MP} \leq 8$ m, $d_{water} \leq 40$m
Isolation casing	16 dB	0.5 - 5 kHz	$D_{MP} \leq 8$ m, $d_{water} \leq 45$m

Several techniques have been developed to mitigate the acoustic impact from off-shore pile driving. The election of the appropriate noise reduction method(s) depends on the pile driving technique, the impact energy and the diameter of the MP (D_{MP}). The current noise mitigation techniques are noise barriers or enclosures, such as an acoustic bubble curtain and an isolation casing. These structures are designed to block or absorb sound waves, reducing the intensity of the noise that is transmitted to the surrounding environment. Currently all mitigation techniques are under development to withstand the increasing sizes of the MP (Koschinski and Lüdemann, 2020). Table 1.1 contains the maximal noise reduction, the frequency range at which that reduction is most optimal and the current limitations in relation to the MP diameter and the water depth at which the MP is driven into the seabed (Koschinski & Lüdemann, 2020).

The average power capacity of off-shore wind turbines in Europe keeps growing every year, according to each year report of Windeurope (2018-2021), shown in table 1.2. This growing capacity forces the wind turbine installation to get bigger as well as the MP foundation. Those bigger MPs shift the radiated noise to frequencies below 1 kHz, which becomes a challenge for traditional noise mitigation techniques. The high noise waves in the low-frequency spectrum are interfering with the low-frequency sound waves the marine mammals use for communication and so on as mentioned above. All mitigation techniques are under constant development to improve their performance and are currently used by combining different techniques to reach the necessary noise reduction, but with limited success. While failing to reach acceptable noise attenuation levels, such strategies only increase installation time and cost (Koschinski & Lüdemann, 2020; Vasconcelos et al., 2022). New mitigation techniques focus on changing the transmission of the impact energy to reduce noise peaks. These techniques will make the mitigation independent of the water depth at which the MP is installed and eliminates the external vessels needed during installation.

Table 1.2: Average power capacity per year for off-shore wind turbines in Europe (Windeurope, 2018-2021)

Year	2018	2019	2020	2021
Avg. power capacity	6.8 MW	7.8 MW	8.2 MW	8.5 MW

1.1. Research description

The mitigation techniques currently in use or in development lack the ability to filter the sound pressure peaks at low-frequency ranges. For this reason, an elastic meta material-based structure, called Meta Cushion, was numerically designed to reduce low-frequency noise during off-shore impact pile driving in a full-scale case (Vasconcelos et al., 2023). The Meta Cushion is placed between the MP and the hammer and is used to filter the energy at the frequencies of an incoming wave which are related to high noise level outputs. The radial displacement of the wall of the MP at its eigenfrequencies are directly coupled to the peaks in the sound pressure waves in the water during off-shore pile driving, as shown in figure 1.1, and therefore most important for the noise levels (Woolfe, 2012). The energy at this sound pressure peak is shifted towards other frequencies by the Meta Cushion reducing the peak value, while the remaining energy is kept for the pile driving process.

A proper validation of the proposed mitigation technique is required. Before implementing the mitigation technique on a full scale, a small-scale test will assess its effectiveness in reducing noise in a controlled environment. Small-scale testing provides a better understanding of the effectiveness of the cushion and gives an opportunity to improve it, which can lead to better results when implemented on a larger scale. Additionally, testing on a smaller scale is generally less expensive than testing on a larger scale, making it a cost-effective way to assess the functionality of the Meta Cushion. This research focuses on designing a small-scale impact testing setup to validate the numerical results presented in Vasconcelos et al. (2023), which will demonstrate the effectiveness of the Meta Cushion in practise. This test is a joint effort of Delft University of Technology and Huisman Equipment B.V..

Research objectives

For this research a small-scale test setup is designed and built to asses the functionality of the Meta Cushion. The setup will be scaled using scaling laws on the large-scale appliance and the instrumentation is properly selected to perform the measurements required to quantify the wave propagation. The small-scale test setup will first asses the functionality of the meta-material unit cell, by testing a modular Meta Cushion made from three different materials: aluminium; acrylic; and nylon. For each Meta Cushion a cushion with the same stiffness, a Conventional Cushion, will be designed and built. From the results and experience of the experiments an aluminium non-modular Meta Cushion, and its Conventional Cushion, will be designed and built to withstand the stresses during an impact test with a higher

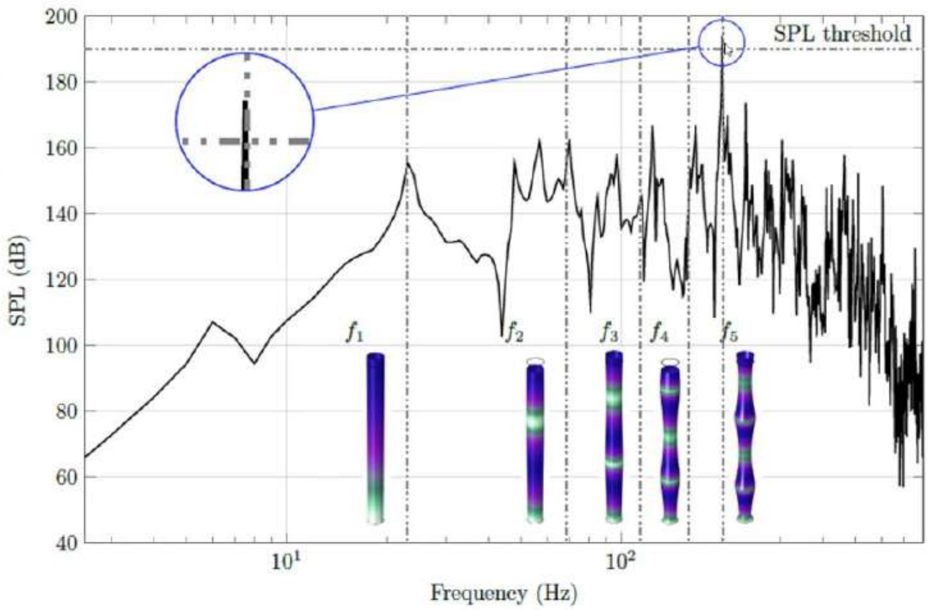

Figure 1.1: Correlation between eigenfrequencies of a MP and peaks in the Sound Pressure Levels. The eigenfrequencies of the MP are indicated by the vertical dashed lines and the SPL is plot for that MP, with the peak SPL circled and zoomed in. The SPL threshold value is indicated by the dotted horizontal line, which is the SPL threshold value in the frequency domain (Vasconcelos et al., 2023)

impact force. The non-modular cushions are tested on their stiffness to validate the simulations, after which both cushions will be tested in the small-scale impact test. The various tests will asses to what extend the small-scale test setup is evaluating the noise reduction and the functionality of the Meta Cushions. This thesis will provide data of the sound pressure in the water and the wall displacement of the MP as a result of an impact force for all cushions.

The main research question for this experimental study is: How to design a small-scale pile driving test to assess the ability of filtering unwanted sound pressure peaks via a Meta Cushion?

To address the design steps involved in the main research questions, the following sub research questions are elaborated:

1. Why is there a demand for new mitigation techniques?
2. What are the fundamentals for a small-scale impact test?
3. What are the key performance indicators of the Meta Cushions?
4. What methodology is used for a small-scale impact test to evaluate a mitigation technique?
5. To what extent is the small-scale test setup evaluating the noise reduction?

Research scope

The small-scale impact test should be the best possible representation of the actual large-scale offshore MP driving process. The environment during offshore MP installation is unpredictable due to influences such as current, wind and waves; these influences are left out of the scope of this experiment. Another concession is the scaling, the ocean is an almost infinite test tank, while the small-scale test tank has a limited size. The wall effect resulting from the limited size of the test tank will be damped using damping foam at the sides, while the soil will contribute in damping the sound waves at the bottom surface.

1.2. Report structure

The structure of this report will follow the sequence of the sub questions. In chapter 2 the background for this research is provided. The necessity of a new mitigation technique for off-shore pile driving is expressed. In the next chapter the fundamentals of the small-scale impact test for this research are shown. In chapter 4 the Meta Cushions are introduced; the requirements for the Meta Cushions and their equivalent, the Conventional Cushions, are explained; and the key performance indicator for its design is shown. The manufacturing of the test components and the small-scale test setup is discussed in chapter 5. The methodology of the stiffness determination of the non-modular cushions is shown in chapter 6. Chapter 7 discusses the methodology of the small-scale pile driving test and the analysis of the data from the sensors. Finally the results are shown and discussed in chapter 8 and the main research question will be answered. The report will end with the conclusion and recommendations for future research.

2 Background

In this chapter the background for this research is provided. The necessity of a new mitigation technique for off-shore pile driving is expressed. First the impact pile driving process will be explained and the effect of the noise pollution on marine life will be given. Then the threshold values for the noise levels in the Netherlands are expressed and explained. Some traditional mitigation techniques and their limitations are discussed. The state-of-the-art solutions are then provided including the Meta Cushion. The chapter will end with the research gap for this experiment.

2.1. Impact pile driving

Offshore wind turbines are an important source of renewable energy, and the foundation design plays a crucial role in the overall performance and stability of the turbine. As mentioned, the most commonly used foundation type for offshore wind turbines is the MP. A MP consists of two cylindrical tubes with different diameters, welded together by a hollow tapered piece. The length of these MPs can vary from 10 m to 110 m and are still increasing in size (Nordenham, 2020). This large-diameter steel pile is driven into the seabed using either an impact hammer or vibration techniques. In figure 2.1 the newest installation vessel, Orion is shown, which carries two MPs and is putting a third MP in position for the pile driving process.

Impact pile driving involves using a large, heavy hammer, shown in figure 2.2, to repeatedly strike the top of a MP, causing it to penetrate the soil. The hammer operates by lifting a drop weight to a certain height. When the desired height is reached, the weight is released and accelerated downwards until it hits the MP head. The impact force generated by the drop weight transfers energy that is used to drive the pile into the soil. However, impact pile driving also transmits significant noise and vibrations to the water, which can have negative impacts on marine life, including the potential for hearing loss and behavioural changes (Andersson et al., 2017). The high noise levels can cause permanent hearing damage (called permanent threshold shift, or PTS) or temporary hearing loss (called temporary threshold shift, or TTS) in both marine mammals and fish. The PTS involves damage to the hair cells of nerve fibres inside the hearing organ of marine mammals. TTS occurs due to the swelling of specific nerve endings of the hearing organ for both fish and marine mammals. This damage can interfere with the ability of these animals to communicate and navigate, which can have negative impacts on their reproductive success and survival.

Figure 2.1: DEME's new offshore installation vessel, Orion, lifting a MP to the correct position to be driven into the seabed. The vessel also carries two extra MPs onboard (Buitendijk, 2022)

Figure 2.2: The newest design of a hydraulic impact hammer from IQIP (IQIP, 2020a)

2.2. Threshold noise levels

There are two common measure units of noise that are used to regulate the levels of noise generated during offshore MP driving. SEL is a measurement of the total sound energy that is received by an individual or a population over a given period of time, and are typically measured in decibels (dB). The SEL is used to express hearing injury thresholds of marine life. The regulations and literature use two values for the SEL: the SEL_{ss}, which expresses the Sound Exposure Level of a single pulse of the impact hammer; and the SEL_{cum}, which is the cumulative sound that a swimming animal experiences throughout the pile driving process and gives an idea of how much energy a given stationary point at a certain distance has received.

The SPL is a measurement of the intensity of a sound at a specific point in time and is also typically measured in dB. The peak value SPL_{peak} is easy to measure for each hammer strike during the impact pile driving process. There are three ways to express this peak pressure: $SPL_{z,p}$, $SPL_{p,p}$ and SPL_{rms}; $SPL_{z,p}$, zero-to-peak, is calculated using only the highest peak pressure value, as shown by the green arrow in figure 2.3; $SPL_{p,p}$, peak-to-peak, is calculated via the pressure difference between the positive peak and negative peak, as shown by the pink arrow in the figure; The SPL_{rms}, uses the root-mean-squared value of the signal to express the sound pressure, indicated by the red dotted line in the figure.

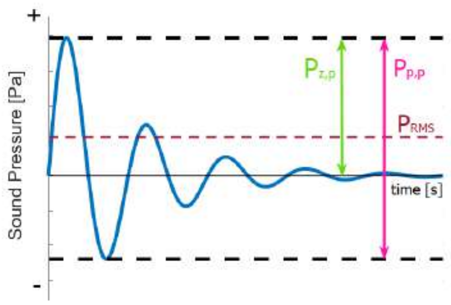

Figure 2.3: Sound pressure signal with indication of the different ways to use the pressure value to obtain the SPL

Table 2.1: Threshold values for pile driving in Dutch and Belgium waters measured from a distance of 750 m from the project (DHV, 2020; Faijer et al., 2020; Heinis et al., 2015; Staat, 2018)

Noise Level	Threshold
SEL_{ss}	168 dB re 1 $\mu Pa^2 s$
SEL_{cum}	199 dB re 1 $\mu Pa^2 s$ over 24h
$SPL_{z,p}$	185 dB re 1 $\mu Pa^2 s$

During offshore MP installation, SELs and SPLs are typically measured using hydrophones or other specialized sensors. These sensors can be placed at various distances from the MP driving equipment to determine the levels of noise that are being transmitted through the water. The distance from the noise source can have a significant effect on the measured SELs and SPLs, as the sound energy has been dispersed to a larger area the further it is away from the MP. The sound energy can also be absorbed or scattered by the water, the seabed, or other underwater features (Andersson et al., 2017). For each region and country the threshold for the noise levels are different. There are also no standardised methods on how to measure these values.

The German guidelines state that at least three hydrophones should measure the noise levels at different distances. Those distances are 750 m and 5 km from the MP (Andersson et al., 2017). The Dutch guidelines for the threshold of the noise levels are not specified specifically for offshore pile driving, but they are for offshore drilling. These values are taken as guidelines for this research and are shown in table 2.1. The guidelines are meant for measurements taken 100 m from the pile driving project.

2.3. Noise mitigation techniques

The sound caused by the pile driving needs to be damped to stay below the values given in table 2.1. Several mitigation techniques are used during the pile driving process and they are currently even combined with each other. The pile driving technique, the impact energy, and the diameter of the MP can provide information about the potential noise levels, allowing for the election of appropriate noise reduction methods. Traditional mitigation techniques are secondary mitigation techniques, focusing on the reductions of the sound pressure waves in the water using noise barriers or enclosures. New mitigation techniques, currently in development, are commonly primary mitigation techniques, which try to prevent high pressure waves in the pile wall causing the peak sound pressure waves in the water, such as the Meta Cushion.

Traditional mitigation techniques

One traditional approach to reduce noise during pile driving is the use of noise barriers or enclosures. These structures are designed to block or absorb sound waves, reducing the intensity of the noise that is transmitted to the surrounding environment. The best known noise barrier used during MP driving is an acoustic Big Bubble Curtain (BBC) (M. A. Bellmann, 2014). Figure 2.4 shows the pile driving vessel, Svanen, using a double BBC as a sound damper during the installation of a MP. A BBC is a system that generates a continuous curtain of air bubbles around the MP from the seabed to the water surface. The bubble curtain absorbs, reflects and scatters the noise generated by the pile driving, reducing the noise transmitted through the water. The effectiveness of this technique depends on the size and distribution of the bubbles, and it may not be effective in reducing noise at long distances from the MP. The damping range of acoustic bubble curtains is typically in the range of 5-18 dB depending on the number of curtains and bubble sizes (Koschinski & Lüdemann, 2020). The performance of the curtain depends on conditions such as current, waves and water depth (Andersson et al., 2017). Another disadvantage of a bubble curtain system is that it is relatively expensive to install and maintain, especially if it is used for larger offshore wind farms. Installing larger wind turbines can pose challenges, as they require larger MPs placed in deeper waters. To overcome these challenges, the use of double bubble curtain systems can provide solutions for the installation of larger monopiles. Additionally, the bubble curtain can be combined with other noise reduction techniques, such as an isolation casing, a Hydro Sound Damper (HSD), or reduced blow energy, to meet legal noise standards, especially in deeper waters or with larger pile diameters, which tend to emit higher levels of noise (M. Bellmann et al., 2018). So far, the combination of BBCs with these additional noise mitigation measures has proven effective in reducing noise levels. However, the noise frequencies best attenuated are those above 1 kHz, while the disturbance of the marine mammals is strongest at frequencies below 1 kHz (Dähne et al., 2017; Dyndo et al., 2015).

Another damping technique using a noise barrier is an isolation casing. With this technique, a steel tube is placed around the MP as a cast (Andersson et al., 2017). The space between this cast and the MP can be filled with a bubble curtain or HSD to increase the damping effect. The advantage of this technique is the sustainability of the cast, since it is reusable. It has been proven a robust and reliable system which has no impact on installation times. The isolation casing has a damping potential between 15 and 20 dB (Andersson et al., 2017). The isolation casing system in combination with the bubble curtain inside the cast has an effective frequency band of 500–5000 Hz (Wilke et al., 2012). The increasing diameter and length of MPs creates a growing disadvantage for this method as this growth forces these casing to also increase its length for the water depth covering and its diameter, which increases the weight of the cast. These adaptations have reached the limits of the currently used cranes (Koschinski and Lüdemann, 2020).

An HSD has been designed to improve the bubble curtain and decrease the dependency on weather conditions. An HSD system reduces the transmission of noise from vibrations through the structure of the MP. The damper typically consists of a gas-filled chamber and a flexible membrane, which vibrates in response to the sound and vibration waves generated by the pile driver (M. A. Bellmann, 2014). The vibration of the membrane creates a pressure wave in the water, which absorbs and dissipates the energy of the sound waves. Besides withstanding the current, the resonance frequency is also adjustable when using an HSD (Koschinski and Lüdemann, 2020). The highest performance of the HSD is measured at a frequency between 100 Hz and 800 Hz, and is 13 dB at best (Andersson et al., 2017). Currently available HSDs can be used with monopile diameters up to 10 m, where for larger diameters, specific adaptations are needed. A downside of the HSD system is regular maintenance requirement, for example checking the water level and quality, as well as replacing the flexible membrane if it becomes damaged or worn.

Pulse prolongation impact hammers

New techniques focus on the mitigation of the sound at the hammer to be independent of the circumference of the MP and the water depth at which the MP is driven. The state-of-the-art for the impact hammer is discussed since this hammer method is used in this research. A traditional impact hammer has a short pulse with a high energy amplitude. One state-of-the-art approach is to distribute that energy over a longer period of time, reaching the same energy with a smaller impact force. Two examples of such hammers are the PULSE and the BLUE piling Hammer. Both hammers use a combination of mass damping and energy dissipation to reduce the noise that is transmitted to the surrounding environment (IQIP, 2020b; Koschinski & Lüdemann, 2020). These new techniques are expected to significantly

Figure 2.4: Van Oord's heavy lift vessel, Svanen, driving a MP into the seabed using a double bubble curtain system (Buitendijk, 2020)

Figure 2.5: The Blue Hammer in its large-scale test phase (NT.nl, 2018)

reduce foundation installation costs for offshore wind turbines. The PULSE hammer, shown in figure 2.2, is one of such hammers that uses pulse prolongation. The BLUE hammer, shown in figure 2.5, uses a large water column driven by combustion to deliver two blows to the MP, rather than a steel ram with one blow. This distribution of the impact reduces the forces and therefore the noise. These techniques are also scalable, allowing for the installation of large MPs. Both hammers, and variations of them, are still under development. The PULSE hammer shows a reduction of 9 dB by the numerical model, and the BLUE hammer reduces the SEL up to 24 dB during the tests (Koschinski and Lüdemann, 2020).

Meta Cushion

The state-of-the-art mitigation technique in this research is a Meta Cushion. When the hammer hits the MP, a transition piece is placed in between them, which is called a Conventional Cushion. Instead of changing the energy distribution of the hammer, the Meta Cushion is installed between the hammer and the pile, replacing the Conventional Cushion, to partially filter the impact energy at certain frequencies.

When the hammer hits the MP, pressure waves travel through the pile. Those pressure waves travel in the axial and circumferential directions over the MP. The displacement caused by these waves generates waves in the water and air around the pile. The radial eigenfrequencies of the MP are directly coupled to the peaks in the sound pressure waves in the water during off-shore pile driving (figure 1.1), and therefore most important for the noise levels (Woolfe, 2012).

A Meta Cushion is a cushion made from an elastic meta material-based structure composed with single-phase resonant structures (Vasconcelos et al., 2022; Vasconcelos et al., 2023). It is designed to obtain a transition loss in the low frequency range at the eigenfrequencies of the MP, reducing the SPL peak around that frequency range, while the remaining energy can still drive the MP into the seabed. The curve from figure 1.1 is plot again in figure 2.6 using a red dotted line and shows the SPL of the MP with a Conventional Cushion overshooting the SPL threshold. The black solid curve in the figure shows a transition loss around that frequency, shifting the energy towards other frequencies, reducing the SPL peak value to below the threshold.

The Meta Cushion is placed between the hammer and the MP, which makes it a primary noise mitigation technique. The Meta Cushion can be implemented in the design of the impact hammer. The hammer needs to be adjusted per MP batch and can therefore be taken into consideration during this process step. The Meta Cushion eliminates the necessity of external vessels during the impact pile driving, which decreases operational costs substantially. This Meta Cushion is the main focus of this research. The functionality of the cushion and the necessity for it are explained in chapter 4.

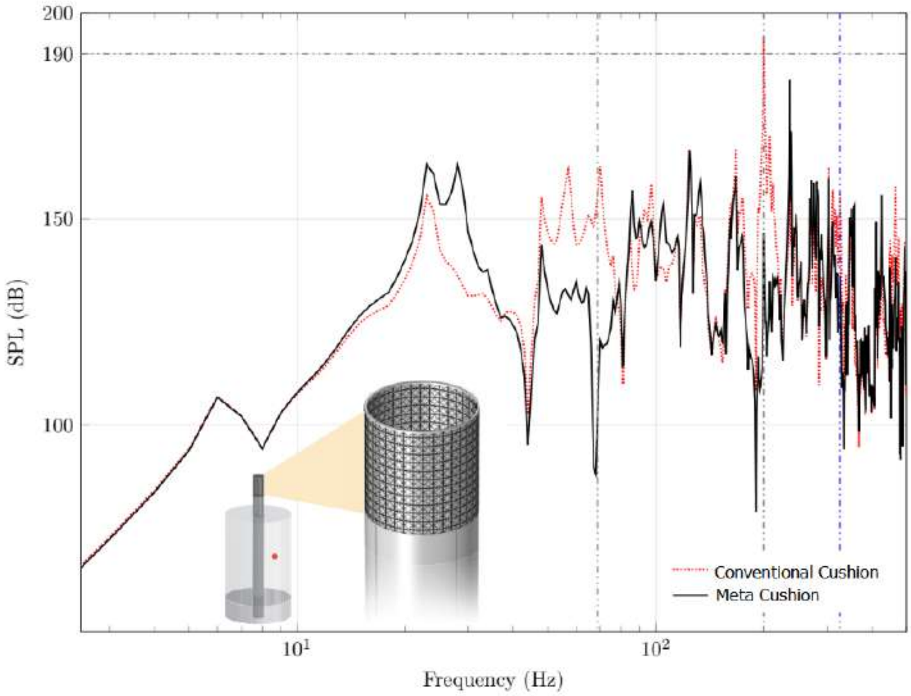

Figure 2.6: SPL comparison between the Conventional Cushion (red dotted curve) and the Meta Cushion (solid black curve). The meta-interface contains 12 layers of periodically distributed unit cells; each layer has 36 unit cells at the radial direction. The SPL threshold is highlighted by the dashed horizontal line. The gray vertical lines indicate the frequencies where the noise reduction was obtained by the local resonance of the Meta Cushion, while the blue vertical line shows the frequency that the SPL decreased due to shift of the eigenfrequency of the Meta Cushion. A reduction of 48 dB is observed in the region with the highest SPL, which occurs around 200 Hz (second vertical dashed line) (Vasconcelos et al., 2023)

2.4. Research Gap

The Meta Cushion has shown promising numerical results to reduce under water noise. This cushion will be taken a step closer to the stage where it actually saves the life of marine animals by manufacturing prototypes and test those cushions on a small-scale. A small-scale impact test setup will be designed and built to assess the effectiveness of the Meta Cushions in reducing noise in a controlled environment. The small-scale test provides a better understanding of its effectiveness and gives an opportunity to improve the cushion. First a modular Meta Cushion using different materials will be designed, built and tested. From that experience a non-modular Meta Cushion will be designed and tested, which could withstand a higher impact force. Testing on a smaller scale is generally less expensive than testing on a larger scale, making it a cost-effective way to assess the effectiveness of the Meta Cushion. The design of the cushion prototypes can be found in chapter 4. This is the first time small-scale testing has been done using a Meta Cushion to mitigate sound pressures caused by MP driving. Small-scale impact tests measuring noise levels caused by MP driving have been executed before. Those experiments form the base of this experiment and their research is changed to fit our experimental setup and goals.

The small-scale impact test setup will demonstrate that the Meta Cushion is more effective than their Conventional Cushions in reducing low-frequency peak noise levels during the small-scale impact test, and the data obtained from the experiments will provide insights for improving the Meta Cushion design for better noise reduction when implemented on a larger scale.

3 Fundamentals for experimental setup

In this chapter the fundamentals for the experimental setup are discussed. First the scaling laws are shown to determine the correct scaling for the setup. Then the setup is discussed briefly, after which each component is explained in more detail. The chapter will end with the equations for the transfer function and the noise levels.

3.1. Scaling laws and similitude

The down scaling plays an important role for the test setup. The monopile and its eigenfrequencies are the biggest influence on the peak values in the noise, as shown in figure 1.1. The dimensions of the MP are therefore leading for the scaling factor, and the eigenfrequencies of the MP are a result from those dimensions.

The geometrical similarity theory was used to scale the Field dimensions down to the Lab dimensions, as shown by Xinquan et al. (2014). When the Field Model (FM) and the Laboratory Model (LM) meet the conditions of this principle, the two physical phenomena are similar. The structure size of the FM and the LM should be proportional to each other to satisfy this similarity theory. The next four equations prove this theory, the subscript F and L stand for the Field Model and the Laboratory Model, respectively.

- Length, radius, and thickness ratio:

$$\frac{L_F}{L_L} = \frac{R_F}{R_L} = \frac{t_F}{t_L} = C_l, \tag{3.1}$$

- Area ratio:

$$\frac{A_F}{A_L} = \frac{\pi(2R_F t_F - t_F^2)}{\pi(2R_L t_L - t_L^2)} = C_l^2, \tag{3.2}$$

- Modulus of section:

$$\frac{W_F}{W_L} = \frac{\pi[R_F^4 - (R_F - t_F)^4]/[2R_F]}{\pi[R_L^4 - (R_L - t_L)^4]/[2R_L]} = C_l^3, \tag{3.3}$$

- Moment of inertia:

$$\frac{I_F}{I_L} = \frac{\pi[R_F^4 - (R_F - t_F)^4]/2}{\pi[R_L^4 - (R_L - t_L)^4]/2} = C_l^4, \tag{3.4}$$

where the C_l is the length coefficient. For this research, the MP was custom made to meet all these scaling laws, therefore the Lab MP and the Field MP have the same aspect ratio and wall thickness-to-radius ratio.

3.2. Small-scale impact test

A small-scale impact test is the best possible representation of the actual large scale offshore monopile driving process. There already have been a few experiments done on a small-scale MP using a hydrophone that is comparable with this research. Jiang et al. (2022) conducted an impact test to analyse the noise reduction between two types of MPs. A comparison was made between a single and a double walled small-scale monopile using an impact test and a hydrophone. The most important similarity between their research and the one presented here is the conversion of the data to Sound Pressure Levels in the frequency domain to show the impact of the noise reduction. The report of Woolfe (2012) developed a downscaled physical model to investigate noise generated by a partially submerged pile under impact loading. This paper will be the theoretical input for this report.

The test setup for this research is built at Huisman Equipment B.V. and shown in figure 3.1, and consists of a water tank filled with water and soil. In the middle of the tank a small-scaled MP is placed

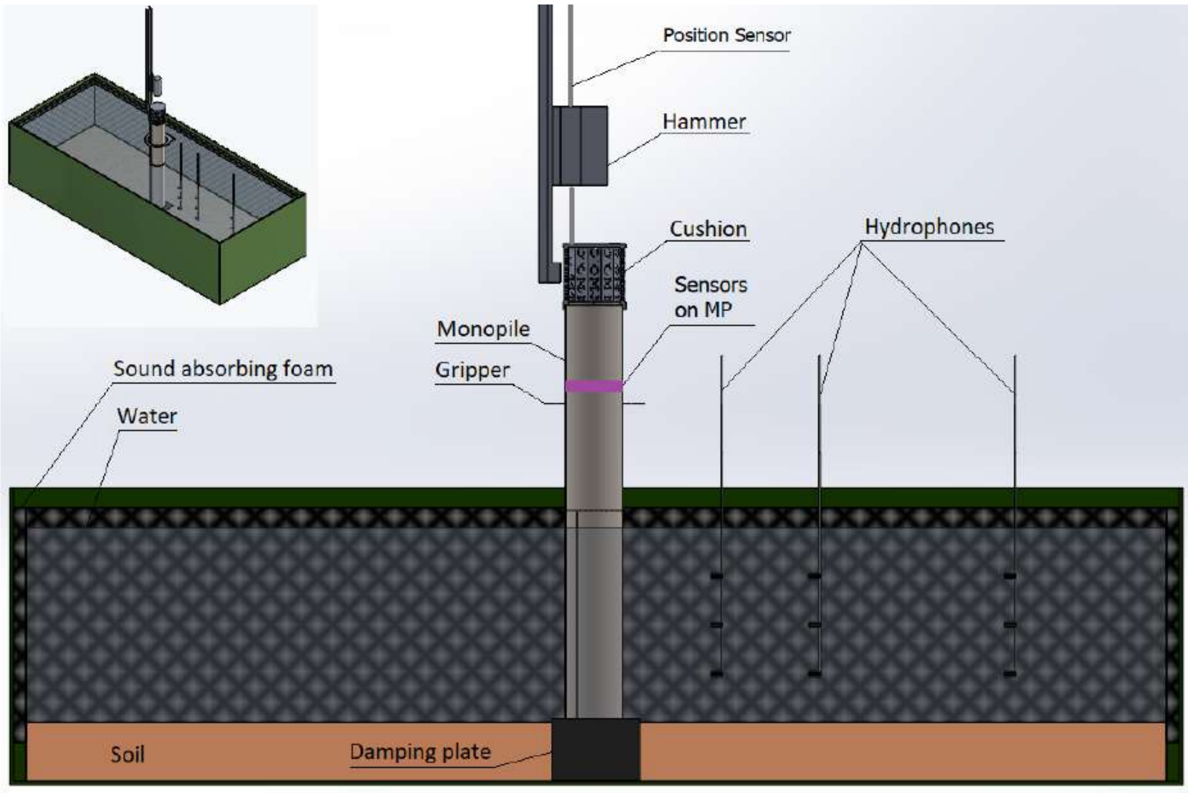

Figure 3.1: Section view of the experimental setup for the small-scale impact test with labeled components

with the cushion clamped on top of the pile. On that cushion a weight is dropped from a certain height, by the impact hammer shown in the top middle of the figure, generating a transient force, causing a compression wave in the pile. This wave and its associated radial displacement motion is measured by an accelerometer and two strain gauges, indicated by the purple band on in the figure. The compression wave causes a sound pressure wave in the water which is measured by a hydrophone, shown on the right side of the MP in the figure.

3.3. Monopile

An actual MP is built from steel compartments welded together on top of each other, as mentioned in section 2.1 and shown in figure 2.1. The length, diameter and the thickness of each compartment of the monopile varies over the length of the pile, and the pile is contructed from steel S355ML. In this report the large-scale monopile is referred to as the Field MP, and its rounded dimensions are shown in figure 3.2a. For the simulation and the small-scale lab experiments a thin walled cylinder with constant wall thickness was used as the MP for simplification, referred to as the Lab MP. The dimensions of the cylindrical Lab MP were based on the bottom half of the Field MP since that part is in the water at the start of the pile driving process. The diameter and associated thickness that occur most frequently over that length of the Field MP were chosen as the foundation to calculate the dimensions of the Lab MP, which is a diameter of 8300 mm and an average thickness of 56.3 mm.

The Field MP was scaled to the Lab MP by using the geometrical similarity theory, with a C_l of 28. The Lab MP was custom made for the small-scale test to meet this theory, and a wall thickness (t_{MP}) of 2 mm was determined. The dimensions of the Lab MP are shown in 3.2b and an impression of the difference in size between the two piles is shown in figure 3.2c. The length of the Lab MP (L_{MP}) will be 2029 mm and the outer diameter (D_{MP}) will be 295 mm. The Lab MP will be constructed from two steel plates, S152-3N, with the material properties: Young's modulus, E_{steel}, of 210 GPa; a density, ρ_{steel}, of 7850 kg/m^3; and a Poisson's ratio, μ_{steel}, of 0.28.

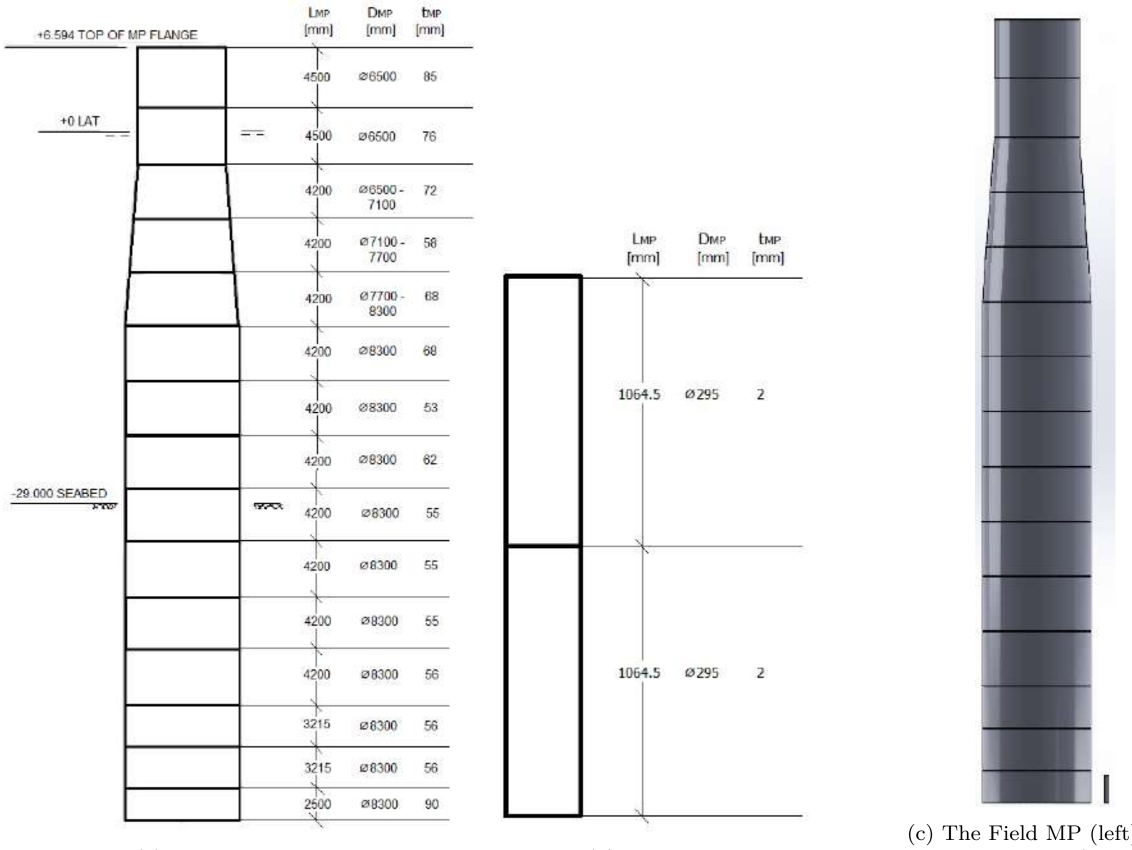

(a) Field MP

(b) Lab MP

(c) The Field MP (left) and the Lab MP (right)

Figure 3.2: Schematic drawing of the Field MP and the Lab MP with the dimensions per compartments, and an impression of the difference in size between the two piles

Prediction of eigenfrequencies MP

The radial eigenfrequencies of the MP are directly coupled to the peaks in the sound pressure waves in the water during off-shore pile driving as mentioned in section 1.1 and shown in figure 1.1. An eigenfrequency is the natural frequency of vibration of a structure, in this case a MP, and it is determined by the physical properties of the MP, such as its mass, stiffness, and damping. When a force is applied to a MP, it may cause the structure to vibrate at its eigenfrequency. This can result in a resonant vibration, which can lead to large amplitude vibrations and large sound pressure peaks.

The Meta Cushion is designed based on the eigenfrequencies of the MP, and this design process is explained in chapter 4. The eigenfrequencies of the MP are predicted via COMSOL Multiphysics®, and are validated in the test setup. The results of these tests can be found in section 8.1.

The MP is partly submerged in water during the impact test, as shown in figure 3.1. The COMSOL® simulation will be built without the water. The eigenfrequencies of the MP in water are expected to be slightly lower because of the high radiation damping underwater. The simulation for the eigenfrequencies of the pile is built as follows: a 2D axisymmetric model is used with a solid mechanics interface. The MP is displayed as a rectangle with the thickness of the Lab MP, t_{MP}, as its width and the length of the Lab MP, L_{MP}, as its height. The rectangle has a displacement in radial direction of the inner radius of the pile, $R_{in,MP}$ of 146.5 mm, and is given the build-in material 'structural steel' with the same density, Young's modulus and Poisson's ratio as the actual Lab MP. The pile wall is a linear elastic material. The movement at the bottom of the pile will be constrained by the test tank and a rubber damping plate during the actual test. The bottom horizontal line of the rectangle is therefore fixed in the simulation. The top of the pile will be constrained by the cushion during the test. The cushion and pile tip are however free to move in all directions, and are therefore not constrained in the simulation.

A mesh of the structure was made using a mapped distribution of 20 by 2 elements over the length of the pile and the thickness of the pile wall respectively. The eigenfrequency study is a built in function and results in the predicted eigenfrequencies of the MP shown in table 3.1.

Table 3.1: first ten eigenfrequencies of the Lab MP extracted from COMSOL Multiphysics®

eigenfrequencies	f_1 [Hz]	f_2 [Hz]	f_3 [Hz]	f_4 [Hz]	f_5 [Hz]	f_6 [Hz]	f_7 [Hz]	f_8 [Hz]	f_9 [Hz]	f_{10} [Hz]
Simulation, air	365	595	1100	1775	1840	2575	2920	3310	3975	4045

3.4. Water tank

The test setup consists of a steel tank provided by Huisman Equipment B.V. with a length of 6000 mm, a width of 2440 mm and a depth of 1500 mm. The MP is placed in the middle of the tank. The tank is filled with a layer of soil and fresh water, as shown in figure 3.1. The Field MP is designed for a water depth of around 30 m. The C_l of 28 results in a water level for the test setup of 950 mm. The soil level is constrained to a maximum height of 300 mm, since the tank will be filled till 250 mm under the tank edge. The soil consists of regular filling sand, which was spread over the tank bottom. Figure 3.3a shows an isometric view of the tank setup, and figure 3.3b shows a section view of that CAD drawing with the most important dimensions.

The density of this sand is around 1500 kg/m³, which is not dense enough to keep the pile from touching the tank bottom. For this reason a damping plate is added under the MP. The damping plate has had an extra advantage by keeping the starting position of the pile in the same place, making it easier to repeat the tests with the same starting conditions. Since the pile will not move deeper into the sand the friction between the pile and the sand is not important for this test setup. The sand only acts as a damper of the sound waves around the seabed and neglects the influence of the tank bottom on those waves. In the middle of the tank floor a rubber damping plate was installed with the dimensions 450 x 450 x 45 mm. The damping plate consists of four layers of Styreen Butadieen Rubber (SBR) sheets with a thickness of 5 mm each, glued on top of a granulate rubber tile with a thickness of 24 mm. The stiffness of the damping plate is determined with a bench press stiffness test shown in chapter 6. The damping plate will be raised till the total damping construction has a height of 345 mm to form the stand for the MP.

The walls of the tank will reflect the sound pressure waves causing a disturbance in the measurements of the hydrophone. This reflection is damped by attaching a sound absorbing bubble foam to the tank walls, using a similar setup as Jiang et al. (2022). The bubble foam absorbs low frequency sound waves in air, and has a thickness of 65 mm. It will cover the whole tank wall except the bottom part which is covered by the soil.

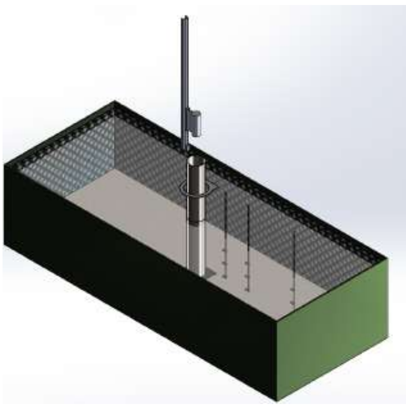

(a) Isometric view of the experimental setup

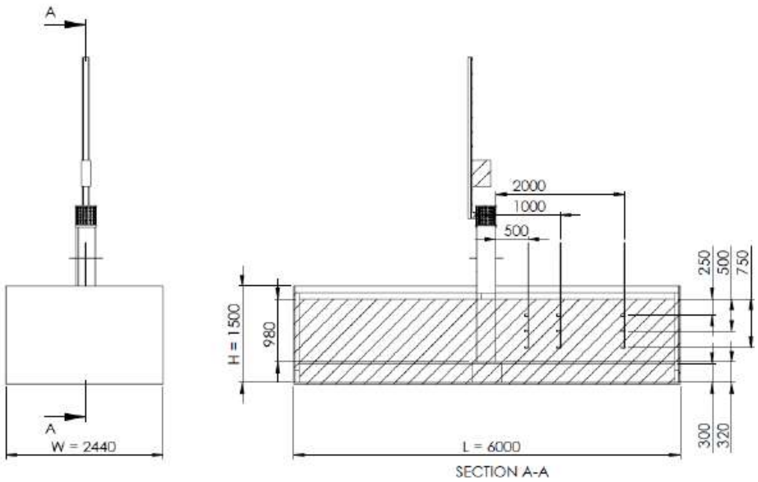

(b) Section view of the technical drawing with the dimensions of the most important components

Figure 3.3: CAD impression for the experimental test setup

Prediction of eigenfrequencies water tank
The eigenfrequencies of the water tank will interfere with the measurements. The eigenfrequencies of the tank could amplify the pressure waves due to resonance. The bottom covered with a damping plate and sand, and the sides covered with the damping foam will muffle these reflected waves as much as possible. The eigenfrequencies of the tank will however still be calculated and determined via the hydrophones by an experiment prior to the actual experiment. Some simplifying assumptions are made for the complexity of the tank shape and the added soil and damping foam.

The bottom of the water tank is covered by a thick layer of soil, and can therefore be kept out of consideration when calculating the eigenfrequencies. The tank walls have a flat surface at the inside of the tank, and are reinforced by stiffeners on the outside. Only the flat inside wall is taken into account for the calculation, and the wall is assumed to be rigid so that the normal component of the particle velocity vanishes at the tank wall. The water of the tank has a height of around 1 m, and therefore the height of the walls are taken as 1 m in the formulas. The natural wave numbers are calculated in the three directions of the tank; over the length of the tank, L_{tank}, as function of l; over the width of the tank, W_{tank}, as function of m; and over the height of the tank, H_{tank}, as function of n. The formulas used are:

$$k_L(l) = l\pi / L_{tank}, \tag{3.5}$$

$$k_W(m) = m\pi / W_{tank}, \tag{3.6}$$

$$k_H(n) = (2n+1)\pi / (2H_{tank}), \tag{3.7}$$

with the length, width and height in meters. The eigenfrequencies can be calculated by combining those three formulas in to

$$f(l,n,m) = \frac{c_{water}\sqrt{k_L(l)^2 + k_W(m)^2 + k_H(n)^2}}{2\pi}, \tag{3.8}$$

with c_{water} as the speed of sound in water of 1490 m/s.

The ten lowest non-degenerated predicted eigenfrequencies are shown in table 3.2. Those predicted values are determines using a continuous wave analysis, and with a very simplified tank. The eigenfrequencies will also be determined when the test setup is complete. This experiment is a part of the test to measure the background noise prior to the impact tests. The test results are shown and discussed in section 8.1.

Table 3.2: Ten lowest non-degenerated predicted eigenfrequencies for the test tank

l,m,n	1,0,0	0,1,0	0,0,1	1,1,0	0,1,1	1,0,1	1,1,1	2,0,0	0,2,0	0,0,2
f(l,m,n) [Hz]	390	496	1110	511	1158	1116	1164	444	757	1850

3.5. Hammer impact energy

There are two types of impact hammers used during the experiments: A pivot hammer for the modular cushions; and a drop weight hammer for the non-modular cushions. Two distinct types of hammers were selected due to the necessity of ensuring that the non-modular cushions were capable of enduring a significantly greater magnitude of impact force.

The pivot hammer consists of a hammer attached to a pivot arm, which pivots via a hinge attached to the frame around the test setup, as shown in figure 3.4. The pivot arm is manually released from an angle of around 90 degrees, after which the hammer hits the cushion in the centre. The impact energy,W_{hammer}, caused by the hammer is calculated via the work done by the hammer head:

$$W_{hammer} = m_{hammer} g s_{hammer}, \tag{3.9}$$

where W_{hammer} is in Joule; the mass of the hammer, m_{hammer}, is in kilograms ; the gravitational acceleration, g, is in m/s^2; and the path traveled by the hammer tip , s_{hammer}, is in meter, calculated by:

$$s_{hammer} = 2\pi r_{hammer} \frac{\alpha_{pivot}}{360}, \tag{3.10}$$

where α_{pivot} is in degrees and the pivot arm r_{hammer} is in meters. The input values and the results from these equations are shown in figure 3.3.

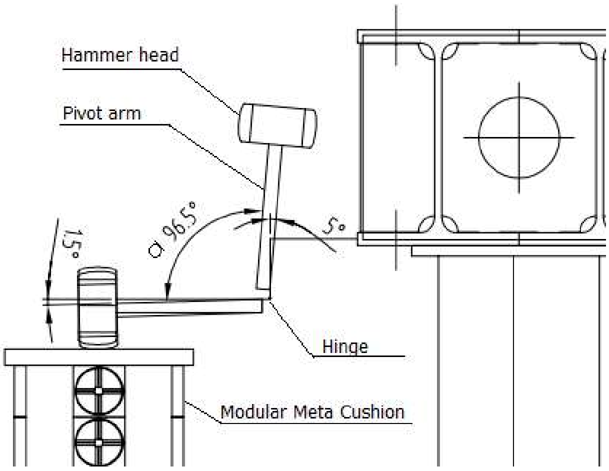

Figure 3.4: Technical drawing of the pivot hammer used for the impact tests on the modular cushions in its upright position and in its impact position

Table 3.3: Input and output variables of the pivot hammer

Quantity	value
m_{hammer}	2.3 kg
r_{hammer}	320 mm
α_{pivot}	96.5°
s_{hammer}	0.54 m
W_{hammer}	12 J

For the non-modular cushions a drop weight impact hammer is used to generate a higher impact force. During those tests a drop weight, so called ram, is lifted and released from a certain height above the cushion and pile. This ram should hit the centre of the cushion each test, therefore it is attached to a guide rail, as shown in figure 3.3a. The friction caused by the rail is the same for each test, and will be neglected.

The pile, cushion and ram can be simplified by a mass-spring system to calculate the maximal impact force of the hammer on the cushion, and is shown in figure 3.5. The MP will not move into the soil and therefore the MP does not act as a damper, but as a spring. The cushion and the pile will be modeled as two springs in series. The conservation of energy between gravitational potential energy of the ram and elastic potential energy of the pile and cushion is used to calculate the displacement of the cushion by the impact force of the ram, u_{ram}, and the resulting hammer force F_{hammer}. The conservation of energy equation is as follows:

$$E_{pot} = E_{spring}, \tag{3.11}$$

The gravitational potential energy of the ram, E_{pot}, is calculated via:

$$E_{pot} = m_{ram} g(DH_{ram} + u_{ram}), \tag{3.12}$$

where m_{ram}, g, DH_{ram} and u_{ram} are the mass of the ram, the gravitational acceleration, the drop height from which the hammer is release and the displacement of the ram into the cushion and pile during impact respectively. The elastic potential energy of the pile and cushion, E_{spring}, is calculated via:

$$E_{spring} = \frac{1}{2}(\frac{1}{k_{cushion}} + \frac{1}{k_{MP}})^{-1} u_{ram}^2, \tag{3.13}$$

where $k_{cushion}$ and k_{MP} are the axial stiffness of the cushion and the pile respectively and are extracted from COMSOL®.

From these three formulas the maximal displacement of the ram, u_{ram}, is determined. This displacement is used to calculate the reaction force from the cushion and MP to the hammer with the formula;

$$F_{ram} = (\frac{1}{k_{cushion}} + \frac{1}{k_{MP}})^{-1} u_{ram}, \tag{3.14}$$

the input variables for these equations and resulting outcomes can be found in table 3.4.

During the experiment a position sensor along the rail measures the position of the hammer over time. With this data the impact velocity, v_{impact}, and the impact energy of the drop weight can be determined using the kinetic energy formula:

$$E_{kin} = \frac{1}{2} m_{ram} v_{impact}^2, \tag{3.15}$$

where the kinetic energy is in Joule.

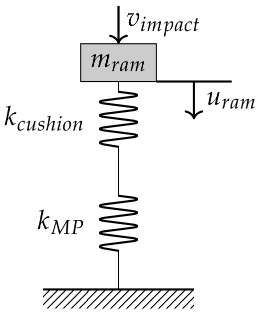

Figure 3.5: Mass-spring system of the ram, cushion and MP

Table 3.4: Input and output variables of the energy conservation equations

Quantity	value
m_{ram}	47 kg
DH_{ram}	300 mm
$k_{cushion}$	600 kN/mm
k_{MP}	170 kN/mm
u_{ram}	1.4 mm
F_{ram}	200 kN
E_{ram}	140 J

3.6. Sensor placement

The experiments were observed with different sensors on and around the pile and cushions, which will be discussed next.

Hydrophone

The hydrophone used in this research is the TC4013. The scarcity in sensors allowed the use of one hydrophone only, therefore the hydrophone will be placed in different spots in the tank per test. The receiving sensitivity of the hydrophone is -211dB re 1V/μPa. This value is used to convert the output signal of the hydrophone from Volt to Pascal. The data from the hydrophone is converted to a sound pressure in the time domain, p(t), by dividing the data by the hydrophone sensitivity.

The eigenfrequencies of the MP determine the near field region and the far field region of the sound pressure waves in the water. It is important to determine the far and near field regions when measuring sound pressure waves in water, because the acoustic behavior of sound waves in water changes depending on the distance from the source. The near field region is the region close to the source where the sound waves are still changing in pressure and intensity. In this region, the sound waves are not well defined and can be influenced by the shape of the source, reflections from nearby surfaces, and other factors. It can be difficult to accurately measure sound pressure in the near field region. On the other hand, the far field region is the region farther away from the source where the sound waves have stabilized and become more uniform in their shape and intensity. In this region, the sound waves are more predictable and easier to measure accurately. Knowing the boundary between the near field and far field regions is important, because it helps to determine the appropriate measurement techniques and instrumentation required for accurate measurements.

The near field ends at ten times the wavelength, when the ratio of circumference to wavelength equals five (Woolfe, 2012). The circumference of the outside diameter is taken for this calculation, resulting in a wavelength of 185 mm, therefore the near field region ends at 1800 mm from the MP wall. The far field region starts at ten times the wavelength of the first eigenfrequency of the MP. For the eigenfrequency of 365 Hz this results in a distance of 41 meters from the MP, which is far outside of the test tank. The hydrophone is placed in the near field region at 500 mm, 1000 mm and 2000 mm from the pile wall over the middle of length of the tank, as shown in figure 3.3a and 3.3b, to minimize the reflections of the tank wall.

The compression wave in the MP caused by the impact hammer and its associated radial displacement motion move downward over the MP. This downward traveling wave generates an acoustic field in the shape of an axisymmetric cone, known as a Mach cone (Reinhall and Dahl, 2011). This cone is created because the speed of the radial displacement wave traveling downward in the MP is higher than the speed of sound in the water. The Mach cone dominates the peak pressure in the underwater noise field.

Once the compression wave reaches the bottom of the MP, it is reflected upward since there is an impedance mismatch between the pile and the sediment. This reflected wave produces an upward-moving Mach cone, and the sound field associated with this cone propagates up through the sediment and into the water. The depth of the hydrophone in the water will vary between 250, 500 and 750 mm from the water level, which divides the water level into four quarters. The functionality of the soil in the tank can be checked this way. The different positions of the hydrophone is shown in figure 3.3a.

The figure shows nine hydrophones while only one was used at a time.

During the test on the modular cushions the hydrophone will be placed in one position: 500 mm from the pile wall, and in the middle of the water at a depth of 500 mm.

Sensors on monopile
The sensors used in this experiment on the pile are one accelerometer and two sets of strain gauges. These wall-motion sensors are attached to the outside wall of the MP and at a distance of 1.5 times the diameter from the tip of the pile. This is a standard for dynamic testing of piles in the field specified by the American Society for Testing and Materials (D4945, 2008).

The accelerometer is attached to the pile via a corner piece for which the accelerometer sensor is in a horizontal position. This sensor will measure the relatively low level of acceleration of the pile wall in three directions. The surface under the strain gauges is cleared of paint for better conductivity and the sensor is glued directly onto the pile wall.

3.7. Noise Levels in the time domain

The noise levels will be calculated in the time domain and compared between the two cushions, since the threshold value of table 2.1 is measured from a larger distance from the MP with a different impact energy.

Sound Exposure Level
The Sound Exposure Level (SEL), explained in section 2.2, is calculated by taking the time-averaged sound pressure squared over the duration of the measurement period, and then integrating this quantity over the time range of the sound. For this research the SEL_{ss} is determined since the tests in this research are done with only one hammer impact pulse each test. The SEL_{cum} can not be measured, it could however be predicted by multiplying the SEL_{ss} over a certain period of time. The Sound Exposure (SE) is calculated with the equation:

$$SE_{ss} = \int_{t_0}^{t} p(t)^2 \, dt, \tag{3.16}$$

where the t_0 is the moment the sound pressure wave reaches the hydrophone, and p(t) is the pressure measured by the hydrophone over time. This SE is used to calculate the SEL via:

$$SEL_{ss} = 10 \log^{10} \frac{SE}{p_{ref}^2}, \tag{3.17}$$

where the p_{ref} is the reference pressure in water in Pa^2s, resulting in a SEL expressed in dB (re 1 $\mu Pa^2 s$).

Sound Pressure Level
The Sound Pressure Level (SPL) is a measurement of the intensity of a sound at a specific point in time and is also typically measured in dB. The peak value SPL_{peak} is easy to measure for each hammer strike during the small-scale impact pile driving test. There are three ways to calculate this peak pressure, as described in section 2.2. The SPL used in this research is the $SPL_{z,p}$, which calculates the SPL with the pressure difference between its peak value and zero ($p_{z,p}$) during the impact test via the formula:

$$SPL_{z,p} = 10 \log^{10} \frac{p_{z,p}^2}{p_{ref}^2}, \tag{3.18}$$

where the SPL is expressed in dB (re 1 μPa), and the p_{ref} is 1 μPa for water.

3.8. Fast Fourier Transform

The signals of the sensors will be transformed to the frequency domain, via the methodology used by Heinzel et al. (2002). The hydrophone measures the total sound pressure as a function of time of the pressure wave, at a given point at a radial distance from the pile and depth in the water. This pressure will be expressed in the discrete data string p[k,r,z] in Pascal. The output signal of the hydrophone is expressed in a voltage, and is transformed to a pressure via the receiving sensitivity. The data from the accelerometer and the strain gauges are measured at one point on the pile wall and can therefore be written as the discrete functions a[k] and s[k], respectively. The data from the sensors on the pile wall and the hydrophone will all be padded with zeros to a length of the next power of two, resulting in N data points. Next the Fast Fourier transform (FFT) is done on each data string, which takes the vector of N complex numbers x[k], k=0, ..., N−1, and transforms it into a vector of N complex numbers y[m], m = 0, ..., N−1. The data in the frequency domain is then normalized by dividing them by the number of data points N.

The sample period, T_s, for the data in the time domain is dependent on the sample frequency, f_s, via the equation:

$$T_s = \frac{1}{f_s}, \tag{3.19}$$

which results in the time vector:

$$t[k] = kT_s, \tag{3.20}$$

for k = 0, ..., N-1.

The data in the frequency domain is taken from 0 to the Nyquist frequency, f_{Ny}, which is $f_s/2$, since the signal is mirrored at the f_{Ny} in the frequency domain. The width of the frequency between two data points in the frequency domain, is called the frequency resolution, f_{res}, and is calculated by

$$f_{res} = \frac{f_s}{N}, \tag{3.21}$$

which results in the vector for the frequency of

$$f[m] = mf_{res}, \tag{3.22}$$

for m = 0 .. N/2, to exclude the data after F_{Ny}.

The formulas used for the FFT are:

$$P[m,r,z] = \frac{1}{N}\sum_{k=0}^{N-1} p[k,r,z]e^{-i2\pi\frac{mk}{N}}, \tag{3.23}$$

for m = 0, ..., N/2, where P[m,r,z] is the pressure measured by the hydrophone in Pascal.

$$A_x[m] = \frac{1}{N}\sum_{k=0}^{N-1} A_x[k]e^{-i2\pi\frac{mk}{N}}, \tag{3.24}$$

for m = 0, ..., N/2, where A_x is in m/s^2. The same formula will be used for acceleration in y and z direction and for the strain gauges:

$$A_y[m] = \frac{1}{N}\sum_{k=0}^{N-1} A_y[k]e^{-i2\pi\frac{mk}{N}}, \tag{3.25}$$

$$A_z[m] = \frac{1}{N}\sum_{k=0}^{N-1} A_z[k]e^{-i2\pi\frac{mk}{N}}, \tag{3.26}$$

$$S[m] = \frac{1}{N}\sum_{k=0}^{N-1} S[k]e^{-i2\pi\frac{mk}{N}}, \tag{3.27}$$

for m = 0, ..., N/2, where the accelerations are in m/s^2 and the unit for the strain gauges in Volt.

Linear spectrum
The data in the frequency domain is compared using the linear spectrum or amplitude spectrum (LS) for each signal in the frequency domain, since the units will be the same as the original in the time domain. The LS is the square root of the power spectrum (PS), which is the data in the frequency domain squared and multiplied by two, to keep the same energy. The LS for the sound pressure, is the Sound Pressure Spectrum (SPS) measured by the hydrophone is shown in the next equation:

$$SPS[m,r,z] = \sqrt{2}|P[m,r,z]|, \tag{3.28}$$

for m = 0, ..., N/2, where the SPS is in Pascal. The SPS will show a trough around the desired frequency band gap if the Meta Cushion works, while the Conventional Cushion shows a peak.

The same formula is used for the data from the accelerometer, to make the Acceleration LS in the 3 directions:

$$A_x LS[m] = \sqrt{2}|A_x[m]|, \tag{3.29}$$

$$A_y LS[m] = \sqrt{2}|A_y[m]|, \tag{3.30}$$

$$A_z LS[m] = \sqrt{2}|A_z[m]|, \tag{3.31}$$

for m = 0, ..., N/2, in [m/s^2].

Lastly the LS from the stain gauge shows the stress energy in the MP, and is calculated with:

$$StrLS[m] = \sqrt{2}|S[m]|, \tag{3.32}$$

for m = 0, ..., N/2, resulting in the StrLS in volt. The stain gauges will show if the eigenfrequency of the pile is filtered by the Meta Cushion, by showing a lower value at the designed frequency band of the Meta Cushion.

Sound Pressure Level

The SPL in the frequency domain is calculated with the same principle as for the time domain. The SPS is used as the pressure input to calculate the SPL$_{\text{peak}}$ in the frequency domain with:

$$SPL_{peak}[m, r, z] = 20 \log^{10} \frac{SPS[m, r, z]}{p_{ref}}, \tag{3.33}$$

where the SPL is expressed in Decibel [dB], and the p$_{\text{ref}}$ is 1 μPa for water.

4 Meta Cushion

The fundamentals for the small-scale test have been discussed and the scale of the experimental setup has been determined. The next step is to introduce the Meta Cushions, and show their key performance indicators (KPIs).

The Meta Cushion consists of arrays containing single-phase resonant structures, called unit cells. The resonators in these unit cells are designed to obtain a local resonance band gap - a bandwidth where waves are attenuated - at the desired frequency range, causing a transmission loss (TL) which shifts the energy around that frequency towards other frequencies (Vasconcelos et al., 2022). The desired frequency band gap of the unit cells will be around the eigenfrequencies of the MPs, since the sound pressure peaks are at those eigenfrequencies as discussed in 3.3.

The impact hammer needs to be adjusted per MP batch and the Meta Cushion can be implemented during this process step. The Meta Cushion is independent of the water depth at which the MP is installed and eliminates the necessity of external vessels or casings during the impact pile driving, which decreases the operational costs substantially.

For each Meta Cushion, a Conventional Cushion is designed with the same stiffness and from the same material. The cushion act as a spring, as explained in section 3.5. The Conventional Cushion forms the baseline to compare the Meta Cushion with to eliminate the influence of the spring constant and see the functionality of the meta-material itself.

4.1. Elastic mechanical meta-material

Elastic mechanical meta materials are a type of engineered material that has the ability to deform and change shape in response to external forces, while maintaining their structural integrity. These materials are made up of a complex structure of tiny interconnected parts, each designed to contribute to the overall mechanical properties of the material. In the spectrum from pure natural materials that possess intrinsic mechanical properties to large-scale structures that are characterized by highly design-specific structural properties, meta-materials are somewhere in between (Zadpoor, 2016).

The term meta-material was first used in the optics and electromagnetism section, but has emerged in the mechanical direction during the last few years (Zadpoor, 2016). The mechanical meta-material is a designed structure that exhibits constitutive mechanical properties that are not found in naturally occurring materials (Vasconcelos et al., 2021). They are created by introducing structural irregularities into the material, called unit cells. This unit cell is composed to exhibit an arbitrarily chosen set of mechanical and physical properties, such as acoustic/elastic cloaking, negative refractive index, negative permeability, acoustic imaging and acoustic/elastic dampers (Vasconcelos et al., 2021; Zadpoor, 2016). The meta-material composition in this research is designed to obtain a local resonance band gap at the eigenfrequency of the MP used in the experiment, using acoustic absorbing resonators.

Functionality Periodic Unit Cell

The core of the Meta Cushions consist of arrays containing six periodic unit cells (PUC), with each core made from a different material: aluminium, acrylic or nylon, with the material properties shown in table 4.1. The geometry of the different PUCs are shown in figure 4.1. The external shape of the PUC is a square shaped frame, which holds a resonator. The resonators are cut out of the array using water cutting, therefore the array can be produced from one material piece. The resonators consist of

Table 4.1: Material properties for the Meta Arrays

material	Aluminium	Acrylic	Nylon
E [GPa]	70	3.2	9
ρ [kg/m^3]	2700	1190	1150
μ [-]	0.33	0.35	0.4

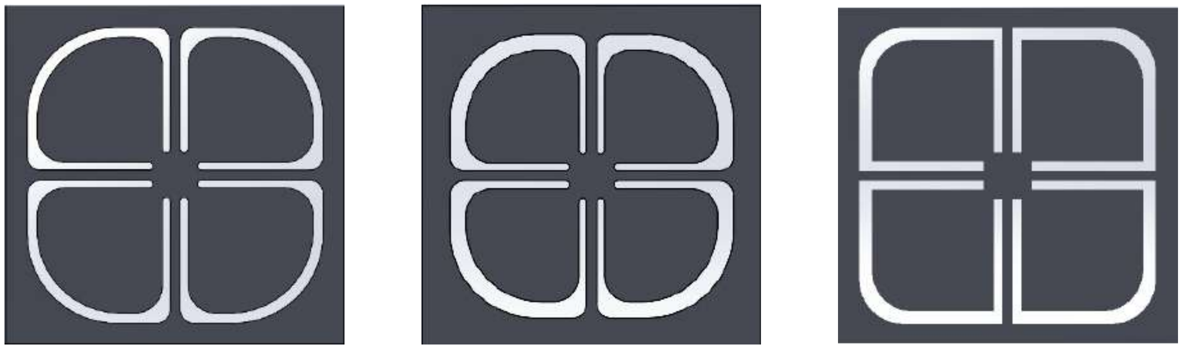

(a) Aluminium PUC (b) Acrylic PUC (c) Nylon PUC

Figure 4.1: PUCs for the modular Meta Cushions designed for this research

a centered mass which is connected to the unit core by beams. The thickness of the beam, t_{beam}, is crucial for the functionality of the resonator and needs to be manufactured with the highest accuracy. The PUC functions as a resonator with a conventional mass-in-mass system behaviour, which filters the energy from the impact load applied on the cushion.

The movement of the resonator causes a TL at the desired frequency, as described by Vasconcelos et al. (2023). The TL is observed when the resonator is moving out of phase compared to the frame, and defined by the formula

$$TL = 20 \log^{10} \frac{||U_2||}{||U_1||}, \tag{4.1}$$

where U_1 and U_2 are the displacements at points x_1 (at the tip of) and x_2 (at the end) of the array respectively, as shown in figure 4.2.

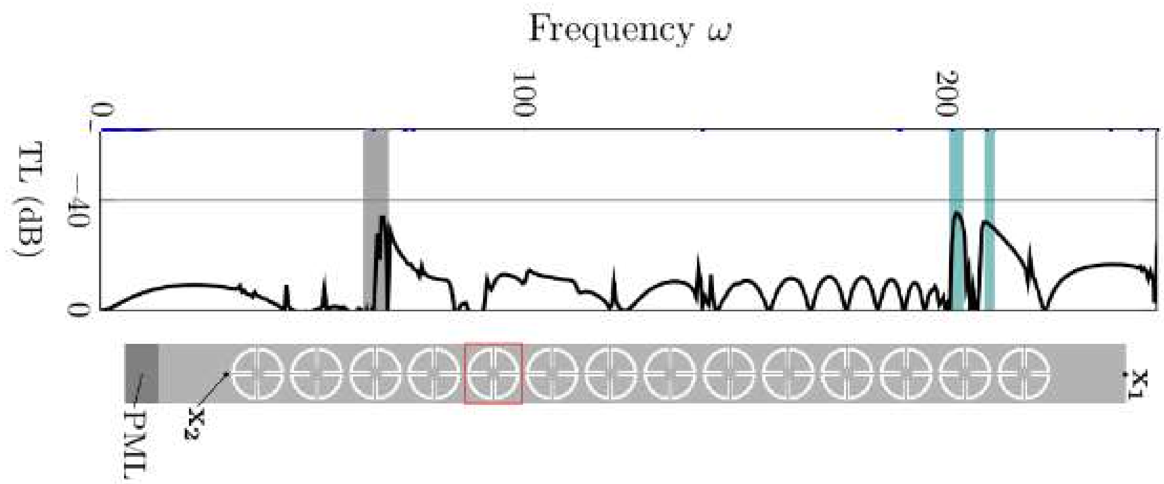

Figure 4.2: Band structure of a periodic unit cell (PUC) and transmission loss diagrams for an array composed by 14 PUCs. The grey area identifies a complete bandgap with range ω = [63.2 Hz - 68.1 Hz]. Partial bandgaps are also identified at frequencies ranging from 201.1 Hz and 215 Hz (blue areas) (Vasconcelos et al., 2023).

4.2. Modular Meta Cushion

The functionality of the meta-material PUCs will be tested by a modular Meta Cushion. This cushion contains four arrays which are clamped between a top and a bottom part, and are interchangeable for each cushion. The KPIs of these cushion cores will be discussed next.

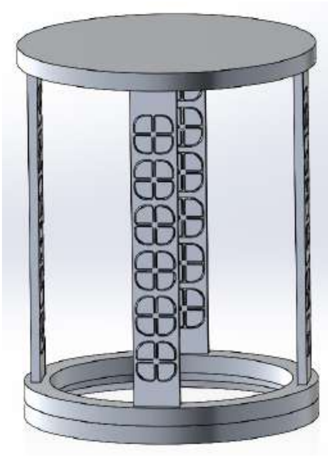

(a) Modular Meta Cushion

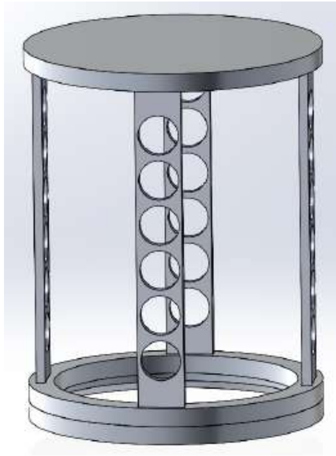

(b) Modular Conventional Cushion

Figure 4.3: CAD impression of two Modular Cushions

Key Performance Indicators
Each cushion was designed for a different TL frequency. This numerical TL frequency for each cushion is shown in table 4.2. The TL frequency depends on the mass of the resonator and the thickness of the beam holding those resonators. After the arrays were manufactured the actual TL frequency was determined using a Frequency Response Function (FRF) test with a laser. During these tests the array is kept in the horizontal position with a vibration machine attached one side of the array as shown in the picture in figure 4.4a, vibrating the array with all frequencies in a range from 1 Hz to 3000 Hz. On the tip of the free side of the array, a laser is measuring the frequency response function of the array, from which the TL diagram can be plot.

The numerical and experimental TL diagram for all the different arrays are shown per array in figure 4.4, where the numerical results are shown with a blue solid curve and the experimental results from the FRF-tests are shown with a black solid curve. The numerical transmission loss diagram for the aluminium array is shown in figure 4.4b, where the designed TL is visual at a frequency of 2500 Hz. The resonator is moving out of frame compared to the array at this frequency, which caused this dent in the plot. The experimental TL diagram for the same array obtained via the FRF-test shows an actual TL around a frequency of 2250 Hz. The aluminium modular Meta Cushion is expected to show the TL at this experimental TL frequency during the small-scale impact tests. The same applies for the other two arrays were the numerical and experimental TL results are shown in the figures 4.4c and 4.4d. The TL frequencies at which the arrays were designed, and the actual TL frequencies determined by the FRF-experiments are shown in table 4.2.

The difference in the numerical and experimental values can be assigned to the designed t_{beam} and actual t_{beam} of the PUCs, which are shown in the next chapter.

Table 4.2: Numerical and experimental TL frequencies for each array used in a Meta Cushion

Meta Cushion	Modular			Non-modular
Material	Aluminium	Acrylic	Nylon	Aluminium
Numerical TL [Hz]	2500	1027	592	350
Experimental TL [hz]	2250	1150	600	220
TL attenuation [dB]	-50	-40	-35	-25

Geometry
The Meta Arrays consist of six PUCs, as mentioned before and shown in figure 4.3a. On both ends of the arrays an extra length is added of 40mm, resulting in a total length of 382.4 mm. The thickness of the arrays are 10 mm for the aluminium and acrylic arrays and 9.45 mm for the nylon arrays. The width of the arrays are the same as for the PUCs, 50.4 mm.

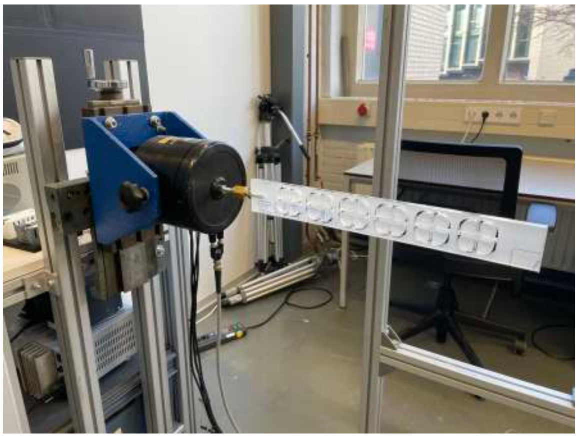

(a) Setup for the FRF-tests with the acrylic Meta Array

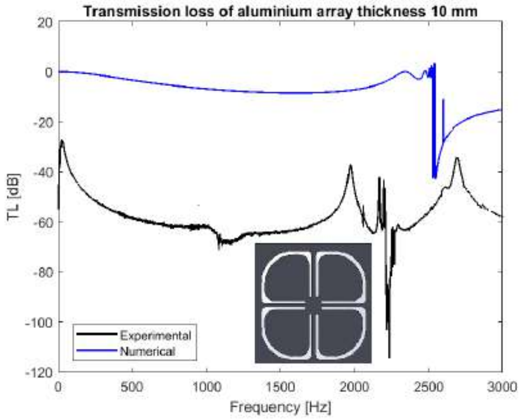

(b) Aluminium array

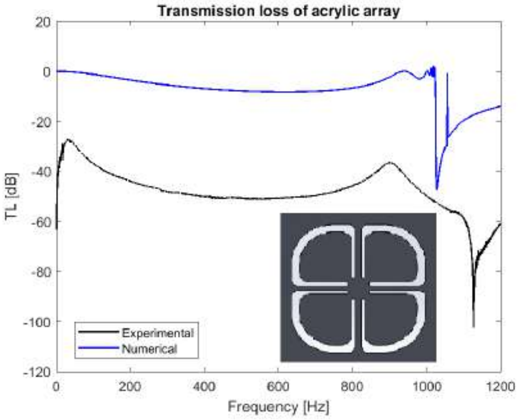

(c) Acrylic array

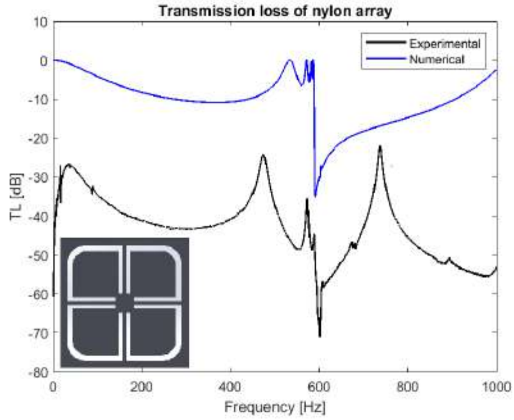

(d) Nylon array

Figure 4.4: Numerical (blue curve) and experimental (black curve) TL diagram for the different arrays with the displacement field during the TL visualised in the top PUC

These four arrays per cushion are clamped between a top plate and a bottom part. The top plate is an aluminium plate with a diameter of 325 mm and a thickness of 20 mm, which will distribute the impact force of he hammer over the arrays. The plate holds the arrays in place during the experiments via four slots which can fit all different arrays. The cushions itself also needs to be kept in position during the impact tests, therefore a clamp was designed, as shown in the cad drawings in figure 4.3. This clamp consists of two circular plates with a thickness of 20 mm and an outer diameter of 325 mm. The bottom plate has an inner diameter of 295.5 mm to have a thigh fit around the MP tip. The top plate of the clamp has an inner diameter of 265 mm, and contains four slots with the same dimensions as the top plate to hold the arrays.

The Conventional Array should have the same stiffness as its Meta Array. The Conventional Arrays will have the same length, width and thickness as the Meta Arrays, but contains six holes instead of resonators, as shown in figure 4.3b. The dimensions of those holes determine the stiffness of the array and this axial stiffness is extracted via a COMSOL® simulation.

The CAD drawing of the Meta Cushion array is loaded into the solid mechanics interface of COMSOL®, and is simulated as a linear elastic material. The corresponding material properties are assigned to the array, which can be found in table 4.1. The bottom of the array is constrained in all three directions and on top of the array a rigid connector was assigned with a prescribed axial displacement. On this rigid connector the summation over the nodes of the reaction forces is taken, which results in an axial stiffness, $k_{\text{axial,Meta}}$, shown in table 4.3. The same simulation setup was used for the Conventional Arrays, which determined the axial stiffness, $k_{\text{axial,Conv}}$, while changing the diameter of the holes, D_{hole}, in the array. The resulting diameter of the hole and axial stiffness are shown in table 4.3.

Table 4.3: Stiffness prediction for the arrays of the modular cushions

Array	Aluminium	Acryl	Nylon
$k_{axial,Meta}$ [kN/mm]	20.26	1.15	0.47
D_{hole} [mm]	42	41	44
$k_{axial,Conv}$ [kN/mm]	18.34	1.15	0.50

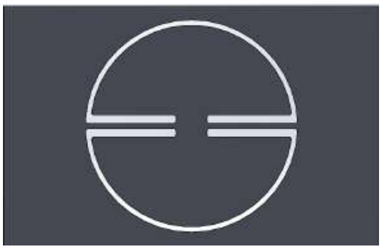

(a) CAD impression

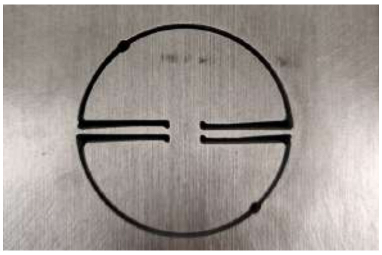

(b) Picture of the back of array after watercutting

Figure 4.5: Unit cell for the aluminium non-modular Meta Cushion

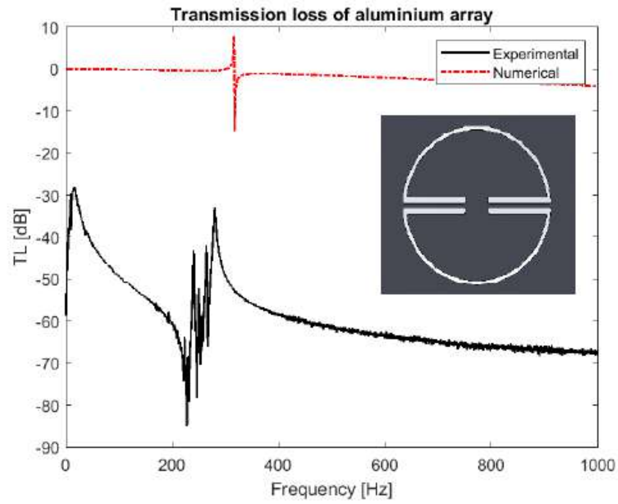

Figure 4.6: Numerical (red) and experimental (black) TL diagram of the aluminium array for the non-modular Meta Cushion with the displacement field during the TL visualised in the top PUC

4.3. Non-Modular Meta Cushion

The non-modular cushion will be designed to obtain a higher impact force as mentioned in section 3.5. This cushion will be the next step towards the final large-scale implementation, where the cushion is exposed to even higher internal stresses. The non-modular cushions are both made from the same material, aluminium 6082. This aluminium has a yield strength of 260 MPa and is easy to use for welding, which is pleasant for constructing the core of this Meta Cushion.

Key Performance Indicators

The numerical and experimental TL diagram for the non-modular Meta Cushion is shown in figure 4.6, where the numerical results are shown with a red dotted curve and the experimental results from the FRF-tests are shown with a black solid curve. The numerical TL is visual around a frequency of 350 Hz with an attenuation of 15 dB. The FRF-experiments started with a high peak after which the curve decreased in value, with a TL visible around 220 Hz of 15 dB, after which the array shows TLs and peak values until the frequency of 320 Hz where it reaches a peak value.

The difference in the numerical and experimental values can be assigned to the designed and actual t_{beam} of the PUCs, shown in figure 4.5. All beams were designed with a thickness of 1 mm, while the actual thickness of the beam varied from 0.53 mm up to 0.8 mm. This could be the reason for the reduction in TL frequency and the spreading in the plot.

Geometry

The non-modular Meta Cushion consist of twelve arrays containing six PUCs each. The geometry of the unit cell is a bit different than that of the modular cushions, as shown in figure 4.5a, however the working principle stays the same. The external shape of the PUCs is a square with a length of 46 mm, holding a resonator with two beams. The twelve arrays form a do-decagon, as shown in figure 4.7a, which is linked to the dimensions of the wall diameter of the MP, therefore the width of the array is larger than the width of the unit cell. The inside width of the array is 72 mm, the thickness of each array is 20 mm and the length of the array is six times the length of a PUC (276 mm).

(a) Non-modular Meta Cushion

(b) Non-modular Conventional Cushion

Figure 4.7: CAD impression of the non-modular cushion designed for this research

On top of the core a top plate is added with the same dimensions as the top plate of the modular cushions, and on the bottom a clamp with the same dimensions is used (both without the slots). This cushion has to withstand an higher impact force, therefore an extra top plate is placed on top of the existing top plate with diameter of 325 mm and a thickness of 10 mm. The final mass of the non-modular Meta Cushion is 22 kg.

Internal stress Meta Cushion
During the experiments the impact hammer hits the top of the cushion with an dynamic impact force, creating internal stresses in the cushion and the MP. The internal stress experienced by this cushion should not exceed the yield strength of the material, Aluminium 6082, which is 270 MPa.

The internal stresses and displacements of the Meta Cushion are predicted using COMSOL Multiphysics®. The impact force of the hammer is a dynamic, time dependent phenomenon, however the peak value of the force causing peak internal stresses can be modeled using a stationary study. The CAD drawing of the Meta Cushion is loaded into the solid mechanics interface of COMSOL®, and is simulated as a linear elastic material with the material properties of aluminium. To simulate the axial hammer force a circle with the diameter of the hammer, 140 mm, was drawn on top of the top plate. On this area a boundary load in the axial direction of 200 kN is prescribed. The plate of the clamp engaging with the top of the MP is constrained in all three directions.

The Von Mises stresses are subtracted from the simulation using built-in domain probes. If the internal Von Mises stress do not exceed the yield strength the criteria states there is no plastic deformation. The simulation will calculate the maximal Von Mises stress in the top plates, in the cushion core and for the resonators separately. The maximal displacement of the cushion top plates and the top of the core wall are also extruded. The results from the simulation can be found in the first row of table 4.4, and the stress distribution can be seen in figure 4.8a.

During the simulation the hammer force acts exactly in the middle of the top plate, while during the experiments the hammer could have an offset from the centre. The simulation is therefore repeated with an offset of the impact force of 10 mm, and the results are shown in the second row of table 4.4.

The simulation considers the cushion core and the two top plates are a single object, while in reality all three parts are separated from each other. The stress distribution shows the highest stresses at the top of the cushion core which is probably a result of high shear stresses, caused by the deformation of the top plate. During the impact test the core and the top plates are not attached to each other and therefore these high shear stresses will not occur. The core is therefore also simulated without the top plates, with the axial force directly on the top of the core walls. This reduces the Von Mises stress in the arrays and resonators, as shown in the third row of table 4.4, and is a better representation of reality. The displacement extracted from the simulation will be used during the validation of the stiffness prediction in chapter 6.

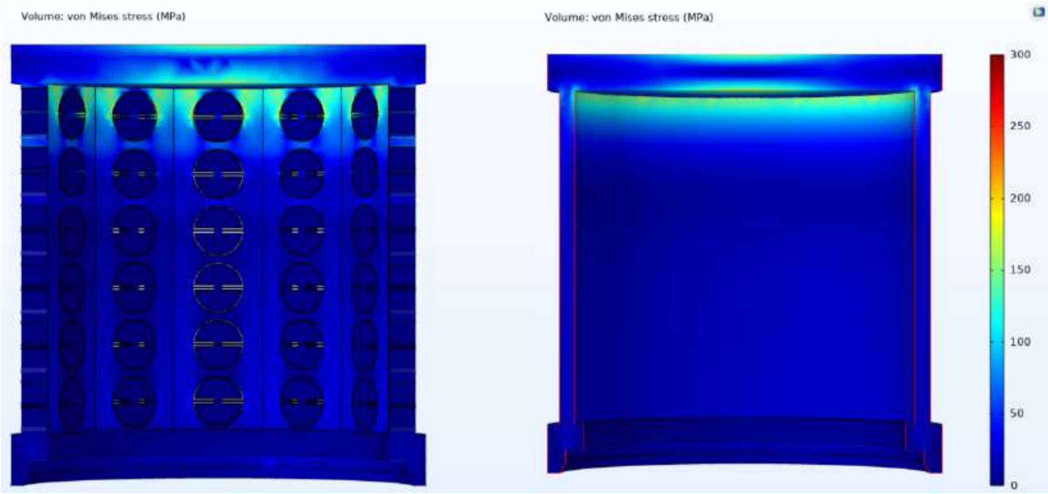

(a) Meta Cushion (b) Conventional Cushion

Figure 4.8: The numerical Von Mises stress distribution for both non-modular cushions showed for the cross-section view, with the legend from 0 MPa (blue) to 300 MPa (red)

Table 4.4: Predicted Von Mises stress for the non-modular cushions with the hammer centred and with an offset, and for all components separately. These values should not exceed the yield strength of 270 MPa

		Top plate		Core		Resonators
		Von Mises stress [MPa]	Displ [mm]	Von Mises stress [MPa]	Displ [mm]	Von mises stress [MPa]
Meta	Hammer offset 0 mm	160	0.77	260	0.17	205
	Hammer offset 10 mm	160	0.76	275	0.20	225
	Only core	-	-	160	0.15	110
Conv.	Hammer offset 0 mm	170	0.79	210	0.17	-
	Hammer offset 10 mm	175	0.78	215	0.11	-

The resonators will vibrate under the dynamic impact stress, this is not taken into account during the stationary simulation. The vibration will increase the stress in the beams of the resonators, and can cause the beams to elongate through plastic deformation.

Predicted axial stiffness non-modular Meta Cushion

The axial stiffness of the Meta Cushion is extracted from the COMSOL® simulation, for the design of the Conventional Cushion. The previous simulation setup can be used by replacing the boundary load with a rigid connector with a prescribed axial displacement, which simulates the displacement on the cushion top caused by the hammer. The summation over the nodes of the reaction forces on this connector is taken, which results in an axial stiffness for the Meta Cushion, $k_{axial,Meta}$, of 595 kN/mm.

The simulation models the cushion as a single object, as stated before. During the experiments the cushion core and its clamp are expected to act as linear helical springs, and the two top plates as two parallel disc springs. The axial stiffness of the cushion core and both top plates are simulated separately. The axial stiffness of the cushion core is determined by assigning the rigid connector with the prescribed displacement directly on top of the core wall. The axial stiffness for the both top plates is predicted by applying a displacement on top of the plate with the diameter of the hammer. The bottom of the plate is constrained in all directions at the area in contact with the cushion core. The results can be found in table 4.5, where the axial stiffness of the whole cushion is the stiffness that will be used to make the Conventional Cushion. To validate this data a stiffness test is performed on the cushion using a bench press, for which the methodology and the results are discussed in chapter 6.

Table 4.5: Prediction of the axial stiffness for the Meta Cushion and the resulting Conventional Cushion

	t_{wall} [mm]	$k_{axial,cushion}$ [kN/mm]	$k_{axial,core}$ [kN/mm]	$k_{axial,Top20mm}$ [kN/mm]	$k_{axial,Top10mm}$ [kN/mm]
Meta Cushion	-	595	2350	740	140
Conv. Cushion	12.65	605	2820	620	115

4.4. Non-Modular Conventional Cushion

The Conventional Cushion has the same axial stiffness and preferably the same mass as the Meta Cushion. The core of the cushion is changed, while the top plates and bottom part are kept the same as for the Meta Cushion. The core of the Conventional Cushion is a cylinder with an inner and outer diameter that should be determined. These dimensions have to meet the following requirements to fulfill the demand:

- the core should be aligned with the wall of the MP;
- the length of the cylinder should be the same as the core of the Meta Cushion;
- the stiffness of the conventional core should be the same as the core of the Meta Cushion;

An aluminium cylinder with an inside diameter of 280 mm was chosen, with a wall thickness of 15 mm. This wall thickness will be reduced to the desired thickness to meet the stiffness requirement.

Axial stiffness and internal stress and geometry

The stiffness of the core of the Conventional Cushion is determined via the same methodology as the Meta Cushion, while varying the outside diameter of the core. A wall thickness of 12.65 mm showed best result for the axial stiffness and is shown in table 4.5.

The internal Von Mises stress is also extracted from COMSOL® for the final cushion dimensions, and are shown in table 4.4 and figure 4.8. For both simulations, with the hammer perfectly centered and with an off set of 10 mm, the Von Mises stress in the cushion will not exceed the yield strength of 270 MPa.

The final dimensions of the cylinder used as the Conventional Cushion core are an inner diameter of 280 mm, a wall thickness of 12.65 mm and a length of 276 mm. The total cushion has a mass of 17.5 kg, which is lighter than the Meta Cushion. For this reason the non-modular Conventional Cushion meets the requirements set before:

- $D_{in,Conv}$ (280 mm) $<$ D_{MP} (295 mm) $<$ D_{Conv} (305.3 mm)
- $L_{core,Conv}$ (276 mm) $=$ $L_{Core,Meta}$ (276 mm)
- $k_{axial,cushion,Conv}$ (605 kN/mm) $\approx$ $k_{axial,cushion,Meta}$ (595 kN/mm)

5 Experimental Setup

Most components for the experimental setup were custom made. The production and assembly of those components, and building the experimental setup will be discussed in this chapter.

5.1. Monopile

The test MP was scaled down from a real size MP and simplified, as mentioned in section 3.3. The material used for the test MP is steel, ST52-3N, which comes in sheets with a thickness of 2 mm and a maximal length of 1500 mm. The MP was therefore constructed from two cylinders with an equal length of 1064.5 mm, which were rolled into a cylinder shape and welded with a seam weld to get an outside diameter of 295 mm, with a deviation of 1 mm. The two cylinders were then welded on top of each other with the vertical weld on opposite sides of the MP, resulting in a final MP length of 2129 mm, with a tolerance of 0.1 mm. During the experiments the MP was continuously exposed to water, for this reason the MP was protected from corrosion by applying a paint coating.

Sensors on monopile

As mentioned in section 3.6, the sensors in this experiment used on the pile are one accelerometer and two sets of strain gauges. These wall-motion sensors were attached to the outside wall of the MP, at a distance of 1.5 times the diameter from the tip of the pile.

The accelerometer was attached to the pile via a corner piece for which the accelerometer sensor is in a horizontal position, as shown in figure 5.1b indicated by the circled A. The ENDEVCO® 773-200-u accelerometer will measure the relatively low level of acceleration of the pile wall in three directions: the x-, y- and z-direction measure the acceleration of the pile wall in circumferential, radial and axial direction respectively as shown in figure 5.1c. When the sensor is subjected to a shock motion, it will generate a signal via unique variable capacitance micro-sensors. The accelerometer has a 200 g range, and operated with an applied voltage of 24 V. The accelerometer provides single-ended output with a 2.5 V output bias voltage.

The surface under the two sets of strain gauges is cleared of paint for better conductivity and the sensors are glued directly onto the pile wall, as shown in figure 5.1a indicated by the circled 1, and in figure 5.1b indicated by a circled 2. The strain gauges are used to measure mechanical strain, which refers to the deformation or change in shape of the MP wall under stress. As the MP undergoes deformation by the compression wave, the strain gauge's resistance changes proportionally to the level of strain being experienced. The output signal of the strain gauge is a voltage that is directly proportional to the amount of mechanical strain being applied to the MP. The sensors will operate by a 24 V power supply, which causes the sensors to heat during the experiments, and change the resistance over time. The sensors were calibrated each three test, to prevent an offset in the output data.

5.2. Cushions

The modular cushion consist of a top plate, a clamp and four arrays and will be discussed first. The non-modular Meta Cushion consist of two top plates a clamp and 12 arrays, and its Conventional cushion of a cylinder instead of the arrays.

Arrays

The nylon Meta Arrays were made using a laser sintering printing technique, and the other arrays for the modular and non-modular Meta Cushions were manufactured using watercutting with a tolerance of the waterlaser of 0.1 mm. Each array contains six resonators with the geometry shown in figure 4.1 and figure 4.5a, which was cut out of the array. The resonator is the most sensitive part of the manufacturing process, with the thickness of the beams as the most important factor for the frequency band gap, and was handled with the most precision. The waterjet will not start around the beams of the resonator, but at an angle of 45 degrees from the beam, visible in the picture in figure 4.5b.

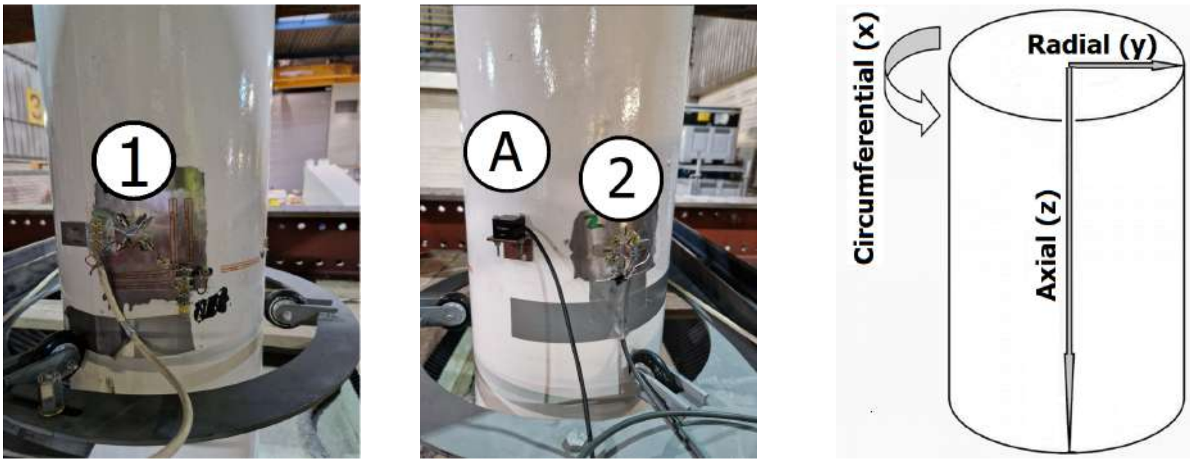

(a) The first set of strain gauges (indicated by 1) attached to one side of the MP

(b) The accelerometer (indicated by A) and strain gauges (indicated by 2) attached to the other side of the MP

(c) Directions of the wave propagation on the MP measured by the accelerometer

Figure 5.1: The sensors secured on the MP

The Conventional Arrays for the modular cushions were watercut from the same material with the same outside dimensions and tolerance as the Meta Arrays, after which the holes were extracted using a drill press. The arrays for the modular cushions are shown in figure 5.2, and the dimensions for these arrays are shown in table 5.1. The actual dimensions were used to recalculate the stiffness per array using the COMSOL® simulation, and the difference between the axial stiffness of the Meta Arrays compared to the stiffness of the Conventional Array was calculated and also expressed in the table.

The aluminium arrays for the non-modular Meta Cushion had a thickness of 20.4 mm, a length of 276 mm and a width of 82.7 mm. All beams were designed with a thickness of 1 mm, while the actual thickness of the beam varied from 0.53 mm up to 0.8 mm, as mentioned in section 4.3. The thickness of the array caused distortion in the shape of the resonator as shown in figure 4.5b, which should be taken into account during the discussion of the results from the impact test.

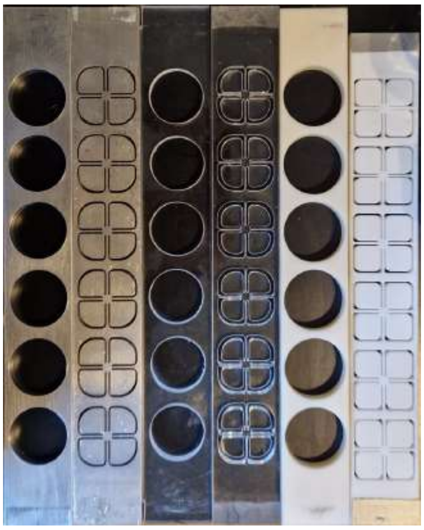

Figure 5.2: pictures of the arrays for the modular cushions: aluminium (left); acrylic (middle) and nylon (right)

Table 5.1: Actual dimensions of the arrays for the modular cushions with the new axial stiffness calculated via COMSOL®

Material	Aluminium	Acryl	Nylon
$L_{array,Meta}$ [mm]	380.5	381	381.5
$L_{array,Conv}$ [mm]	380.5	382	400.1
$W_{array,Meta}$ [mm]	50.4	50.2	50.2
$W_{array,Conv}$ [mm]	50.4	52.5	49.7
$t_{array,Meta}$ [mm]	10.2	10.2	9.7
$t_{array,Conv}$ [mm]	10.2	9.9	12.1
$t_{beam,Meta}$ [mm]	1.3-1.6	1.1-1.4	1.5-1.6
$D_{hole,Conv}$ [mm]	42	40	44.6
$k_{axial,Meta}$ [kN/mm]	20.607	1.134	0.466
$k_{axial,Conv}$ [kN/mm]	23.457	1.455	0.528
difference k_{axial} [%]	12	22	12

(a) The Meta Cushion core, showing the welds on the inside (b) Finished Meta Cushion (c) Finished Conventional Cushion

Figure 5.3: Pictures of the non-modular cushions

Modular Cushions
The top plate for the modular cushion is made from aluminium 6082 with an outside diameter of 325 mm with a tolerance of 0.1 mm and a thickness of 20.4 mm. The clamp on the bottom of the cushions consists of two cylindrical plates, as described in 4.2. The plates are made from the same aluminium, with the desired dimensions and attached on top of each other by two component adhesives for metal parts, with a strength of 220 kg/cm^2. The components were pressed together during the drying process of the glue by placing 100 kg weights on top of the parts. The slots for the arrays have a length of 50.7 mm, a width of 10.1 mm and a depth of 15 mm, which were made using a milling machine. The arrays were clamped in these slots during the experiments.

The nylon arrays had to be adjusted to fit into the slots: the Meta Arrays were too thin, therefore the thickness on the top and bottom of the array was increased using duct-tape; the thickness of the Conventional Arrays was too large to fit into the slots and were adjusted to the correct size on both ends.

Non-modular Cushions
A similar top plate and clamp were used for the two non-modular cushions (without the slots), but a thin top plate was added on top with a thickness of 10 mm. The two plates were placed on top of the core during the experiments, and were centred after each test.

The core of the non-modular Meta Cushion was formed by 12 arrays shaped in a do-decagon with a maximal width of 82.7 mm. The sides of the arrays were milled to make a 75 degree angle over the length, after which the arrays were welded to form the core of the Meta Cushion, as shown in figure 5.3a. The weld, when applied on the inside of the cushion core, tightens the core structure during the welding. The top and bottom of the core were then smoothed by a lathe machine, after which the clamp was attached to the core by two component adhesives for metal parts using the same methodology as for the clamp itself. Figure 5.3b shows the final result of the non-modular Meta Cushion.

The Conventional Cushion, shown in figure 5.3c, is made from the same aluminium as the other aluminium components. The cylinder forming the core originally had an inside diameter of 280 mm and a wall thickness of 15 mm. The wall thickness of this cylinder was reduced using a CNC turning lathe machine to an outside diameter of 305 mm with a tolerance of 0.1 mm. The inside diameter had a higher deviation, resulting in a wall thickness between 12.3 to 13 mm.

5.3. Small-scale impact test setup

The small scale impact pile driving test setup was built in the lab facilities of Huisman Equipment B.V. and is shown in figure 5.4 and 5.6. The setup consists of a steel tank with the dimensions: 6000 x 2440 x 1500 mm. On the tank walls sound absorbing foam was attached using double sided tape and glue to minimize the wall effect as shown in figure 5.4.

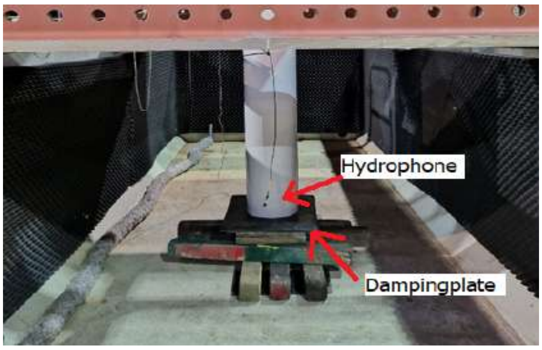

(a) Without sand

(b) With sand

Figure 5.4: The inside of the test tank used during the small-scale impact test setup before the water was added, with the hydrophone and the damping plate indicated in the left picutre

As mentioned in section 3.4, in the middle of the tank floor a rubber damping plate was installed to separate the MP from the tank bottom. In the middle of the tank floor two layers of three wooden beams with a height of around 100 mm were placed, with two steel tiles with a height of 50 mm on top of those beams. On top of this base the rubber damping plate was positioned, as shown in figure 5.4a. The damping plate consists of one bottom layer of a rubber granulate tile with a thickness of 24 mm with 4 SBR sheets with a thickness of 5 mm each glued on top of the tile. The total thickness of the damping plate is 45 mm. The total construction had a height of 345 mm, and formed the stand for the MP. The soil consists of four cubes regular filling sand, which was spread over the tank bottom, as shown in figure 5.4b. The sand height was measured randomly and a height of 280 mm with a deviation of 20 mm was reached.

The MP was placed in the middle of the tank, on top of the damping plate, with the cushion clamped on top. During off-shore pile driving of MPs a gripper puts the MP in the correct position and keeps it in that position during the installation. To keep the MP in vertical position in the small-scale test a gripper was formed by two circular parts connected by a hinge on one side and a lock on the other side. The gripper is shown in the picture in figure 5.1a, and was installed just below the sensors on the MP as shown in figure 5.6a. On the inside three soft wheels were connected to allow the MP to move in axial direction. The wheels contain a small spring that although they constrained the MP in radial direction, they did not interfere with the pressure wave in the pile wall.

Frame construction

Around the tank a construction was build to hold among other things the hammer mechanism. The base of this frame consists of two blocks on each of the tank sides as shown in the back in figure 5.6a, forming a tower. These towers hold two beams crossing the tank on each side of the MP, shown in the bottom corners of the picture. On these beams a third beam was placed to hold the MP gripper in the correct position. On top of the towers a platform was created across the tank. That platform was raised by a block on each side of the MP, and holds the top beam to which the hammer drop mechanism is attached, as visible in the top of the picture in figure 5.6a.

Hammer drop mechanism

The pivot hammer used during the impact tests on the modular cushions was attached to the frame construction, as shown in figure 5.5. The hammer was constrained by a vertical beam for the same initial position, which placed the hammer in a 95° angle compared to the horizon. When the hammer was released from its initial position, it made an impact on the cushion ending in a horizontal position with a deviation of 1.5° varying per cushion.

As mentioned in section 3.5, the impact during the test on the non-modular cushions was done by a drop weight impact hammer. This hammer should hit the centre of the cushion each test, therefore the ram was attached to a guide rail, as shown in figure 5.6a. This rail was attached to the top beam and to the platform to be kept in vertical position. The ram is attached to the rail by four wheels keeping the ram of the hammer in line with the rail and therefore also vertical, as shown in figure 5.6b. An electric winch, also attached to the top beam, was used to lift the ram to the correct height for each test. The

(a) Hammer in vertical position

(b) Hammer in horizontal position

Figure 5.5: The pivot impact hammer used during the tests on the modular cushions

cable of the winch was connected to the ram by a quick release connector to drop the ram when the right impact height was reached. The MP was centered under the ram of the hammer by adjusting the gripper position.

Instrumentation
The hydrophone, TC4013, was placed in the water at the positions indicated in figure 3.1. The position of the hydrophone needed to be changeable in between tests and was attached to a beam crossing the tank using a clip. The beam could be moved to different distances from the pile wall and the clip allowed for varying the depth of the hydrophone in the water.

The movement of the resonators during the impact tests were recorded using a high-speed camera and a stroboscope (with the yellow band), which was attached to the platform above the tank, as shown in the bottom right corner of figure 5.6b.

(a) Picture for the total setup

(b) Close up of the hammer and the high-speed camera (bottom right)

Figure 5.6: The small-scale impact test setup for this research

6 Stiffness test

The stiffness of the Meta Cushion and its Conventional Cushion should be the same to be able to draw conclusions for the meta-material. Both non-modular cushions were tested in a bench press from Mammuth, the SP50HAL, at the test facilities of Huisman Equipment B.V. only the non-modular cushions was tested on its stiffness since the arrays of the modular cushion were to fragile to be tested in this test setup. During the stiffness test, the force was evenly distributed over the whole cushion top, as shown in figure 6.1. This test determined the stiffness of the cushion core as the bending of the top plate is not accounted for. During the actual impact test the axial force is only in the middle of the plate with a hammer diameter of 140 mm, which would reduce the stiffness of the cushion.

Methodology stiffness test cushion core
As shown in the picture in figure 6.1, the cushion was placed on top of a squared steel plate with a thickness of 50 mm and a width of 350 mm, which was aligned to the middle of the test setup with a precision of 1 mm. In the middle of the plate a stand was connected via a magnet, with a distance sensor attached to it, over which the cushion was placed and aligned to the middle of the plate. This way the sensor measured the axial displacement of the bottom of the top plate during the tests. A second plate was placed on top of the cushion to distribute the force of the bench press over the top of the cushion and it was aligned to the centre. This plate had the same dimensions as the bottom plate and had a mass of 52 kg. In the middle of this steel plate a cylindrical press with a diameter of 100 mm pushed to deliver a force.

The test started by building up the pressure on the cushion top via a foot paddle controlling a cylindrical press till a pressure of 350 bar. This pressure was checked via the barometer on top of the bench. The pressure was dropped in steps by manually releasing the air from the press via a plunger, visible in the graph in figure 6.2. The test was finished when the pressure dropped under one bar.

During the tests, the bench press delivers a pressure in bar, which was measured via an analogical barometer on top of the bench press, and via a pressure sensor attached to the foot paddle. This second sensor delivered the input data for the tests, in combination with the distance sensor inside the cushion providing the data for the displacement of the top plate.

Both sensors have a sample frequency of 5 Hz. The distance sensor was set to 0 mm when the pressure is 0 bar. The force in kN was calculated via the following formula:

$$F = 0.78P, \tag{6.1}$$

with the pressure, P, in bar. This formula takes the mass of the steel plate on top of the cushion into account.

The data of the force under 10 kN was not taken into account because of the large variation in data from the distance sensor. The test was repeated at least 4 times for both cushions.

Results stiffness cushion core
The axial force-displacement curve created by the data from all tests is shown in figure 6.3a. The stiffness is calculated by dividing the axial force by the displacement and is shown in the box plots in figure 6.3b.

The stiffness of the Meta Cushion core is 680 kN/mm and for the Conventional Cushion core it is 830 kN/mm, while the predicted stiffness was 2350 kN/mm and 2820 kN/mm respectively. In the stiffness prediction the top plates were not considered, which could reduce the predicted stiffness. The gap between the two top plates could also influence the stiffness calculation. While the predicted stiffness and the stiffness from the tests are not the same, the ratio between the stiffness of the Meta Cushion core and the Conventional Cushion core are around the same value. The box plot also shows a wide variation of outliers which could indicate the measurements did not reach the linear region yet.

Figure 6.1: The bench press stiffness test setup to determine the stiffness of the non-modular cushions, shown with the Meta Cushion

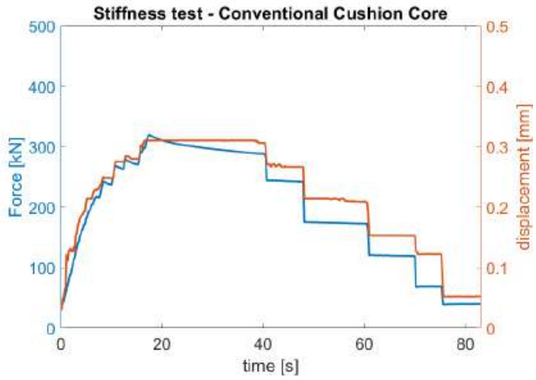

Figure 6.2: Graph of the axial force (blue) and the displacement (red) plot over time to determine the axial stiffness of the non-modular cushions via a bench press stiffness test

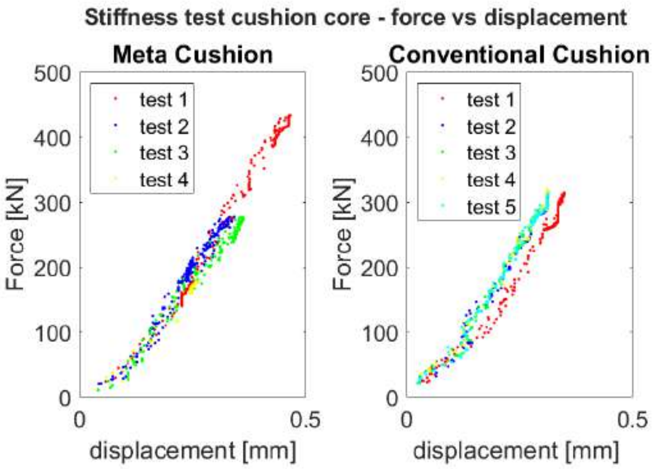

(a) The axial force applied on the top of the cushion plot as a function of the displacement of the top plate. The results for the Meta Cushion on the left, and the results for the Conventional Cushion on the right, with different colours to indicate the different test repetitions

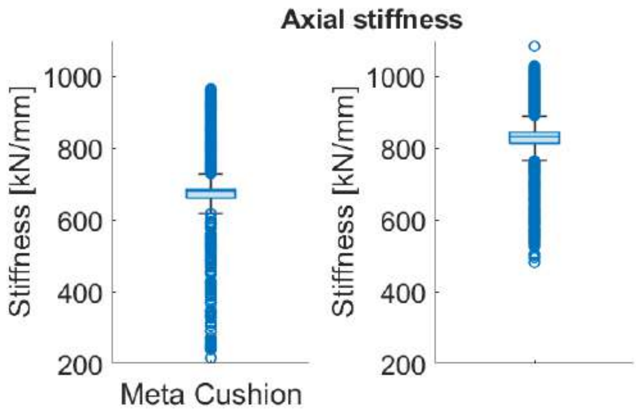

(b) Box plot of the axial stiffness of the Meta Cushion (left) and the Conventional Cushion (right), with a mean value of 680 kN/mm and 830 kN/mm, respectively

Figure 6.3: Results for the bench press stiffness test on the Meta Cushion core and the Conventional Cushion core

Stiffness damping plate
Under the pile a damping plate was added. The stiffness of this plate was also determined using the bench press. The damping plate was made out of rubber, which is hard to simulate in COMSOL®. The damping plate would have to withstand a peak force of around 45 kN, and consists of one bottom layer of a rubber granulate tile with a thickness of 24 mm and 4 layers of SBR rubber sheets with a thickness of 5 mm each glued on top of the tile. The total thickness of the damping plate is 45 mm.

The test setup is shown in figure 6.4. The steel tile used at the bottom of the stiffness test of the cushions was kept in place. On top of that, the damping plate was placed in the middle but turned 45 degrees in radial direction. Next to the damping plate a digital dial indicator gauge was connected to the steel plate by its magnetic base. On top of the damping plate a thin walled steel cylinder with the same thickness and diameter as the MP was set in the middle. And on top of that cylinder a steel cylindrical plate with a diameter of 301 mm was centered.

The stiffness of the steel cylinder and plates were assumed to be infinite compared to the stiffness of the rubber damping plate. The dial indicator was set to 0 before each test, and the data was read off of it during the tests. During the actual impact test a peak force of 45 kN will act on the damping plate, this impact takes only a few milliseconds. The stiffness tests were done with a force up to 2 kN, with the assumption that the damping plate acts as a linear spring. Via a foot paddle the pressure on the cylindrical press was built to a pressure of around 25 bar with steps of around 5 bar. The pressure was checked via the barometer on top of the bench. During the tests, the bench press delivers a pressure in bar. The pressure was converted to the axial force with formula 6.1. The stiffness results for the damping plate are shown in table 6.1

Figure 6.4: The bench press stiffness test setup to calculate the stiffness of the damping plate

Table 6.1: Results of the stiffness tests for the damping plate

Force [kN]	Displacement [mm]	Stiffness [kN/mm]
5.06	2.66	1.90
7.40	4.06	1.82
9.74	6.03	1.62
15.20	9.30	1.63
19.10	12.0	1.60

7 Data Analysis

This chapter will show and discuss the impact test methodology and the analysis of the data from the sensors. During the impact test the data of all sensors is logged, and will be processed using MATLAB®.

7.1. Small-scale impact test methodology

For the small-scale impact test on the modular cushions, the cushion is assembled with the correct arrays and placed on top of the MP. The hammer is placed in a vertical position and the stain gauges are calibrated, after which the experiment could start. The hammer is constrained by a vertical beam to obtain the same starting position each test. When released, the hammer will pivot and hit the middle of the top plate of the cushion. This test was repeated 10 times for each composition, after which the arrays of the cushion were changed, resulting in a total of 60 tests. The data from the accelerometer, the stain gauges and hydrophone logged the impact measurements for all tests, and the strain gauges were calibrated to a zero off-set between every three tests, when necessary.

For the tests on the non-modular cushions, the correct cushion was clamped on top of the MP. The data for the strain gauges were calibrated while the hammer was detached from the cushion and MP, after which the hammer was placed on top of the cushion to calibrate the position sensor. The data for all sensors was logged from the moment the hammer had been lifted to the impact position. The hammer was lifted to the right height above the cushion manually with an electrical winch. The height was directly indicated by the position sensor next to the hammer rail, and the lifting tolerance was 1 mm around the desired lifting height. The hammer was then released by pulling a cord attached to the quick release connector and made an impact on the cushion and MP. The hammer was reattached to the winch and lifted 50 mm to re-centre the top plates on the cushion, each three tests the vertical position of the MP was reset and the hydrophone was relocated if necessary. The test was executed with the hydrophone on nine different locations, repeated three times, resulting in 54 tests in total in this second test round.

The test results were analysed and the setup was changed to reduce the excessive movement of the MP, after which both cushions were tested again. This test round the hydrophone was kept in one location and the test was repeated ten times for each cushion, totalling 20 tests for test round three.

7.2. Data arrival

The data available from each test was:

- data from the hydrophone measuring the sound pressure expressed in Pascal;
- data from the accelerometer measuring the wall acceleration in circumferential-, radial- and axial-direction in m/s^2;
- data from strain gauge 1 measuring the pressure wave through the wall in voltage;
- data from strain gauge 2 measuring the pressure wave through the wall in voltage;
- data from the position sensor measuring the height of the hammer in millimeters;

The data from strain gauge 2 was too sensitive to changes in the surrounding temperature and are left out of consideration for the results.

The data from the sensors were measured with a sampling frequency of 20 kHz. The data of the hydrophone can be changed from voltage to pascal by dividing the data with the receiving sensitivity of $2.81838\ 10^{-5}$ V/Pa for this hydrophone. The sound pressure wave takes time to reach the hydrophone and therefore the moment of impact at that sensor depends on the distance of the hydrophone from the pile.

The data in the time domain is shown in figure 7.1, where the signal of the hydrophone and the sensors on the MP are plotted for the first 3 milliseconds to look at the signal arrival times, with the moment the accelerometer detects the impact pressure wave taken as start. The data for the strain

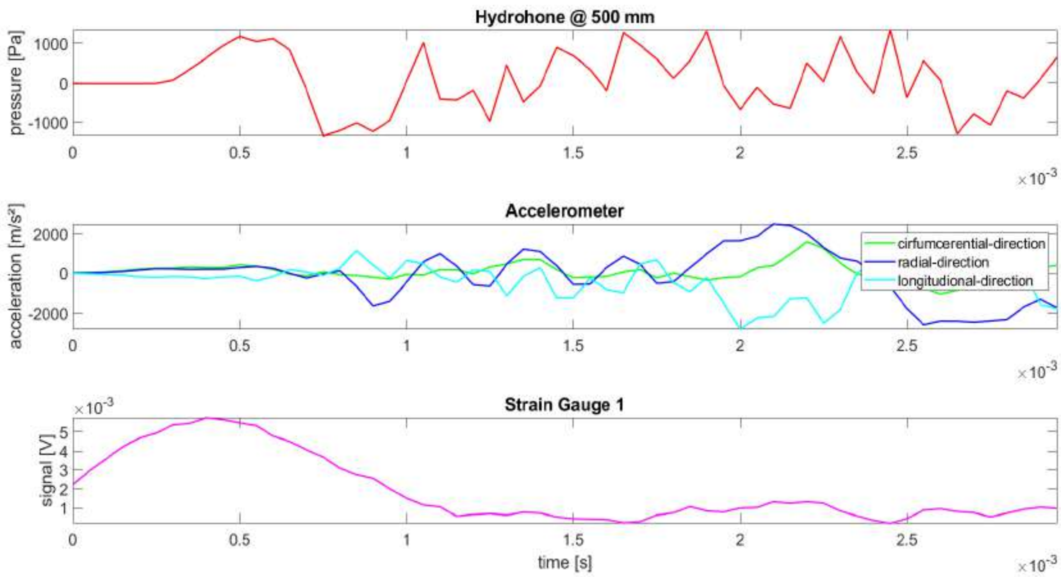

Figure 7.1: Signal arrival for the sensors on the MP and the hydrophone at a distance of 500 mm. The signals are plot for 3 ms from the moment of impact to show the different arrival time depending on the distance from the MP wall

gauge has the same data arrival time as the accelerometer as shown in the figure 7.1 as expected since they are placed on the same height on the MP wall. The delay in the hydrophone signal arrival is clearly visible in the plots in figure 7.2 for the hydrophone at a distance of 500 mm, 1000 mm and 2000 mm from the MP wall, respectively. The speed of sound in water is 1500 m/s, and the distances of the hydrophone are 500; 1000; and 2000 mm. This results in a time difference between the sensors on the pile and the hydrophone of 0.33 ms; 0.67 ms and 1.3 ms respectively, which corresponds with the data in the plots. This delay was taken into account when processing the data.

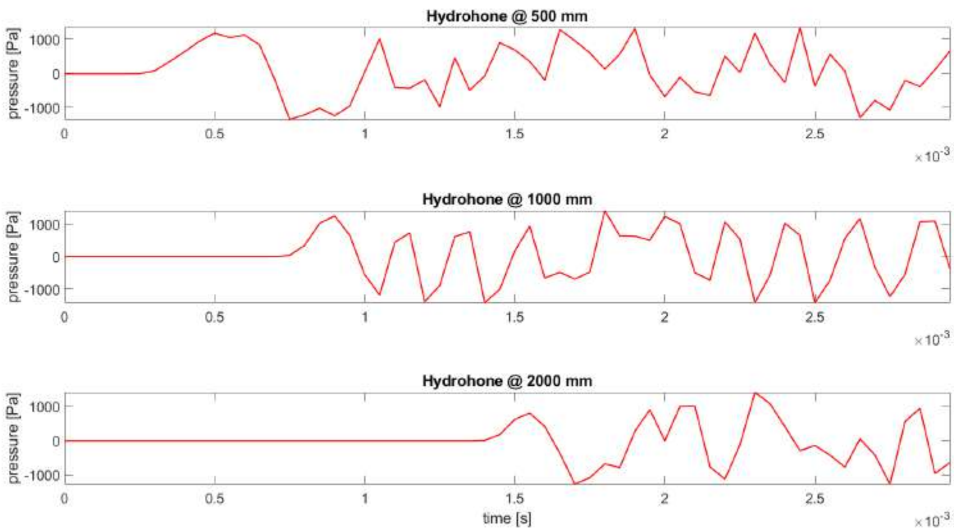

Figure 7.2: Signal arrival for the hydrophones at different distances from the MP wall. The signals are plot for 3 ms from the moment of impact detected by the accelerometer to show the different arrival time depending on the distance from the MP wall

Position sensor

The data from the position sensor was also compared to the signal arrival of the Strain Gauge, as shown in figure 7.3. In this figure the data from the strain gauge is plot by a purple curve and the data from the position sensor is plot by a black curve for 25 ms after the sensors on the MP detect the impact. The hammer shows a delay of 20 ms after the impact detected by the sensors on the pile. This delay was caused by a filter inside the position sensor and was taken into account when processing the data. The signal for the hammer was processed using the measurements from 300 ms before the impact until the moment the hammer changed directions, indicating the maximal displacement of the cushion, MP and damping plate.

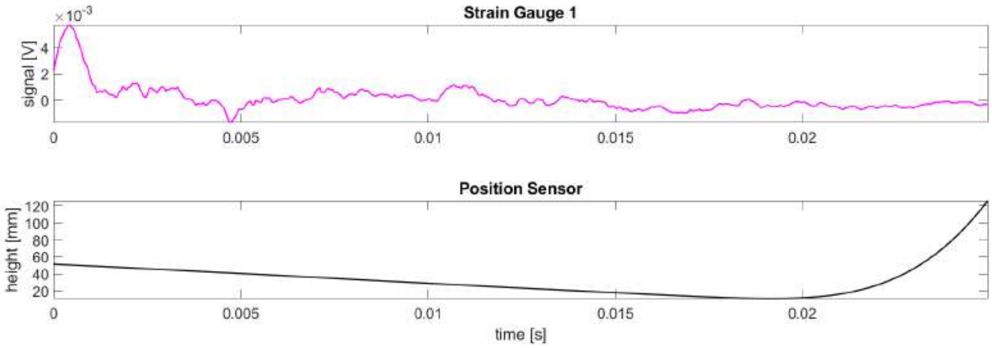

Figure 7.3: Signal arrival for the strain gauge (top) and the position sensor (bottom). The signals are plot for 25 ms from the moment of impact, detected by the accelerometer, to show the delay in the signal arrival of the position sensor

8 Results and Discussion

The results for the small-scale impact test are shown and discussed in this chapter. Prior to the test the background noise and the eigenfrequencies of the tank and MP are determined, after which the impact pile driving tests took place. The functionality of the meta-material was assessed with the modular Meta Cushions during the first test round using the pivot hammer. Next the small-scale impact test setup was assessed using the drop weight impact hammer on the non-modular cushions causing higher internal stresses. During this second test round the MP experienced a backlash from the damping plate, therefore the granulate rubber tile was removed, after which a third test round was done with the same two non-modular cushions and hammer.

8.1. Prior testing

Before the impact tests took place the background noise in the tank and the eigenfrequencies of the tank and MP were determined. For the results of these tests the data from all sensors, except from the position sensor, are transformed to the frequency domain with the methodology described in section 3.8.

Background noise

The test environment produced background noise during the tests, which was measured with the hydrophone before each impact. For these tests the hydrophone was placed 500 mm from the pile wall, at a depth of 500 mm under the water level and 1220 mm from the nearest tank side. A data from the last test round was used with a time duration of 70 ms, to keep the same frequency resolution as for the impact tests using the drop weight hammer. The results are shown in figure 8.1, for the frequencies from 0 to 3000 Hz, since only this low-frequency domain is of interest for this research. The hydrophone shows a peak in the SPL around 1850 Hz, for which the cause could not be determined. This peak would not affect the results for the TL of the Meta Cushions, but should be taken into account when designing and testing future Meta Cushions. The LS for the strain gauges and accelerometer in all directions was also plot for the background noise, and did not show any peak values.

eigenfrequencies monopile

The eigenfrequencies of the MP were extracted using the hydrophone, placed 1000 mm from the pile wall at a depth of 500 mm. The MP was placed in vertical position, without the cushion on top of it. The pile was hit by a synthetic hammer, while the sensors on the pile wall and the hydrophone in the test tank measured the impact results. For the first test round, a thin aluminium plate was placed on top of the pile and was hit manually in the middle of the plate with the hammer. At the second test round, the aluminium plate was removed and the MP was hit on the pile wall around the MP tip.

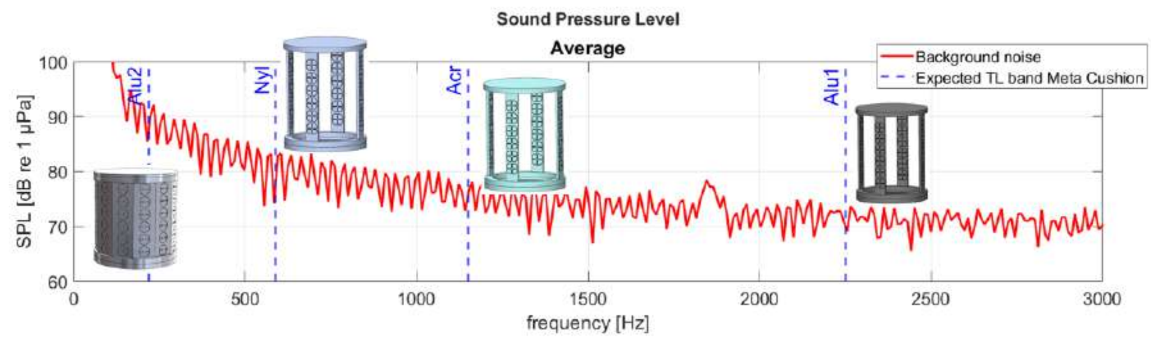

Figure 8.1: Sound Pressure Level for the background noise in the frequency domain from 0 Hz to 3000 Hz, with the expected TL frequencies for the Meta Cushions indicated by vertical blue dashed lines

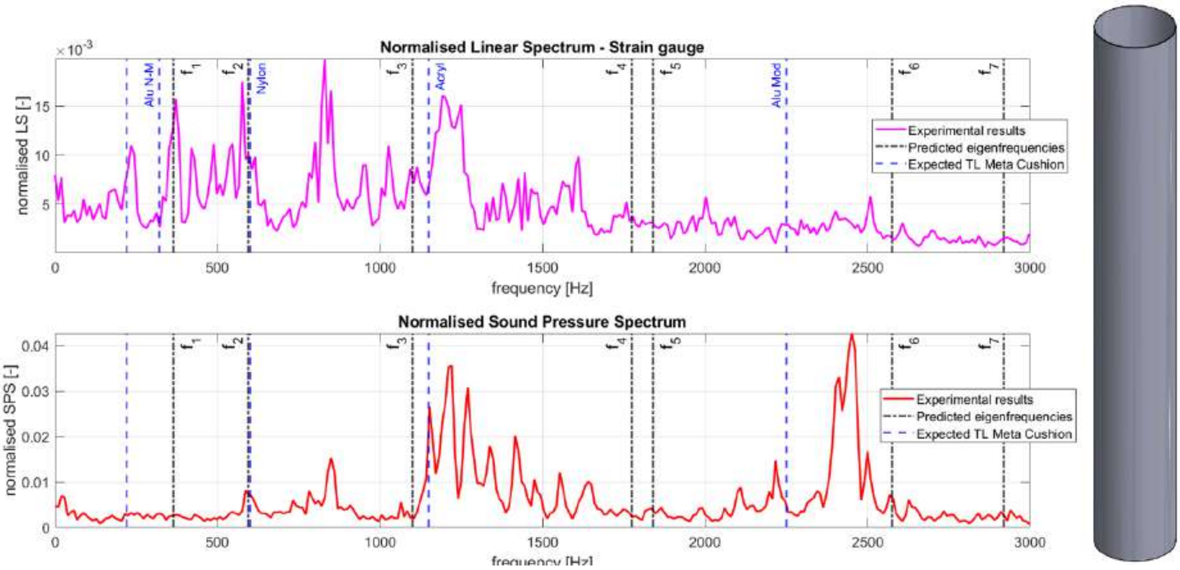

Figure 8.2: The eigenfrequencies of the MP visualised by the normalised LS of the strain gauges on the pile wall (top) and the normalised SPS measured by the hydrophone (bottom) with the predicted eigenfrequencies of the monopile indicated by the dashed vertical black lines. The vertical blue dashed lines indicate the designed TL frequencies of the Meta Cushions

During the last test round, the MP was hit on the top of the pile wall (without the plate). The data from the strain gauges and hydrophone were first normalised, by dividing it with its maximum value to eliminate the variation in hammer impact, after which the normalised LS and SPS were calculated.

The average results from the experiments are plot in figure 8.2, with the predicted eigenfrequencies from table 3.1 indicated by vertical black dashed lines and the expected TL frequencies of the Meta Cushions indicated by vertical blue dashed lines. The peaks in the graph for the normalised LS of the strain gauges and the normalised SPS indicate a high vibration of the pile wall which could be an eigenfrequency of the MP. The peaks in the two plots should be compared with each other, to reduce the influences from noise.

The prediction of the eigenfrequencies was done for a MP surrounded by air, while the MP in the test setup is partly submerged in water. The water level will cause reflection of the internal stress wave traveling trough the MP, and the water itself will act as a damper on those stress waves affecting the eigenfrequencies. The prediction of the eigenfrequencies of a MP partly submerged in water should be improved when used as input values for the design of the Meta Cushions. The peak values shown in the plots from figure 8.2 can be used for the design of new Meta Cushions for the small-scale impact test.

The vertical blue lines indicate the expected TL frequencies of the Meta Arrays determined with the FRF-experiments. The aluminium non-modular Meta Cushion will have a TL around 250 Hz at which the strain gauges show a clear peak. This peak is not visible in the SPS of the hydrophone, so the results are expected to be most visible in the plots from the strain gauges. The nylon arrays from the modular Meta Cushions is designed for the second eigenfrequency of the MP and this eigenfrequency is clearly visible in both plots, therefore it is expected to show a clear TL measured by both sensors. The acrylic arrays are expected to show a TL around a frequency of 1150 Hz, where the SPS shows a peak. The aluminium modular cushions is expected to show a TL around a frequency of 2250 Hz, which occurs around a high peak value in the results from the hydrophone in the plot. The strain gauges do not show reliable results after a frequency of 1750 Hz, therefore will not be used for the results of the aluminium modular cushion.

eigenfrequencies tank
The eigenfrequencies of the tank were also predictedt before the experiments, with the hydrophone at the same position as previous test and the strain gauges. The tank was hit on different places of the tank wall, while the hydrophone measured peaks in the sound pressure waves caused by the eigenfrequencies of the tank. The data from the hydrophone was again first normalised to eliminate the variation in hammer impact, after which the normalised SPS was calculated. The median of the tests

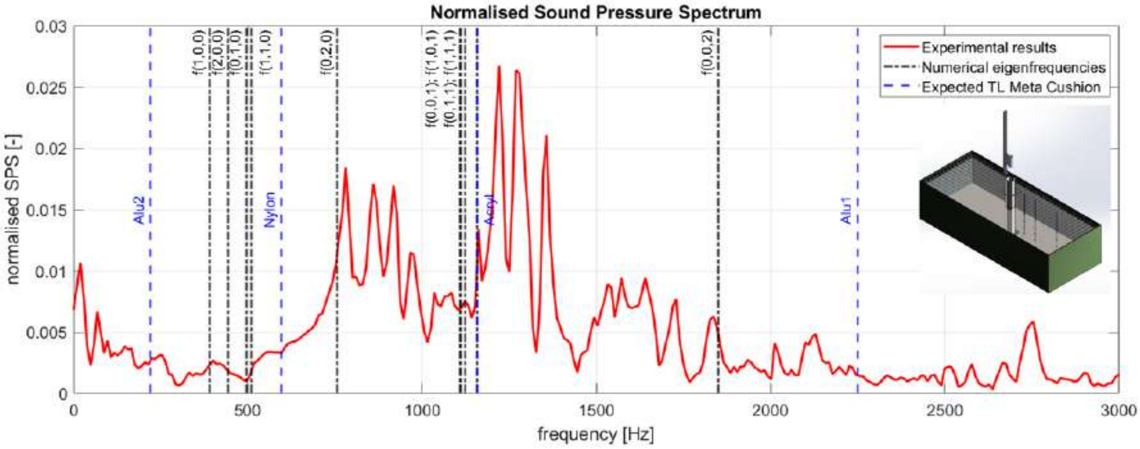

Figure 8.3: Average normalised Sound Pressure Spectrum showing the eigenfrequency of the test tank with a black curve, and the predicted eigenfrequencies of the test tank indicated by the dotted vertical lines. The vertical blue dotted lines indicate the designed TL frequencies of the Meta Cushions

data is plot by the black solid curve in the graph in figure 8.3, with the predicted eigenfrequencies from table 3.2 indicated by the dashed vertical lines. The vertical blue dashed lines indicate the designed TL frequencies of the Meta Cushions.

The predicted eigenfrequencies are not clearly visible in the test results and are probably damped by the sound absorbing foam and the layer of soil. The eigenfrequencies f(0,2,0) at 757 Hz and f(0,0,2) at 1850 Hz are the predicted eigenfrequencies of the tank visible in the plot, but these values are not around the expected TL band gaps of the cushions. The expected TL for the acrylic modular Meta Cushion and the eigenfrequencies f(0,1,1) and f(1,1,1) of the tank interfere with each other, which should be taken into account when discussing these cushion results.

The MP was already in the tank during the eigenfrequency determination, therefore these eigenfrequencies of the MP could also be showing in this plot. The results for both test are therefore plot in one graph shown in figure 8.4, were the results for the MP are plot in a red solid curve and the results for the eigenfrequency determination of the tank are plot in a black dashed line. The TL KPIs for the Meta Cushions are again indicated by blue vertical dashed lines. Both plots show a peak value around the TL frequency of the acrylic modular Meta Cushion, which could mean the peak value is a result from the eigenfrequency of the MP.

8.2. Modular Meta Cushion

The functionality of the meta-material was assessed with the modular Meta Cushions with a small-scale impact test using a pivot hammer. The hammer was assumed to deliver the same impact energy throughout the entire test round on all cushions. The data from the hydrophone, the accelerometer and the strain gauges were taken for a time window of 30 ms after the sensor measured the impact, which results in a frequency resolution of 20 Hz for the results in the frequency domain.

First the SPL and the SEL in the time domain are compared for both cushions, after which the data was transformed into the frequency spectrum and again compared per cushion type. In each graph in the frequency domain the results for the conventional Cushion are plot in solid red, the Meta Cushion is plot is solid blue, and the expected TL frequencies of the Meta Arrays determined with the FRF-experiments is indicated by blue vertical dashed lines.

Pivot hammer impact energy

The impact energy of the impact hammer was assumed to be constant throughout all experiments, and was not determined. However, the frequency spectrum of the impact hammer was clearly visible during the experiments in the LS from the accelerometers shown in figure 8.5. These are the results for the tests on the aluminium modular cushion, and shown a clear peak from 1000 Hz to 1250 Hz. This spectrum could interfere with the results of the acrylic Meta Cushion, and should be taken into account.

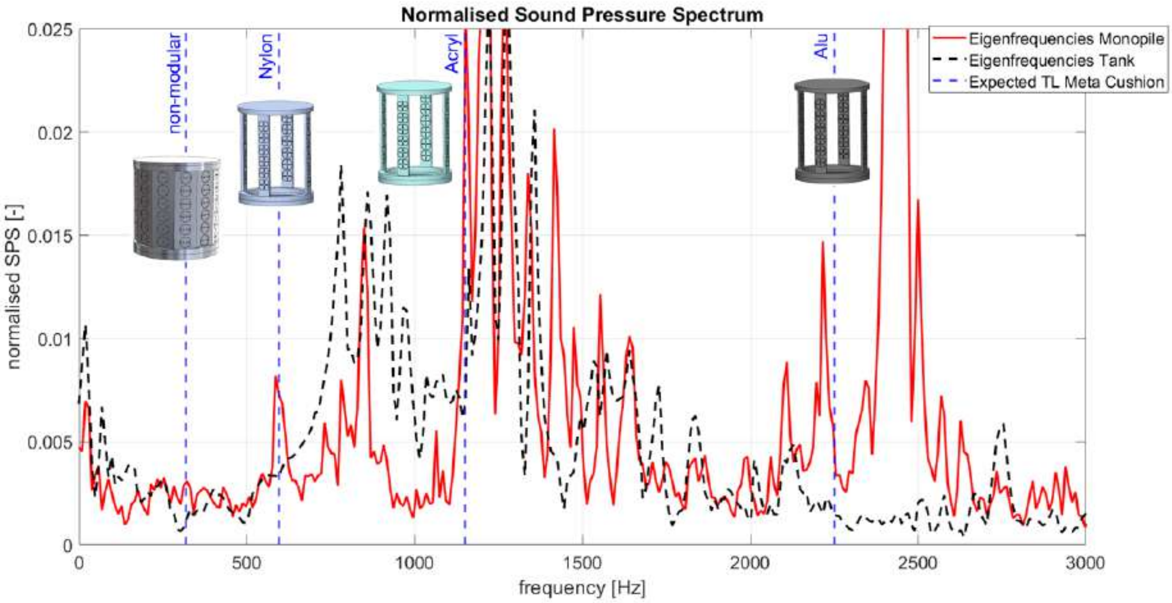

Figure 8.4: Average normalised Sound Pressure Spectrum showing the eigenfrequency of the test tank with a red curve; the predicted eigenfrequencies of the test tank indicated by the vertical black dashed lines; and the vertical blue dashed lines indicate the designed TL frequencies of the Meta Cushions

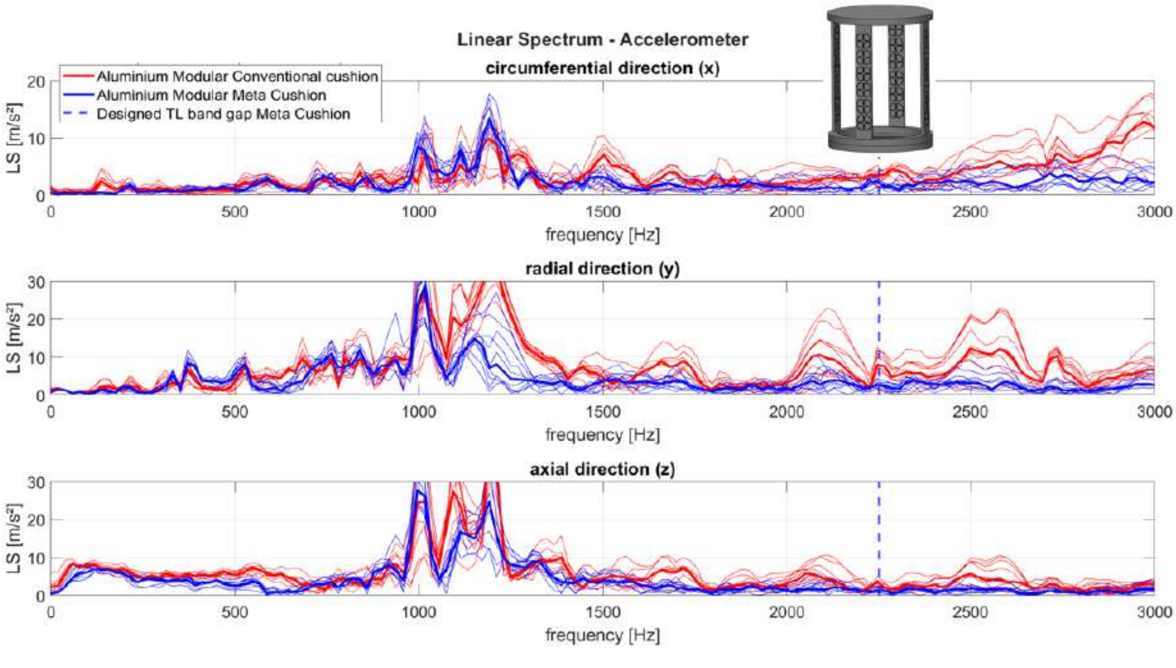

Figure 8.5: Results from the accelerometer for the tests on the aluminium modular Meta Cushion plot from 0 Hz to 3000 Hz, clearly showing the impact hammer frequency between 1000 Hz and 1250 Hz

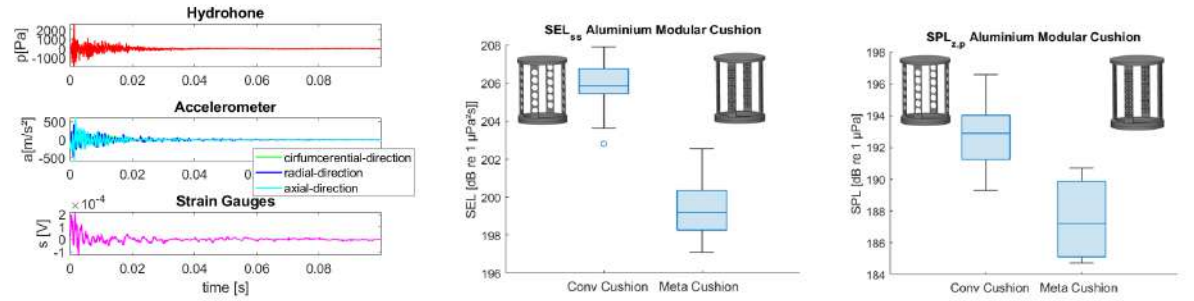

(a) data from the three different sensors plot for 100 ms from one single test

(b) Boxplot for the SEL_{ss} in the time domain for all test on for both cushions

(c) Boxplot for the $SPL_{z,p}$ in the time domain for all test on for both cushions

Figure 8.6: Results for the aluminium modular cushions in the time domain

Aluminium Meta Cushion

The data from the sensors for one of the tests with the aluminium modular Meta Cushion are plot in figure 8.6a for 100 ms. When the aluminium arrays are clamped properly in the top and bottom part of the modular cushion, it results in a clear impact measured by all sensors without any additional noise from a backlash of the hammer or pile, as shown in the plots.

From the signal of the hydrophone the SEL_{ss} and the $SPL_{z,p}$ were calculated for all tests, with the equation 3.17 and A.7, respectively, and shown in a boxplot in figures 8.6b and 8.6c. The mean SEL_{ss} for the Conventional Cushion is 206 dB (re $1\mu Pa^2s$) and for the Meta Cushion its 199 dB (re $1\mu Pa^2s$) for all tests, which indicates an attenuation of 7 dB (re $1\mu Pa^2s$) for the this Meta Cushion. The same difference is obtained in the $SPL_{z,p}$ with 193 dB (re $1\mu Pa$) versus 187 dB (re $1\mu Pa$) for the Conventional Cushion and the Meta Cushion respectively, which is a attenuation of 6 dB by the Meta Cushion. The meta cushion has a lower stiffness compared to the Conventional Cushion, which could also be the reason for the attenuation in the noise levels.

This Meta Cushion was expected to show a TL at the frequency band gap around 2250 Hz. The results from the hydrophone are plot in figure 8.7a from 0 Hz to 3000 Hz, where the top plot shows the results for all tests and the bottom plot in the figure shows the average of the tests for both cushions. The sound pressure waves during the tests on the Conventional Cushion occur in a narrow band width for the tests, which mean the repeatability of the tests was of high quality. The sound pressure waves during the tests with the Meta Cushion showed the same precision till a frequency of 1100 Hz, after which the behaviour of the pressure waves scattered more. The SPL from both cushions have the same value until this frequency after which the Meta Cushion shows lower SPLs throughout the rest of the shown frequency spectrum. The equal SPLs in the low frequency domain could mean the difference in stiffness had not much influence.

The graphs also show clear TL around a frequency of 1950 Hz and around 2200 Hz, where an attenuation of 15 dB and 10 dB is shown respectively via a trough in the Meta Cushion results. The data from the strain gauges did not show consistent results for both cushions in this high frequency range, and is therefore not used.

The results from the accelerometer in the frequency domain are shown in figure 8.7c, where the LS for all three directions is plot from 1500 Hz to 3000, showing a TL around a frequency of 2200 Hz clearly visible in the radial and axial direction. Around a frequency of 1950 Hz no clear TL is shown, however the displacements at that frequency is too small to clearly state a result. There should be more research done in future studies with an higher impact to get clearer results.

Acrylic Modular Meta Cushion

The data from the sensors for the acrylic modular cushions are plot in figure 8.8a for 100 ms. The cushion had a lower mass compared to the aluminium one, causing a clear visible second impact from the impact hammer bouncing back, as shown in the signal. This distortion was cut off, since the data was only processed for a time window of 30 ms.

The SEL_{ss} and the $SPL_{z,p}$ were calculated for the results of these tests and plot into boxplots visible in figure 8.8b and 8.8c. The Meta Cushion again showed some attenuation in the noise levels compared

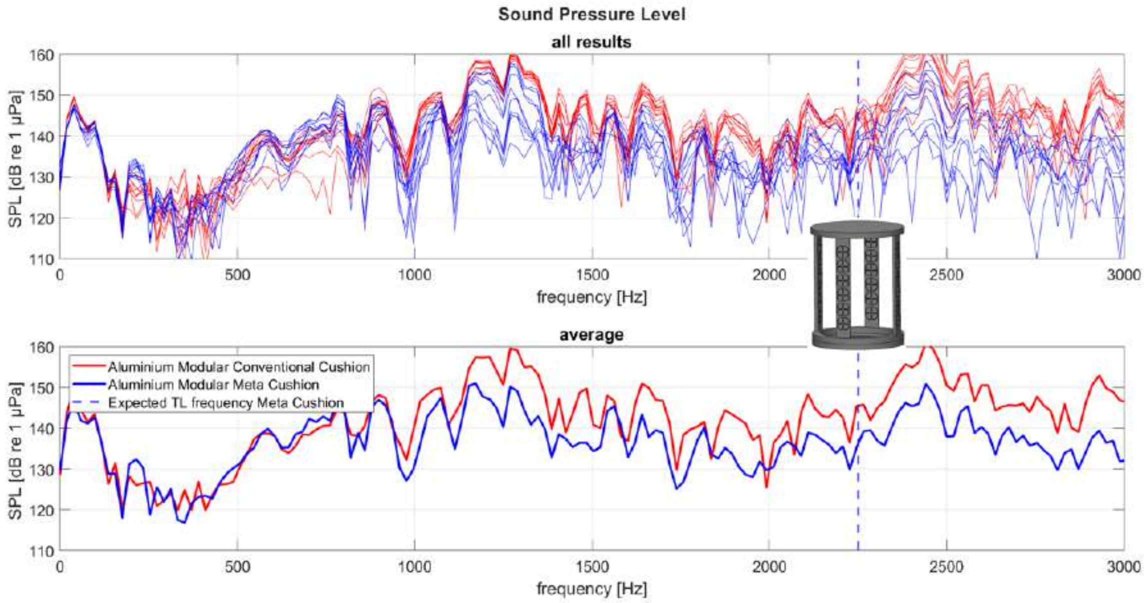

(a) the SPL for all tests in the top graph and the average SPL per cushion plot in the bottom graph

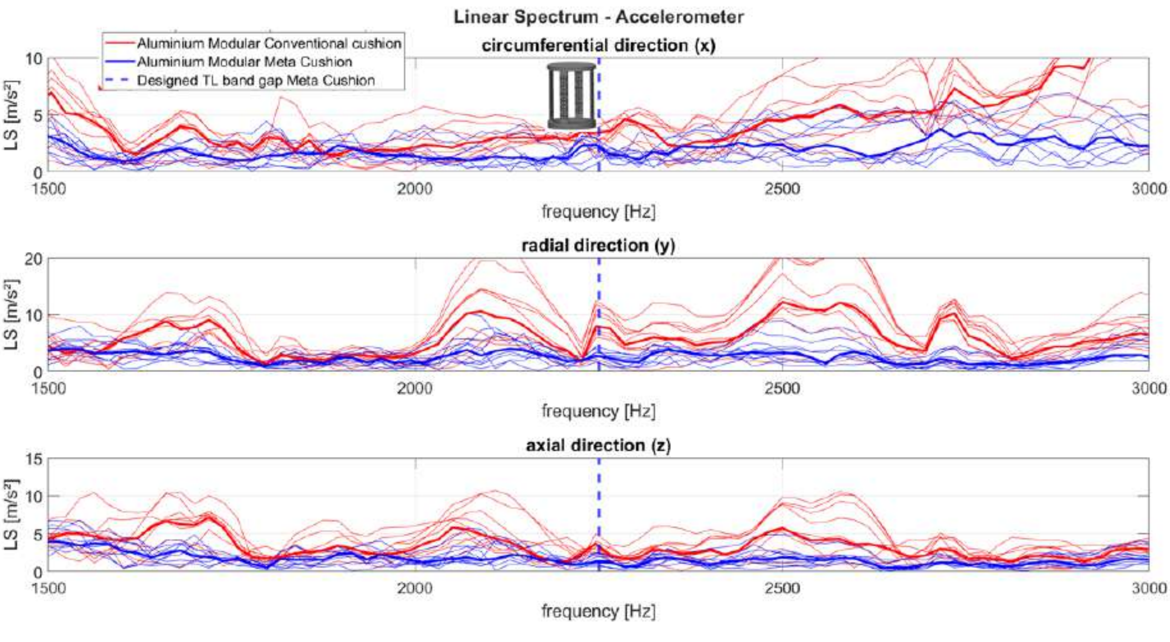

(b) from 1500 Hz to 3000 Hz

(c) LS of the Accelerometer, with the results for all tests and its average per cushion plot in one graph per direction

Figure 8.7: Results in the frequency domain for the aluminium modular cushions. The solid red curves indicate the Conventional Cushion and solid blue the Meta Cushion, the expected TL frequency (2250 Hz) is indicated with a blue dashed vertical line

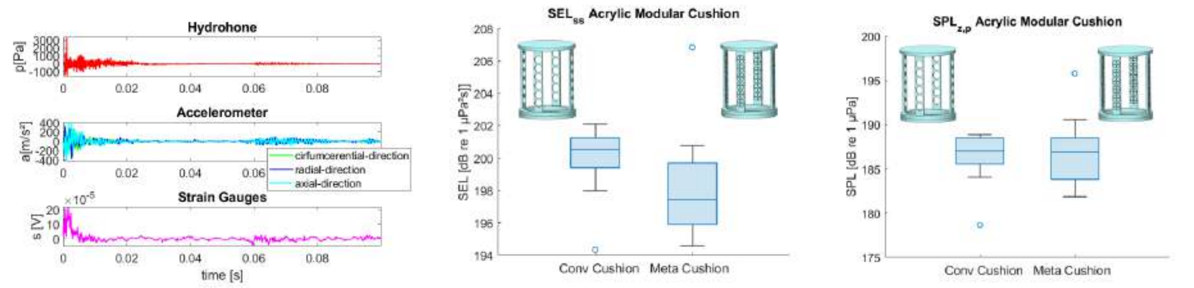

(a) Data from the three different sensors plot for 100 ms from one single test

(b) Boxplot for the SEL_{ss} in the time domain for all test on for both cushions

(c) Boxplot for the $SPS_{z,p}$ in the time domain for all test on for both cushions

Figure 8.8: Results for the Acrylic modular cushions in the time domain

to its Conventional Cushion. The SEL_{ss} for this Conventional Cushion was 200 dB (re 1 $\mu Pa^2 s$), and was 3 dB lower for the Meta Cushion. The average $SPL_{z,p}$ was 187 dB (re 1 μPa) for both cushions.

The Meta Cushion had again a lower stiffness of 22 % compared to the Conventional Cushion, which could also be the reason for the attenuation in the noise levels.

The acrylic modular cushion shows a TL at the frequency around the expected frequency of 1150 Hz, shown in the results from the strain gauges and the results for the radial and axial acceleration of the pile wall, in figure 8.9a and 8.9b, respectively. The SPL does not show a TL at this frequency, which could be caused by the eigenfrequencies of the tank which were expected to interfere with the TL frequencies of this cushion. The expected attenuation in the frequency domain cannot be determined for this cushion, the expected TL frequency, however, is shown in the results.

Nylon Modular Meta Cushion

The SEL_{ss} of the Nylon Conventional Cushion was 194 dB (re 1 $\mu Pa^2 s$), and the $SPL_{z,p}$ was 180 dB (re 1 μPa), while for the nylon Meta Cushion these values were 191 dB (re 1 $\mu Pa^2 s$) and 173 dB (re 1 μPa) for the SEL_{ss} and the $SPL_{z,p}$, respectively. Again for both cushions the resulting SEL_{ss} and $SPL_{z,p}$ are plot in boxplots which can be seen in figure 8.10b and 8.10c respectively.

The size of the nylon arrays were different than that of the other arrays. The length of the Meta Arrays were smaller, because of which a larger impact from the impact hammer was received by this Meta Cushion, they also had to be adjusted to increase its thickness. The Conventional Arrays had to be adjusted to decrease its thickness to fit into the top and bottom part of the cushion. After these adjustments the Meta Cushion experienced large movements during the tests, influencing the results, as shown in figure 8.10a by the second impact detection. The second impact occasionally caused a higher pressure wave compared to the first pressure wave, but was still cut off for the signals used in the frequency domain.

The meta PUCs were designed for a TL around 592 Hz, around this frequency the Meta Cushion showed an increase in the SPL and in the pile wall movement, detected by the strain gauges and accelerometer, shown by the plots in figure 8.11. The results form the strain gauges are shown in the top graph in figure 8.11a, where the Meta Cushion shows peak values compared to its Conventional Cushion around 350 Hz and 500 Hz, where this last frequency peak is also shown in the results from the FRF-test.

Around a frequency of 760 Hz a TL is visible in the LS from the strain gauges and in the LS of the accelerometer in circumferential and axial direction. This could be caused by the design of the Meta PUC, but should be investigated in future research by inspecting the movement of the unit cell during the impact test. The same behaviour can be seen around a frequency of 1100 Hz, which is shown by the strain gauges but not clearly visible in the SPL since there is already a trough around that frequency. The new test should be more aware of the influence of the stiffness of the Meta Arrays compared to the Conventional Arrays, and more care should be taken during the manufacturing of the outside dimensions of the arrays, since the difference in height caused a difference in impact energy during the tests of this cushion. The behaviour of the PUC during the impact tests should also be logged using a high speed camera, to determine its frequency movement.

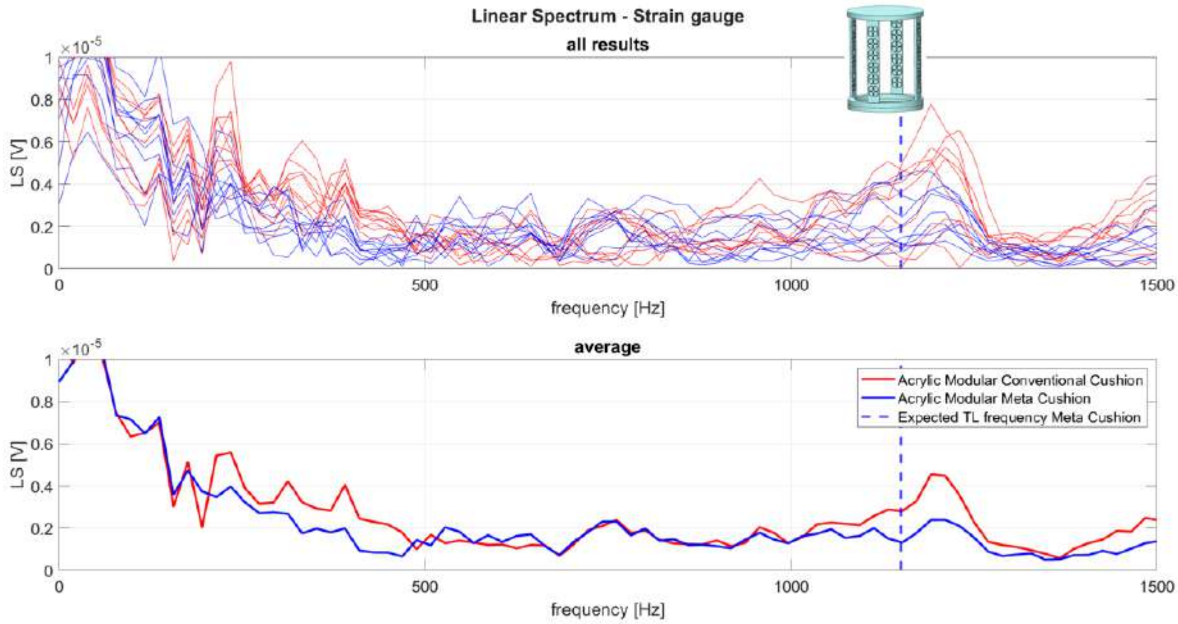

(a) LS of the Strain gauges, with the results for all tests in the top graph and the average per cushion plot in the bottom graph

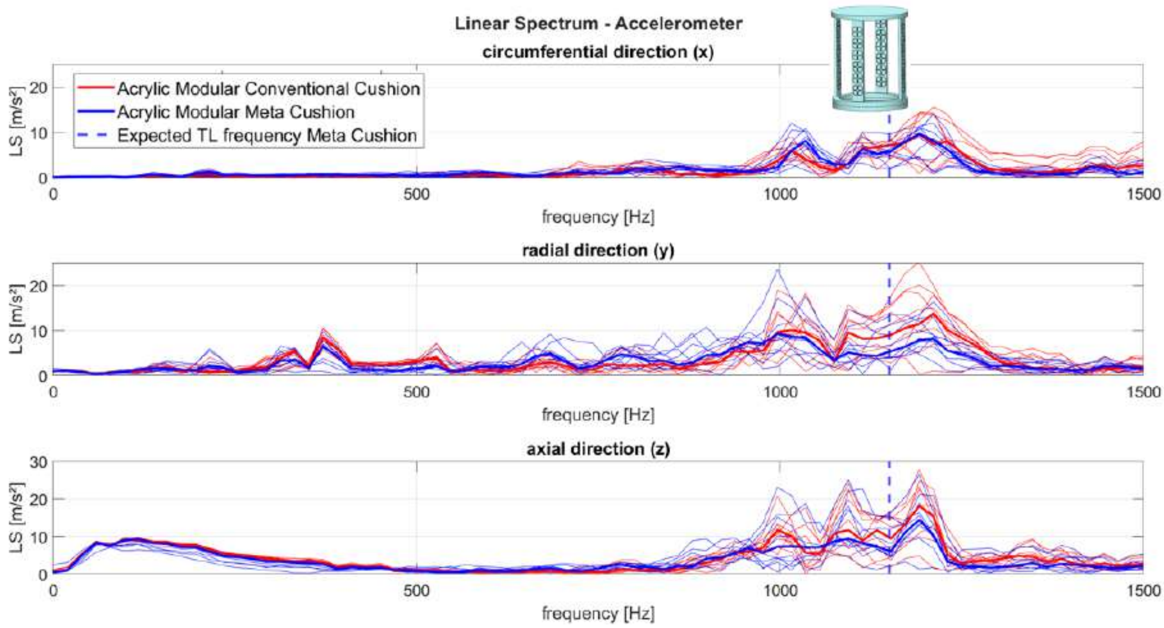

(b) LS of the Accelerometer, with the results for all tests and its average per cushion plot in one graph per direction

Figure 8.9: Results in the frequency domain for the acrylic modular cushions. The solid red curves indicate the Conventional Cushion and solid blue the Meta Cushion, the expected TL frequency (1150 Hz) is indicated with a blue dashed vertical line

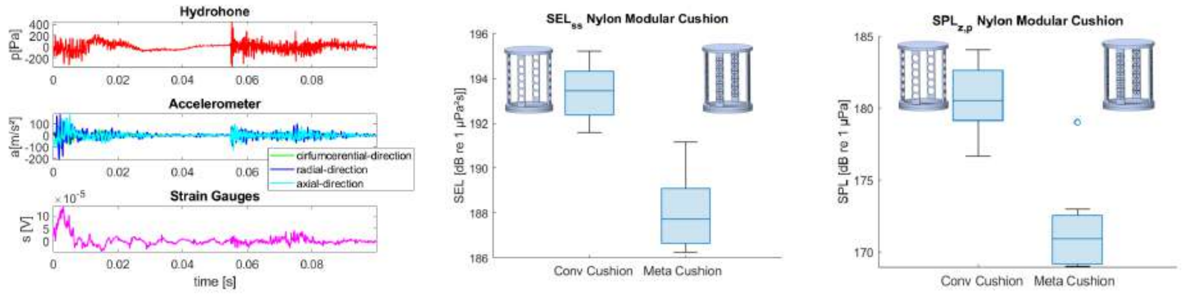

(a) Data from the three different sensors plot for 100 ms from one single test

(b) Boxplot for the SEL_{ss} in the time domain for all test on for both cushions

(c) Boxplot for the $SPS_{z,p}$ in the time domain for all test on for both cushions

Figure 8.10: Results for the Nylon modular cushions in the time domain

8.3. Non-modular Cushion

The non-modular cushion was tested with a higher impact force using the drop weight impact hammer described in section 3.5. The effectiveness of the small-scale impact test setup was assessed during these experiments. During this second test round the MP experienced a backlash from the damping plate, therefore the granulate rubber tile was removed, after which a third test round was executed on the same two non-modular cushions. The data from the hydrophone, accelerometer and the strain gauges were taken for a time window of 70 ms after the sensor detected the impact and the hammer impact was taken for a time window of 300 ms before it detected the impact, as shown in figure 8.12. This time window results in a frequency resolution of 10 Hz for the results in the frequency domain.

Hammer Impact Energy

To calculate the impact velocity of the hammer the time derivative was taken from the data of the position sensor during the free fall. The velocity just before impact, the highest value, was then used to calculate the kinetic energy at the moment of impact. The impact energy during all experiments for both cushions, during the first test round had the same impact energy with a mean value of 124 J, the deviation during the tests on the Meta Cushion was larger, as shown in the boxplot of figure 8.13. After the test setup was changed, the impact energy was again determined and shown in the box plots in figure 8.14. The mean value for the tests on the Conventional Cushion was 138 J with a standard deviation of 10 J and for the tests on the Meta Cushion the mean value was 134 J with a standard deviation of 7 J.

The drop height of the impact hammer had a small variation in height, which could mean the deviation in impact energy is caused by inaccuracy of the position sensor. The data is therefore not normalized by the impact energy.

Assessment experimental setup

To asses the repeatability of the small-scale test setup, the data from the strain gauges on the MP were used. The Linear Spectrum for the data from the strain gauges is determined using formula 3.32. During the second round of experiments with the proposed test setup the MP experienced a large reaction force from the damping plate. The impact energy during the first test round was too small to cause this reaction. The backlash changed the MP position and for each third test the MP had to be reset to the vertical position.

The data from the tests with the original damping plate is shown in the top graph in figure 8.17. The graph shows a large deviation in the results, which indicates a low repeatability of the experiments. The backlash of the MP was also visualised by the high-speed camera, which recorded the movement of the resonators during the impact, the recorded frame is shown in figure 8.16. The camera showed that the resonators were not vibrating in the same phase or frequency.

The damping plate was replaced by four layers of SBR (without the rubber granulate tile), and a third test round was executed. During the third test round the MP stayed in the same vertical position, and the PUCs moved in the same frequency recorded by the high speed camera. The LS for the strain gauges with the new damping plate is visualised in bottom graph in figure 8.17. The repeatability of the

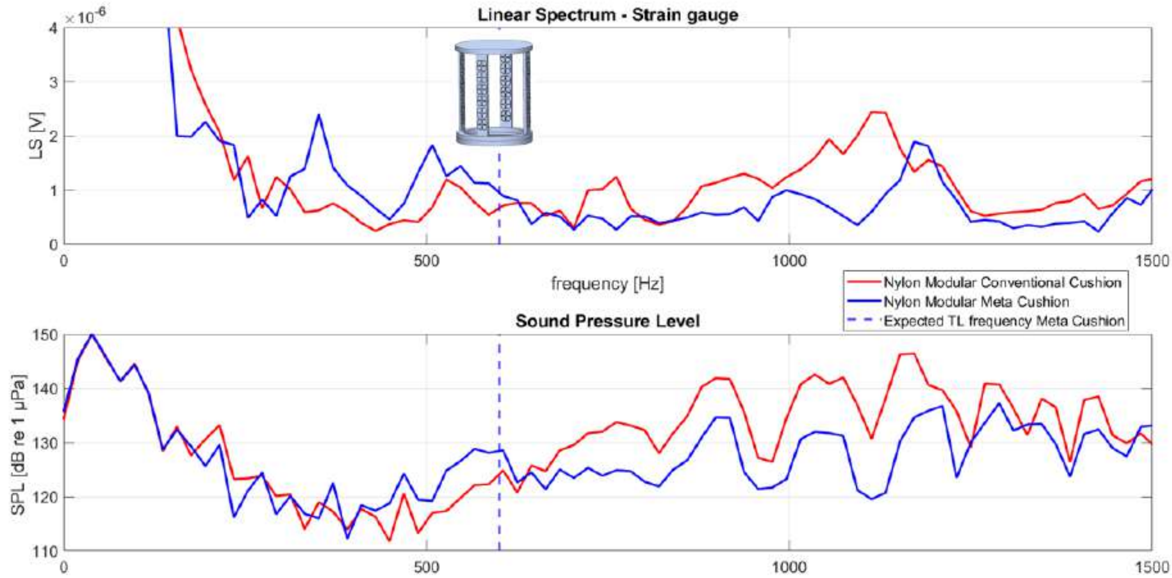

(a) Average LS of the Strain gauges in the top graph and the average SPL plot in the bottom graph for both cushions

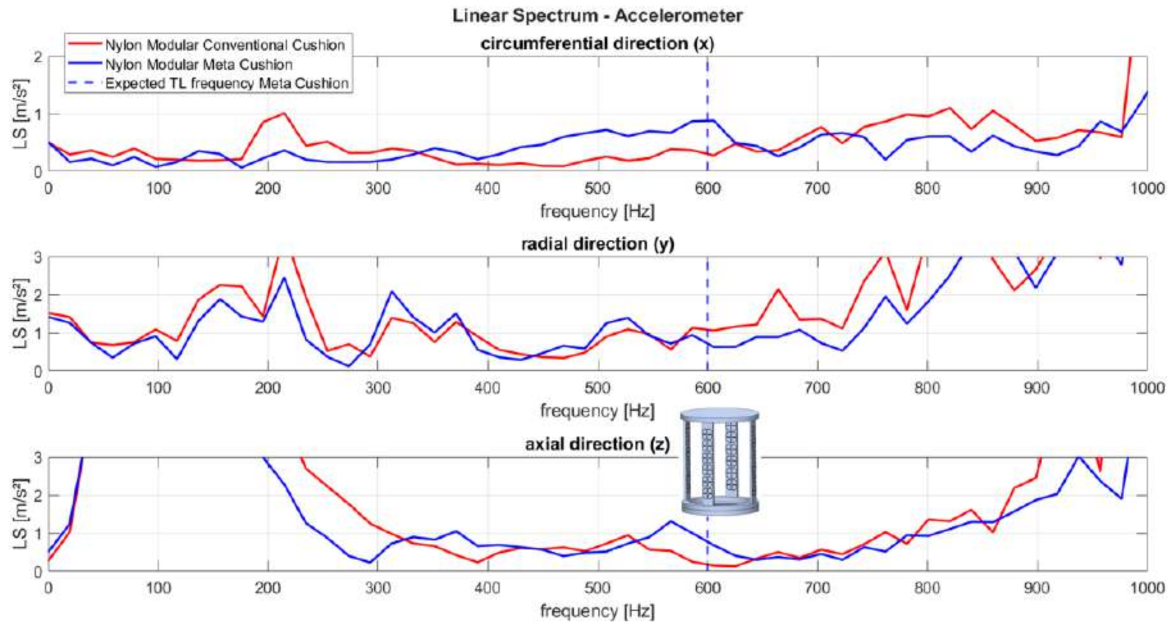

(b) Average LS of the Accelerometer plot for both cushions in one graph per direction

Figure 8.11: Results in the frequency domain for the nylon modular cushions. The solid red curves indicate the Conventional Cushion and solid blue the Meta Cushion, the expected TL frequency (600 Hz) is indicated with a blue dashed vertical line

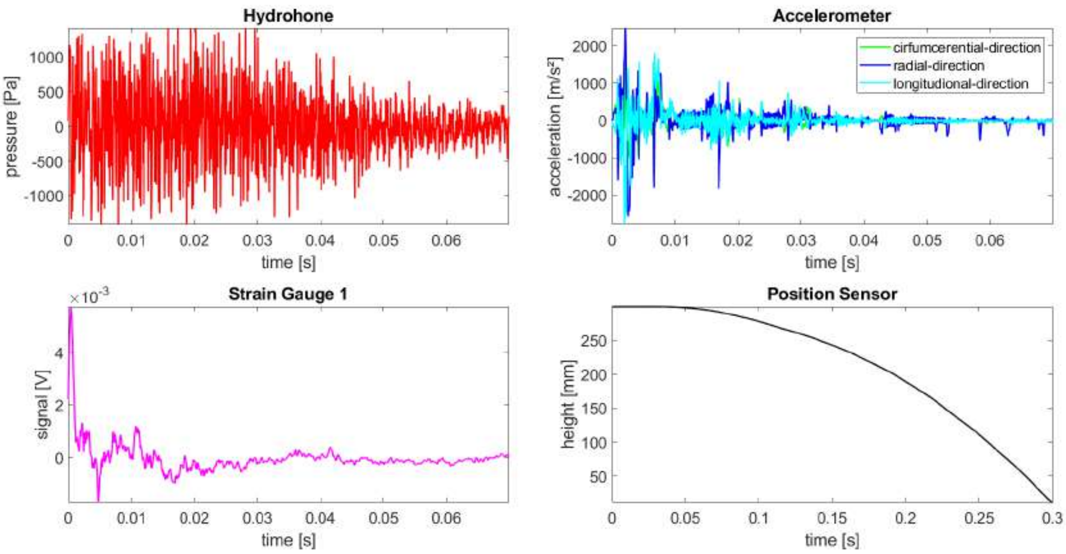

Figure 8.12: The data from the sensors in the time domain for one of the tests on the non-modular cushion used to process the results: the sound pressure measurements by the hydrophone shown in the top left; the acceleration of the MP wall plot in the top right; the strain gauges data shown in the left bottom left; and the height of the hammer above the cushion in the bottom right

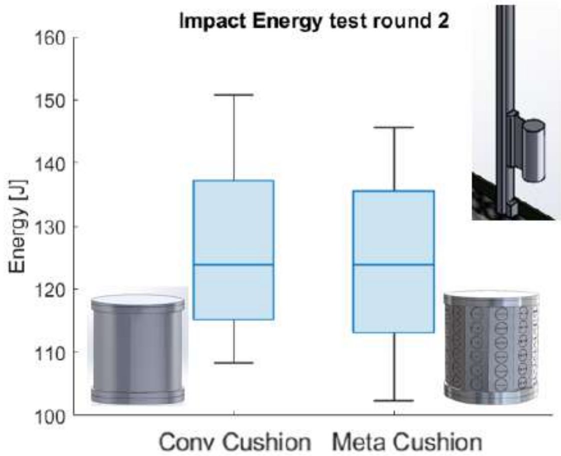

Figure 8.13: Impact energy for the second test round

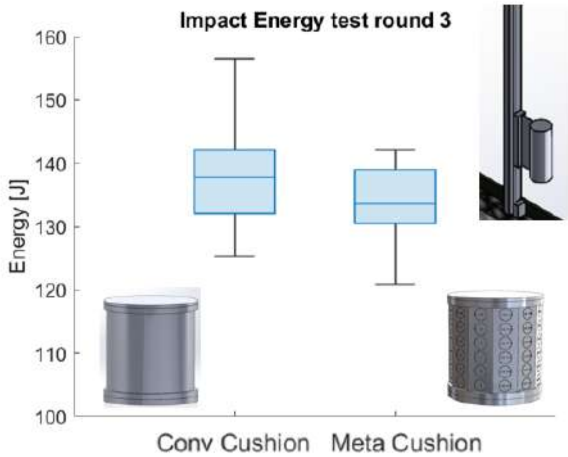

Figure 8.14: Impact energy for the third test round

Figure 8.15: Box plot for the impact energy determined from the position sensor for tests on the non-modular cushions

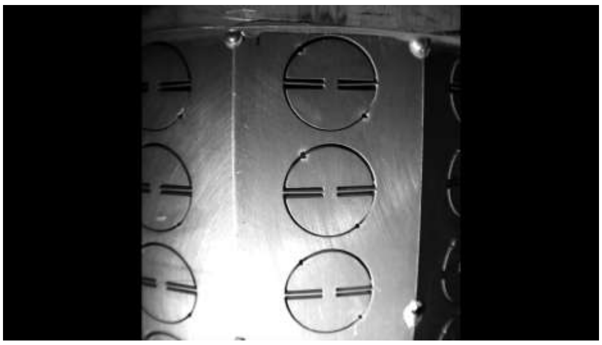

Figure 8.16: Screenshot of the high-speed camera

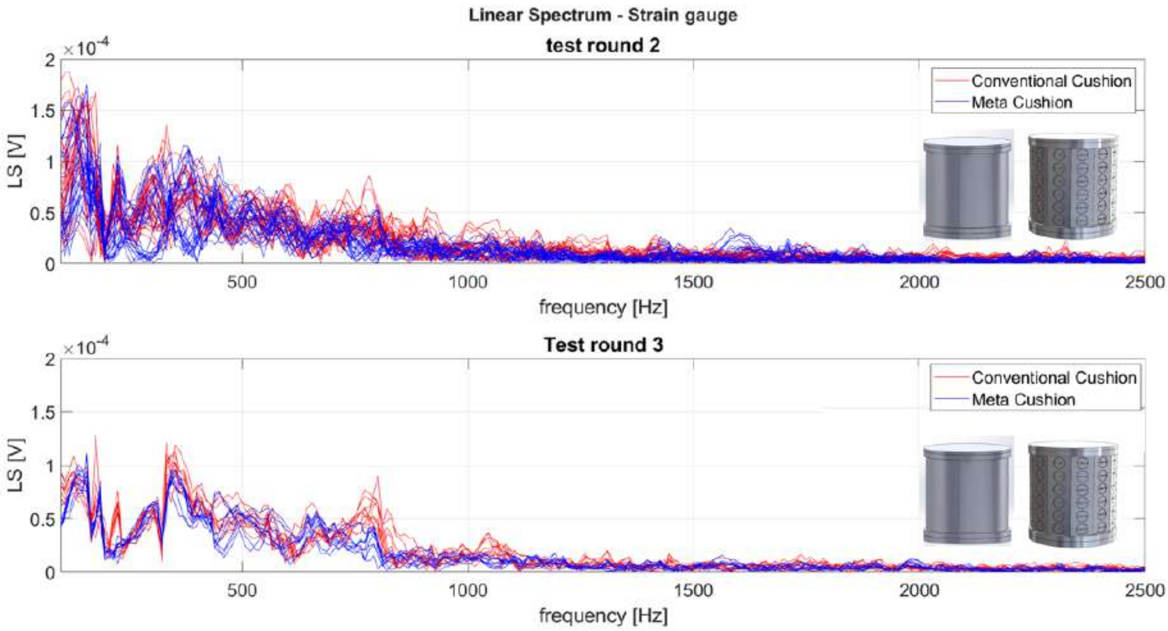

Figure 8.17: Linear Spectrum of strain gauge on the MP before and after improvement

test was improved as the deviation in the results for both cushions decreased, with a standard deviation of the last test round of 10 %. The spectrum of the Meta Cushion and the Conventional Cushion in the frequency domain follow the same pattern, except for the frequency around 220 Hz. Around that frequency range the curve of the Conventional Cushion shows a peak, while the Meta Cushion shows a TL trough caused by the resonators in the Meta Cushion.

Hydrophone location

During the second test round, the hydrophone was placed at three different distances from the MP wall and at three different depths, totalling nine different locations in the test tank. When the distance from the pile wall is increased, the curves show a lot of noise in the low-frequency range. The most optimal position of the nine positions is determined by comparing the data of the tests with the Conventional Cushion, since the out of phase vibrating of the resonators in the first test setup created even more disturbance in the data besides the extra movement of the pile. The results for the tests with the hydrophone at 500 mm and 2000 mm are shown in figure 8.18. The hydrophone shows less deviation between the tests when the hydrophone is closer to the pile for the frequencies above 300 Hz. Future experiments are recommended to measure the sound pressure no further than 500 mm from the MP wall.

The best depth of the hydrophone is determined using the data from the Conventional Cushion at all distances shown in different plots for each depth in figure 8.19. The hydrophone in the middle of the water level, at 500 mm shows the best result. The bottom of the tank reflects waves and causes noise in the signal for the hydrophone at 750 mm depth. The hydrophone at 250 mm depth gets similar reflection waves from the water surface. The depth of the hydrophone should be tested more in future research to determine the influence. For now, the hydrophone in the middle of the water depth is recommended during future research.

Aluminium Non-modular Cushion

The functionality of the non-modular Meta Cushion was tested during the third test round with the changed damping plate and the hydrophone placed on the determined location 500 mm from the MP wall and at a depth of 500 mm. The SEL_{ss} and the $SPL_{z,p}$ were the same for both cushions in the time domain, with an SEL of 206 dB (re 1 μPa^{2}s) and a SPL of 183 dB (re 1 μPa). The TL was expected around the frequencies around 220 Hz for this Meta Cushion. The LS of the strain gauges show a dent for the Meta Cushion around 220 Hz as already shown in figure 8.20. At the frequency around 320 Hz the Conventional Cushion shows a better result compared to the Meta Cushion, which corresponds to

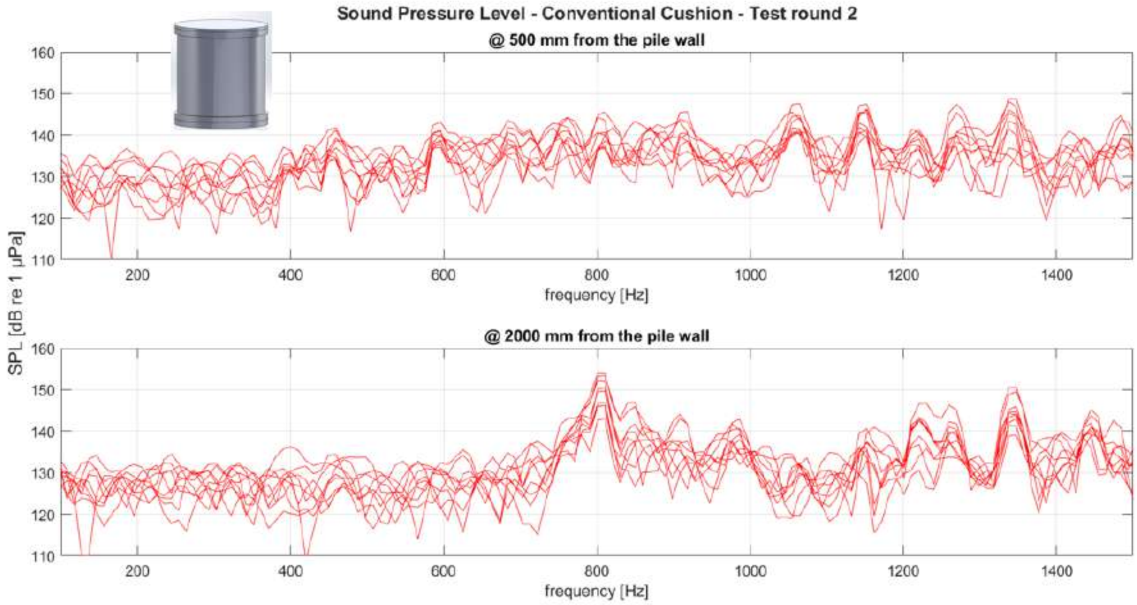

Figure 8.18: Sound Pressure Level for the impact test with a hydrophone distance of 500 mm (top) and 2000 mm (bottom) from the pile wall at all depths for the Conventional Cushion

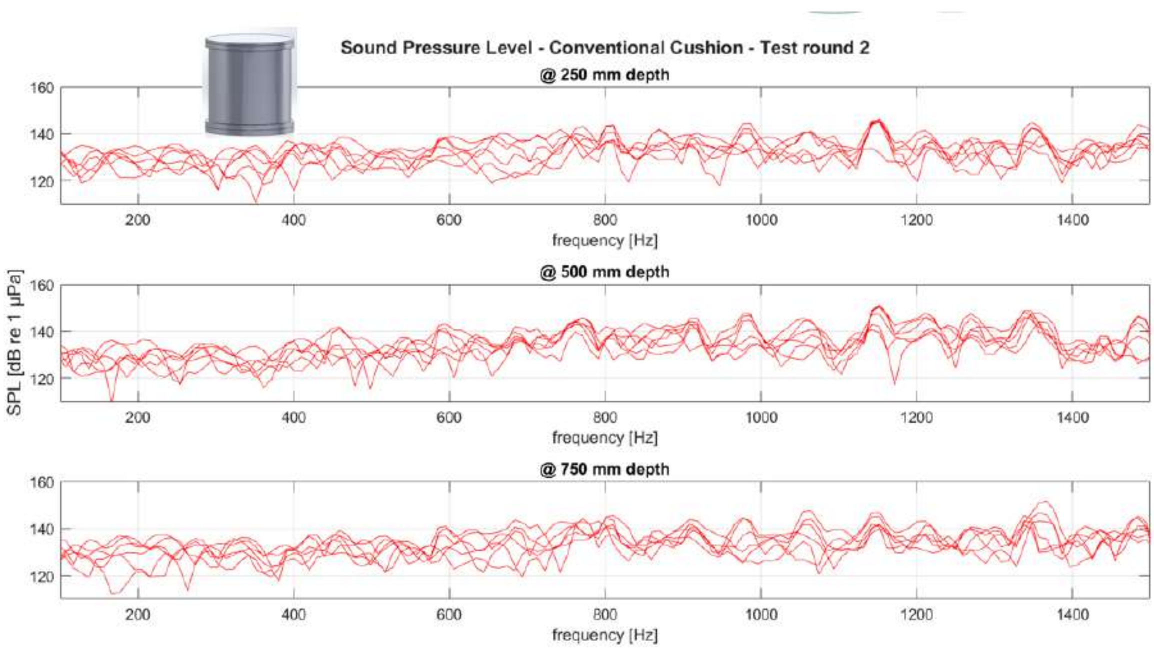

Figure 8.19: Sound Pressure Level for the impact test with a hydrophone at a depth of 250 mm (top); 500 mm (middle) and 750 mm (bottom) at 500 mm from the MP for the Conventional Cushion

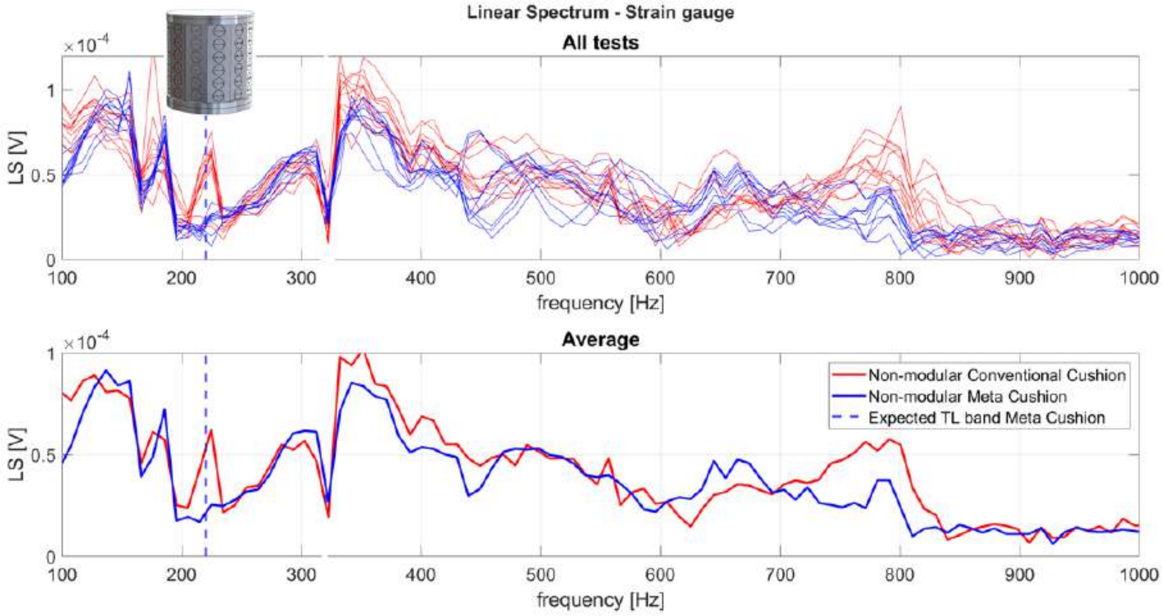

Figure 8.20: LS for the strain gauges for the aluminium non-modular cushions

the peak in the results from the FRF-tests, while between the two frequencies the two cushions show the same behaviour.

The results from the hydrophone experienced too much noise below a frequency of 400 Hz, and the accelerometer did not show reliable results since the sensor had come loose, and are therefore not discussed.

The thickness of the arrays of this Meta Cushion caused problems during the manufacturing process. The water laser diverged causing a smaller thickness of the beams and a different shape of those beams, which influenced the behaviour of the resonators and therefore the Meta Cushion.

During the tests the resonators experienced plastic deformation elongating the beams. This plastic deformation caused the resonators to rotate in plane and this could cause changes in the vibrating behaviour. For future research the vibration behaviour of the resonators and the resulting internal stress in the beams should be explored more, to keep those stresses below the yield strength of the material.

The small-scale impact test setup did demonstrate the Meta Cushion TL at the expected frequencies for almost all cushion. The reduction of low-frequency peak noise levels during the small-scale impact test were only obtained by the aluminium modular Meta Cushion. The data obtained from the experiments provides insights for improving the Meta Cushion design and future small-scale tests for better noise reduction when implemented on a larger scale.

9 Conclusion

To assess the functionality of the Meta Cushion in reducing low-frequency noise during offshore impact pile driving, a small-scale pile driving test setup was designed and built. The increasing demand for RES in the form of offshore wind farms has led to higher levels of underwater noise pollution in the low-frequency range, which harm marine mammals. Current mitigation techniques are dependent on water depth and fail to reduce the noise in this low-frequency range. New and innovative mitigation techniques, independent of water depth, are critical to reduce the impact of underwater noise on marine mammals. These high underwater noise levels have a large impact on marine life as marine mammals rely on sound waves, particularly low-frequency waves. The noise from pile driving damages their auditory systems and can lead to multiple injuries making them more vulnerable to predators. The Meta Cushion was numerically designed to reduce low-frequency noise during offshore impact pile driving in a full-scale case. The small-scale test aimed to validate the numerical results and to provide a better understanding of the cushion's effectiveness. This test was a joint effort of Delft University of Technology and Huisman Equipment B.V..

The small-scale impact test setup was scaled using scaling laws on the large-scale appliance, and the instrumentation was selected to perform the required measurements to quantify wave propagation. A custom-made scaled MP with the same aspect ratio and wall thickness-to-radius ratio as a large-scale MP was used in the test. The eigenfrequencies of this MP were predicted via a FEM simulation without taking into account that the MP was party submerged in water.

The test setup was built using a test tank with sound-absorbing foam attached to its walls and soil at the bottom to reduce the reflection waves of the tank sides. In the middle of the tank the small-scaled MP was placed on top of a damping plate, to protect the MP and the bottom of the tank. This damping plate was changed during the experiments, because the initial plate caused a large backlash on the MP after impact. On top of the MP, different cushions were placed, and on the MP wall, a set of strain gauges and an accelerometer were attached to measure the behaviour of the MP throughout the tests. In the tank, a hydrophone was placed to measure the sound pressure as a result of the impact force.

The small-scale test setup had three test rounds; The first round assessed the functionality of the meta-material unit cell by testing a modular Meta Cushion made from three different materials: aluminium, acrylic, and nylon, while using a pivot impact hammer; the second and third test rounds were performed on two aluminium non-modular cushions, which were designed and built to withstand the stresses during an impact test with a higher impact force, using a drop weight impact hammer. The FRF-experiments were conducted to extract the actual TL frequency and the attenuation caused by it for each cushion.

The sound pressure measured by the hydrophone was used to calculate the $\mathrm{SEL}_{\mathrm{ss}}$ and the $\mathrm{SPL}_{\mathrm{z,p}}$ in the time domain for all cushions, after which the data was transformed into the frequency domain to show the $\mathrm{SPL}_{\mathrm{peak}}$ for the frequencies in the low-frequency range. The data from the sensors on the MP were also transformed into the Linear Spectrum to compare the frequency attenuation of the Meta Cushion with its Conventional Cushion in the frequency domain.

The modular cushions consisted of four arrays, a top plate, and a clamp to secure the cushion on the MP. Each array for the Meta Cushion contained six meta-material unit cells with resonators attached to the arrays by beams, resulting in a 40 dB TL at a specific frequency. To compare the results of the tests, a Conventional Array with the same axial stiffness was manufactured for each meta array. On the Meta Arrays, an FRF-test was performed to extract the actual TL frequency and the attenuation caused by it. The aluminium modular Meta Array was designed for an attenuation around a frequency of 2500 Hz. After the array was manufactured, the TL was detected around 2250 Hz with a value of minus 50 dB. The acrylic array was designed for a TL frequency of 1027 Hz, which was observed at a frequency of 1150 Hz with an attenuation of 40 dB. The nylon array was designed for a TL around a frequency of 592 Hz, which was also the actual frequency determined during the FRF-tests, with an attenuation of 35 dB. The differences in the designed TL frequencies and the actual TL frequencies for the Meta Arrays were caused by the different thickness of the beams attaching the resonators to the arrays.

The non-modular Meta Cushion, designed and built to withstand the stresses caused by a higher impact, consisted of 12 Meta Arrays welded together forming a do-decagon, attached to the same clamp as for the modular cushions. The arrays for this cushion were designed for a TL frequency of 350 Hz with an attenuation of 15 dB. The FRF-experiments showed a TL of 15 dB around a frequency of 220 Hz, after which the array shows TLs and peak values until the frequency of 320 Hz where it reaches a peak value. During the manufacturing of these arrays, the array thickness caused distortion in the shape of the resonator. On top of the cushion core two top plates were placed to keep the internal stresses, caused by the impact force, below the yield strength of 270 MPa. This internal stress and the stiffness of this non-modular Meta Cushion was determined using the FEM programm COMSOL Multiphisics®, where the axial stiffness of 595 kN/mm was used to design the Conventional Cushion. The core of the Conventional Cushion was made from an aluminium cylinder with a wall thickness of 12.65 mm resulting in an axial stiffness for the total cushion of 605 kN/mm during the impact test.

The axial stiffness of the non-modular cushion cores were obtained through a bench press test that involved applying a force on the top plate of the cushion and measuring the corresponding displacement of the cushion core using a displacement sensor. The stiffness of the Meta Cushion core was found to be 680 kN/mm, whereas the Conventional Cushion core was 830 kN/mm. Notably, the predicted stiffness for the cores was much higher at 2350 kN/mm and 2820 kN/mm for the Meta Cushion and Conventional Cushion respectively, the ratio, however, was the same.

The functionality of the modular cushions were tested using a pivot hammer, with each cushion tested ten times. The aluminium modular Meta Cushion showed an attenuation in the SEL_{ss} of 7 dB (re $1\mu Pa^2 s$), and an attenuation in the $SPL_{z,p}$ of 6 dB (re $1\mu Pa$), which could be caused by the lower stiffness of the Meta Array. The Meta Cushion shows a TL around the frequency of 2200 Hz, with an attenuation of 10 dB (re $1\mu Pa$). The cushion also showed a TL around a frequency of 1950 Hz with an attenuation of 15 dB, which could be because of the resonators in the Meta Arrays, further research is necessary to definitively say what causes the TL.

The acrylic modular Meta Cushion showed an attenuation in the SEL_{ss} of 3 dB (re $1\mu Pa^2 s$), but no difference in the $SPL_{z,p}$. The SPL in the frequency domain did not show a TL around the expected TL frequency, which could be caused by the eigenfrequencies of the tank. The strain gauges and accelerometer on the MP did however show a TL at this frequency.

The Nylon Conventional Cushion had an SEL_{ss} of 194 dB (re 1 $\mu Pa^2 s$) and an $SPL_{z,p}$ of 180 dB (re 1 μPa), while the Meta Cushion had an SEL_{ss} of 191 dB (re 1 $\mu Pa^2 s$) and an $SPL_{z,p}$ of 173 dB (re 1 μPa). The length of the Meta Cushion was a lot shorter compared to the other arrays, which caused a larger impact from the impact hammer. The behaviour of this Meta Cushion was the inverse compared to the results from the FRF-tests: The TL was designed for a frequency around 592 Hz, at which the Meta Cushion showed an increase in the SPL and in the pile wall movement detected by the strain gauges and accelerometer. Around a frequency of 760 Hz a TL was visible in the LS from the sensors on the MP. In future tests, more attention should be paid to the stiffness of the Meta Arrays compared to the Conventional Arrays and the manufacturing of the outside dimensions of the arrays. It is also recommended to use a high-speed camera to log the frequency movement of the PUC during impact tests.

The non-modular cushions were tested with a higher impact force using a drop weight impact hammer. During this second test round the test setup was assessed, and it was found that the MP experienced a backlash from the damping plate, therefore the granulate rubber tile was removed. The repeatability of the tests was improved as the deviation in the results for the sensors for both cushions decreased. The hydrophone location showed the best performance at 500 mm from the MP at a depth of 500 mm. The third test round was executed on the same two non-modular cushions to asses the KPIs of the Meta Cushion. The SEL_{ss} and the $SPL_{z,p}$ were the same for both cushions in the time domain. The TL was detected by the strain gauges around the expected frequency of 220 Hz for the non-modular Meta Cushion, which was different from the designed TL frequency of 350 Hz. The thickness of the arrays of this Meta Cushion caused problems during the manufacturing process, where the waterjet diverged causing a smaller thickness of the beams and a different shape of those beams, which influenced the behaviour of the resonators and therefore the Meta Cushion.

During the tests the resonators experienced plastic deformation elongating the beams. This plastic deformation caused the resonators to rotate in plane and this could cause changes in the vibration behaviour. For future research the vibration behaviour of the resonators and the resulting internal stress in the beams should be explored more, to keep those stresses below the yield strength of the material.

The small-scale impact test setup did demonstrate a TL for almost all Meta Cushions at the expected frequencies. The reduction of low-frequency peak noise levels during the small-scale impact tests were only obtained by the aluminium modular Meta Cushion. The data obtained from the experiments provides insights for improving the Meta Cushion design and future small-scale tests for better noise reduction when implemented on a larger scale.

10 Recommendations

The design of the Meta Cushion is based on the eigenfrequencies of the MP, it is recommended that further research should be conducted to improve the prediction of eigenfrequencies via FEM for a partly submerged MP. This can be achieved through a small-scale test focused on the determination of the eigenfrequencies of a MP via hydrophones, strain gauges, and accelerometers. The same should be done for the eigenfrequencies of the test tank.

It is important to note that during this research, all Meta Cushions had a lower stiffness compared to the Conventional Cushion, which could cause lower SPLs. Hence, in future tests, more attention should be paid to the stiffness of the Meta Arrays compared to the Conventional Arrays, as well as the manufacturing of the outside dimensions of the arrays. Using a high-speed camera to log the frequency movement of the PUC during impact tests is also recommended.

Further exploration should be conducted on the most optimal location of the hydrophones by finding the relationship with the dimensions of the MP and the distance of the hydrophone. It is recommended to test the hydrophone at a closer range, where the wave should have enough time to develop while still being close enough to minimize the noise. Additionally, the influence of the noise by the depth of the hydrophone could be tested in future research. The bottom of the tank and the water level seem to reflect the waves, but this is not tested enough to give a hard recommendation. It is also recommended to have more hydrophones available for these tests, and they should be ordered in time.

The TL was shown in the strain gauges with the best results in the low-frequency range till a frequency of around 1250 Hz and for the hydrophone from a frequency around 400 Hz till the Nyquist frequency. Both sensors should be explored more on how this range could be enlarged. More attention should be paid to attaching (and possibly reattaching) the accelerometer, also it is recommended to use multiple accelerometers below each other as for some eigenfrequencies the accelerometer could be at a node of that eigenfrequency.

It is important to note that the environment during offshore monopile installation is unpredictable due to influences such as current, wind, and waves, which were left out of the scope of this experiment. Therefore, for future research, the test should take place at a lake or at the shore of the sea to take these influences into account. The noise should also be taken into consideration when conducting those tests. Another consideration is scaling, as the ocean is an almost infinite test tank, while the small-scale test tank has a limited size. The damping foam, the soil, and damping plate under the pile has damped the wall effect, but further research using a bigger tank could prove to what extend the wall effect is damped.

Future test setups, when the Meta Cushion shows good results, should take the penetration of the MP into the seabed into account. Additionally, the cushion should be designed to withstand even higher impact energy compared to the energy used in large-scale MP driving, and its behaviour over time, after many impact tests, should be examined.

Finally, during the tests, the resonators experience plastic deformation elongating the beams, causing the resonators to rotate in plane and this could change the vibrating behaviour. For future research, the vibration behaviour of the resonators and the resulting internal stress in the beams should be explored more to keep those stresses below the yield strength of the material.

References

[1] Andersson, M. H., Anderson, S., Ahlsen, J., Andersson, B. L., Hammar, J., Persson, L. K., Pihl, J., Sigray, P., & Wikstrom, A. (2017). A framework for regulating underwater noise during pile driving. Vindval.

[2] Bellmann, M., Kühler, R., Matuschek, R., Müller, M., Betke, K., Schuckenbrock, J., Gündert, S., & Remmers, P. (2018). Noise mitigation for large foundations (monopile l xl) - technical options for complying with noise limits. Noise mitigation for the construction of increasingly large offshore wind turbines, Berlin.

[3] Bellmann, M. A. (2014). Overview of existing noise mitigation systems for reducing pile driving noise. itap - Institute for Technical and Applied Physics GmbH, Germany.

[4] Buitendijk, M. (2020). Svanen uses bubbles to silently install offshore foundations in denmark. Retrieved December 30, 2022, from https://swzmaritime.nl/news/2020/09/04/svanen-uses-bubbles-to-silently-install-offshore-foundations-in-denmark/

[5] Buitendijk, M. (2022). In service at last: Deme's orion installs first monopile at arcadis ost. Retrieved December 30, 2022, from https://swzmaritime.nl/news/2022/06/13/demes-orion-installs-first-monopile-at-arcadis-ost/

[6] D4945, A. (2008). A standard test method for high-strain dynamic testing of deep foundations. ASTM International.

[7] Dähne, M., Tougaard, J., Carstensen, J., Rose, A., & Nabe-Nielsen, J. (2017). Bubble curtains attenuate noise from offshore wind farm construction and reduce temporary habitat loss for harbour porpoises. Marine Ecology Progress Series, 580, 221–237. https://doi.org/10.3354/meps12257

[8] Deltares. (2022). New pile installation method for offshore wind monopiles. Retrieved June 20, 2022, from https://www.deltares.nl/en/projects/new-pile-installation-method-offshore-wind-monopiles/#:~:text=The%5C%20dominant%5C%20method%5C%20used%5C%20to,induced%5C%20by%5C%20the%5C%20hammer%5C%20hits.

[9] DHV, R. H. (2020). Deelstudie onderwatergeluid co2 transport en opslag. RoyalHaskoningDHV Nederland B.V.

[10] Dyndo, M., Wisniewska, D., Rojano-Doñate, L., & Madsen, P. (2015). Harbour porpoises react to low levels of high frequency vessel noise. Scientific Reports 5, 11083, 1–9. https://doi.org/10.1038/srep11083

[11] Faijer, M. J., Sosef, M., & Perk, L. (2020). Mer kavel vi windenergiegebied hollandse kust (west). Pondera Consult.

[12] Heinis, F., de Jong, C., & Onderwatergeluid, R. W. (2015). Cumulatieve effecten van impulsief onderwatergeluid op zeezoogdieren. Technical Sciences.

[13] Heinzel, G., Rudiger, A., & Schilling, R. (2002). Spectrum and spectral density estimation by the discrete fourier transform (dft), including a comprehensive list of window functions and some new flat-top windows. https://doi.org/https://pure.mpg.de/pubman/faces/ViewItemOverviewPage.jsp?itemId=item_152164

[14] IQIP. (2020a). Hydrohammer. Retrieved February 8, 2022, from https://iqip.com/products/pile-driving-equipment/hydrohammer/

[15] IQIP. (2020b). In service at last: Deme's orion installs first monopile at arcadis ost. Retrieved December 30, 2022, from https://iqip.com/products/pile-driving-equipment/blue-piling-technology/

[16] Jiang, Q., Wang, X., Yu, M., Tang, M., Zhang, H., & Wu, J. (2022). Theoretical study of vibroacoustics of fluid-pile-soil coupled system and experimental research of noise reduction of small-scale pile driving. Ocean Engineering, 252, 110997. https://doi.org/10.1016/j.oceaneng.2022.110997

[17] Koschinski, S., & Lüdemann, K. (2020). Noise mitigation for the construction of increasingly large offshore wind turbines - technical options for complying with noise limits. Federal Agency for Nature Conservation, Isle of Vilm, Germany.

[18] MediaPower. (2020). Hoe hard klinkt een decibel. Retrieved December 6, 2022, from https://lichtbeeldgeluid.nl/geluid/akoestiek/hoe-hard-klinkt-een-decibel/

[19] Nordenham, S. (2020). Beyond xxl – slim monopiles for deep-water wind farms. Retrieved June 22, 2022, from https://www.offshorewind.biz/2020/05/11/beyond-xxl-slim-monopiles-for-deep-water-wind-farms/

[20] NT.nl. (2018). Blue hammer timmert op maasvlakte. Retrieved December 30, 2022, from https://www.nt.nl/havens/2018/07/24/blue-hammer-timmert-op-maasvlakte/?gdpr=accept

[21] Popper, A. N., & Hasting, M. (2009). The effect of anthropogenic sources of sound on fishes. Journal of Fish Biology, (75), 455–489.

[22] Reinhall, P. G., & Dahl, P. H. (2011). Underwater mach wave radiation from impact pile driving: Theory and observation. The Journal of the Acoustical Society of America, 1209(130). https://doi.org/10.1121/1.3614540

[23] Staat, B. (2018). Actualisatie van de omschrijving van goede milieutoestand vaststelling van milieudoelen voor de belgische mariene wateren. kaderrichtlijn mariene strategie – art 9 10. bmm. Federale Overheidsdienst Volksgezondheid, Veiligheid van de Voedselketen en Leefmilieu, Brussel, België.

[24] Vasconcelos, A. C. A., Schot, D., Jovanova, J., & Aragon, A. M. (2022). Meta-interface for structural resonance shielding. Delft University of Technology.

[25] Vasconcelos, A. C. A., Schott, D., Aragón, A. M., & Jovanova, J. (2021). Single-phase elastic metamaterials for wave filtering. ASME 2021. https://doi.org/10.1115/SMASIS2021-68283

[26] Vasconcelos, A. C. A., Valappil, S. V., Schott, D., Jovanova, J., & Arag´on, A. M. (2023). A metamaterial-based interface for the structural resonance shielding of impact-driven offshore monopiles.

[27] Wilke, F., Kloske, K., & M.Bellmann. (2012). Esra-evaluierung von systemen zur ramsmchallminderung an einem offshore-testpfahl. Stifting Offshore Windenergie.

[28] Windeurope. (2018-2021). Offshore wind in europe - key trends and statistics 2021-2018. Retrieved June 20, 2022, from https://windeurope.org/intelligence-platform/product/offshore-wind-in-europe-key-trends-and-statistics-2020/

[29] Woolfe, K. F. (2012). A scaled physical model for underwater sound radiation from a partially submerged cylindrical shell under impact. https://smartech.gatech.edu/handle/1853/44874

[30] Xinquan, W., Shimin, Z., Juan, L., & Yingsheng, H. (2014). Research and development on similarity principle of model pile. Applied Mechanics and Materials, 581-583, 3106–3110. https://doi.org/10.4028/www.scientific.net/AMM.580-583.3106

[31] Zadpoor, A. A. (2016). Mechanical meta-materials. Materials Horizons, 3(5), 365–462. https://doi.org/10.1039/c6mh00065g

A Evaluation of the ability of a small-scale pile driving test to assess noise reduction in the frequency spectrum

This research paper investigates the design of a small-scale pile driving test to assess the ability to filter unwanted sound pressure peaks in the frequency spectrum. The research questions focus on the fundamentals of the test, the methodology used for evaluating a mitigation technique, and the extent to which the test setup can evaluate noise reduction. The experiment involved the use of strain gauges to measure the behaviour of the pile wall and hydrophones to measure the sound pressure waves generated by the impact of the pile. The results showed that a small-scale impact test can effectively evaluate noise reduction techniques, and that the test setup is reliable and repeatable. The methodology used for the test was shown to be effective in measuring transmission loss (TL) in the low frequency spectrum, and the results demonstrated that the mitigation cushion was able to filter unwanted sound pressure peaks in the frequency spectrum. These findings provide valuable insights into the design of a small-scale pile driving test for evaluating noise reduction techniques and can be used to further develop and optimize the test setup for future experiments in this field

A.1. Introduction

One of the biggest challenges of this century is the fight against global warming. In all sectors people are doing their best to reduce their carbon footprints and their impact on the environment. In the energy sector this is done by utilizing renewable energy sources (RES), such as wind turbines, instead of fossil fuels. This transition to RES and the growing demand of energy results in extensive off-shore wind farms containing large wind turbines. During the installation of these wind turbines, the monopile (MP) foundation is driven into the seabed using an impact hammer, which dissipates a high amount of energy into the water in the form of sound pressure waves.

The average power capacity of off-shore wind turbines in Europe keeps growing every year, which forces the wind turbine installation to get bigger as well as the MP foundation. Those larger MPs shift the radiated noise to frequencies below 1 kHz, into

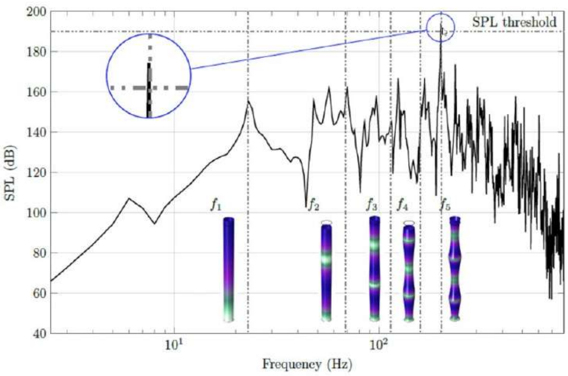

Figure A.1: Correlation between eigenfrequencies of a MP and peaks in the Sound Pressure Levels. The eigenfrequencies of the MP are indicated by the dotted vertical lines and the SPL is plot for that MP, with the peak SPL circled and zoomed in (Vasconcelos et al., 2023)

the low-frequency spectrum interfering with the low-frequency sound waves marine mammals use for communication (Andersson et al., 2017; Popper & Hasting, 2009). The noise from pile driving damages their auditory systems and can lead to multiple injuries making them more vulnerable to predators. For this reason, it is crucial to research methods for predicting underwater noise and reducing the noise during off-shore pile driving operations in the low-frequency domain (Andersson et al., 2017; Jiang et al., 2022). The radial displacement of the wall of the MP at its eigenfrequencies are directly coupled to the peaks in the sound pressure waves in the water during off-shore pile driving, as shown in figure A.1, and therefore the most significant factor affecting noise levels (Woolfe, 2012).

International regulations have been implemented to define maximum noise levels to reduce the impact on marine life around the wind parks, shown in table A.1. In the Netherlands the Sound Exposure Level of a single pulse (SEL_{ss}), which measures the sound energy received by an organism during a single impact pulse, should not exceed 168 dB (re 1 $\mu Pa^2 s$) measured around 750 m from the MP (Faijer et al., 2020). The restriction on the SEL_{cum}, the cumulative sound energy that a swimming animal experiences throughout the pile driv-

Table A.1: Threshold values for offshore pile driving in Dutch and Belgium waters measured from a distance of 100m from the project (DHV, 2020; Faijer et al., 2020; Heinis et al., 2015; Staat, 2018)

Noise Level	Threshold
SEL_{ss}	168 dB re 1 $\mu Pa^2 s$
SEL_{cum}	199 dB re 1 $\mu Pa^2 s$ over 24h
SPL_{peak}	185 dB re 1 $\mu Pa^2 s$

ing process, should not exceed 199 dB (re 1 $\mu Pa^2 s$), usually taken over a period of 24 hours. The Sound Pressure Level (SPL) is a measurement of the intensity of a sound at a specific point in time and should not exceed 185 dB (re 1 μPa) in Belgium waters (Staat, 2018).

Currently, noise barriers or enclosures such as an acoustic bubble curtain and an isolation casing are used as mitigation techniques. These structures are designed to block or absorb sound waves and reduce the intensity of the noise that is transmitted to the surrounding environment, called secondary mitigation techniques - the wave control occurs in the wave propagation path. All mitigation techniques are under constant development to improve their performance and are currently used by combining different techniques to reach the necessary noise reduction, but with limited success while increasing installation time and cost (Koschinski & Lüdemann, 2020; Vasconcelos et al., 2022). Moreover, they lack the ability to filter sound pressure peaks at a specific frequency band in the low frequency range.

To overcome these limitations, new mitigation techniques are being developed that focus on changing the transmission of the impact energy, which is a primary mitigation technique, aiming to reduce noise peaks in the low-frequency range before the wave propagation path. These techniques will make the mitigation independent of the water depth at which the MP is installed and eliminates the external vessels needed during installation. One of these techniques is a mitigation cushion that was numerically designed to reduce low-frequency noise during off-shore impact pile driving in a full-scale case (Vasconcelos et al., 2023).

To assess the effectiveness of this state-of-the-art mitigation technique in a controlled environment, a small-scale test will be conducted before implementation on a full scale. Small-scale testing is less expensive and provides an opportunity to adjust the design for better results on a larger scale. A joint effort of Delft University of Technology and Huisman Equipment B.V. will design and build a small-scale test setup able to evaluate the ability of a mitigation technique to attenuate sound pressure peaks in the frequency spectrum.

The setup will be scaled using scaling laws on the large-scale appliance, and proper instrumentation will be selected to quantify wave propagation and evaluate the noise reduction. The resulting data from this experiment will include sound pressure in the water and wall displacement of the MP caused by an impact force.

The research question for this experiment is: How can a small-scale pile driving test be designed to assess the ability to filter unwanted sound pressure peaks in the frequency spectrum? To address this question, the following sub-research questions will be elaborated:

1. What are the fundamentals for a small-scale impact test?
2. What methodology is used for a small-scale impact test to evaluate a mitigation technique?
3. To what extend can the small-scale test setup evaluate noise reduction?

Similar experiments have been conducted previously on a small-scale MP using a hydrophone, which is comparable to the research presented here. One such experiment was conducted by Jiang et al. (2022) to analyze the noise reduction between two types of MPs using an impact test and a hydrophone. The data was converted to Sound Pressure Levels in the frequency domain to show the impact of the noise reduction, which is similar to the approach taken in this research. Another relevant study is the report by Woolfe (2012), which developed a down-scaled physical model to investigate noise generated by a partially submerged pile under impact loading. This report will be used as theoretical input for this research.

The structure of this report will follow the sequence of the sub questions. The fundamentals of the small-scale impact test for this research are shown first, after which the materials and methodology of the test components and the small-scale test setup are discussed. Then the results are shown and discussed in, and the main research question will be answered. The report will end with the conclusion.

A.2. Fundamentals for experimental setup

Down scaling plays an important role for the test setup. The monopile and its eigenfrequencies are the biggest influence on the peak values in the noise, as shown in figure A.1. The dimensions of the MP are therefore leading for the scaling factor, and the eigenfrequencies of the MP are a result from those dimensions.

The geometrical similarity theory was used to scale the Field dimensions down to the Lab dimensions, as shown by Xinquan et al. (2014). When the Field Model (FM) and the Laboratory Model (LM) meet the conditions of this principle, the two physical phenomena are similar. The structure size of the FM and the LM should be proportional to each other to satisfy this similarity theory, resulting in a scaling factor of 28.

For this research, the MP was custom made to meet all these scaling laws, therefore the Lab MP and the Field MP have the same aspect ratio and wall thickness-to-radius ratio.

The experimental setup for this study was constructed by Huisman Equipment B.V. and comprises a water tank filled with water and soil, with a scaled model of a MP placed at the center of the tank. A hammer is dropped from a predetermined height onto the MP, producing a transient force that induces a compression wave in the pile. The radial displacement motion associated with this wave is measured using an accelerometer and one set of strain gauges. Additionally, the compression wave causes a sound pressure wave in the water, which is measured using a hydrophone.

To simplify the small-scale lab experiments, a cylindrical thin-walled cylinder with constant wall thickness was used as the MP and is referred to as the Lab MP. The Lab MP is a scaled version of an actual MP made of welded steel compartments of varying dimensions. The Field MP refers to the full-sized version. The dimensions of the Lab MP were based on the bottom half of the Field MP since that is the part submerged in water during the pile driving process. The diameter and thickness that occur most frequently over that length of the Field MP were used to calculate the dimensions of the Lab MP.

The Field MP was scaled down to the Lab MP with a length of 2129 mm, an outer diameter of 295 mm, and a wall thickness of 2 mm. The Lab MP was constructed from S152-3N steel, with a Young's modulus of 210 GPa, a density of 7850 kg/m^3, and a Poisson's ratio of 0.28.

The radial eigenfrequencies of the MP are directly related to the peaks observed in sound pressure waves during offshore pile driving, as previously discussed in the introduction and illustrated in figure A.1. An eigenfrequency represents the natural frequency of vibration of a structure, such as the MP, and is determined by the physical properties of the MP, including its mass, stiffness, and damping. When an external force is applied to the MP, it may cause the structure to vibrate at its eigenfrequency, resulting in a resonant vibration and large amplitude vibrations, which can generate high sound pressure peaks.

To mitigate noise peaks at the eigenfrequencies of the MP, it is necessary to predict the MP's eigenfrequencies via COMSOL Multiphysics®. Subsequently, the test setup can be assessed to validate these results. During the impact test, the MP is partly submerged in water, but the COMSOL® model will be simulated surrounded by air. During the impact test, the movement at the bottom of the pile is constrained by the test tank and a rubber damping plate, which results in the bottom of the MP being constrained in all three directions in the simulation. Conversely, the pile tip is free to move in all directions and is thus unconstrained in the simulation.

The eigenfrequency study, which is a built-in function, predicted the eigenfrequencies of the MP as f_1 of 365 Hz and f_2 of 595 Hz, while the other eigenfrequencies were above 1 kHz. However, it is expected that the eigenfrequencies of the MP in water are slightly lower than these extracted frequencies, owing to the high radiation damping that occurs underwater.

The experimental setup for this study consists of a steel tank provided by Huisman Equipment B.V. with dimensions of 6000 mm in length, 2440 mm in width, and 1500 mm in depth. The Field MP is designed for a water depth of approximately 30 m, which results in a water level of around 1 m during the tests based on a C_l value of 28.

The tank has its own eigenfrequencies, which may cause high sound pressure peaks, potentially interfering with sound pressure wave measurements used to evaluate the effectiveness of the mitigation technique. The tank walls and bottom can also reflect these sound pressure waves, causing measurement distortion. To prevent these issues, damping measures are necessary, including covering the tank bottom with a layer of regular filling sand and attaching sound-absorbing bubble foam to the tank walls. The bubble foam, with a thickness of 65 mm, absorbs low-frequency sound waves in air and will cover the entire tank wall except for the bottom portion, which will be covered by soil.

The sand layer will act as a damper for the reflection of sound pressure waves by the tank bottom. The density of the sand is approximately 1500 kg/m_3, which is insufficient to prevent the pile from touching the tank bottom. To address this, a damping plate is inserted beneath the MP to protect the MP from the tank, preventing the pile from moving deeper into the sand, which also enables the repetition of tests with the same starting conditions. As the pile will not move into the sand, friction between the MP and the sand is not a significant factor for this test setup.

To evaluate the effectiveness of the absorption measures, the eigenfrequencies of the water tank will be predicted. These eigenfrequencies, if amplified by resonance, could interfere with hydrophone measurements, unless they are absorbed by the bubble foam and soil. The bottom of the water tank, covered by a thick layer of soil, can be disregarded when calculating the eigenfrequencies. The tank wall is assumed to be rigid, which makes the normal component of the particle velocity vanish at the tank wall. The natural wave numbers are calculated in the three directions of the tank: along the length of the tank, L_{tank}, as a function of l; along the width of the tank, W_{tank}, as a function of m; and along the height of the tank, H_{tank}, as a function of n. The relevant formulas are:

$$k_L(l) = l\pi/L_{tank}, \tag{A.1}$$

$$k_W(m) = m\pi/W_{tank}, \tag{A.2}$$

$$k_H(n) = (2n+1)\pi/(2H_{tank}), \tag{A.3}$$

with the length, width and height in meters. The eigenfrequencies can be calculated by combining those three formulas into

$$f(l,n,m) = \frac{c_w\sqrt{k_L(l)^2 + k_W(m)^2 + k_H(n)^2}}{2\pi}, \tag{A.4}$$

with c_w as the speed of sound in water of 1490 m/s. The non-degenerated predicted eigenfrequencies below 1 kHz are: $f_{1,0,0}$ is 390 Hz; $f_{0,1,0}$ is 496 Hz; $f_{1,1,0}$ is 511 Hz; $f_{2,0,0}$ is 444 Hz; and $f_{0,2,0}$ is 757 Hz.

The test setup involves the use of a drop weight impact hammer that comprises a drop weight, so called ram, which is lifted and released from a specific height above the pile. To ensure consistent test results, the ram must strike the center of the MP in each test, hence it is connected to a vertical guide rail. The friction generated by the rail remains constant throughout the tests and is negligible.

During the experiment, the position of the hammer is measured over time using a position sensor installed along the guide rail. The impact velocity, v_{impact}, and the impact energy of the drop weight can be calculated using the kinetic energy formula:

$$E_{kin} = \frac{1}{2} m_{ram} v_{impact}^2, \tag{A.5}$$

where m_{ram} is the mass of the ram, which is 47 kg, and the kinetic energy is in Joule. The output signal provided by the sensor is calibrated and indicates the distance between the MP and the hammer.

In this research, the TC4013 hydrophone is utilized to measure the sound waves generated during pile driving. It is strategically positioned at three different distances, 500, 1000, and 2000 mm from the pile wall, in the middle of the tank, to avoid reflections from the tank wall. The depth of the hydrophone is also varied between 250 mm to 750 mm from the water level to ensure that the functionality of the soil is properly evaluated.

Furthermore, wall-motion sensors, comprising one accelerometer and one set of strain gauges, are attached to the outside wall of the MP at a distance of 1.5 times the diameter from the pile tip. This placement is conform to the American Society for Testing and Materials (ASTM) standard for dynamic testing of piles in the field.

The accelerometer is attached to the pile using a corner piece, which ensures that it is in a horizontal position to measure the acceleration of the pile wall in three different directions. On the other hand, the strain gauges are directly glued onto the pile wall after clearing the paint on the surface for better conductivity.

Assessing the effectiveness of any proposed noise mitigation technique is crucial to understanding its potential impact on noise levels. To accurately determine the attenuation of the proposed technique, researchers must conduct both a zero measurement and a measurement of the proposed technique. The zero measurement serves as a baseline for comparison, enabling researchers to distinguish the extent to which any observed attenuation is due to the mitigation technique or other factors.

To conduct a zero measurement, a conventional object with properties similar to the proposed mitigation technique should be designed. For example, when testing a mitigation cushion, a conventional cushion with a stiffness equivalent to that of the proposed mitigation technique should be used. It is essential that the conventional cushion is capable of withstanding the same internal stresses as the proposed technique to ensure accurate and meaningful comparisons can be made.

To evaluate the effectiveness of the proposed mitigation technique, researchers should measure noise levels both with and without the mitigation technique in place. This assessment can be achieved by calculating the sound exposure level (SEL) for a specific time window that includes a single impact measurement. The SEL, expressed in dB (re $1\mu Pa^2 s$), can be calculated using the following equation:

$$SEL_{ss} = 10\log^{10}\frac{\int_{t_0}^{t} p(t)^2\,dt}{p_{ref}^2}, \tag{A.6}$$

where the t_0 is the moment the sound pressure wave reaches the hydrophone; and p(t) is the pressure measured by the hydrophone over time; the p_{ref} is the reference pressure in water in [Pa^2s].

The peak SPL during an impact test is determined using the highest measurement of sound pressure (p_{peak}), which is calculated with the following formula:

$$SPL_{z,p} = 20 \log^{10} \frac{p_{peak}}{p_{ref}}, \qquad (A.7)$$

where the SPL is expressed in Decibel [dB], and the p_{ref} is 1 μPa for water.

The effectiveness of new noise mitigation techniques aimed at reducing low-frequency noise peaks, should be assessed by evaluating the transmission losses in the frequency domain, which can be achieved by transforming the signals from sensors on the pile wall and hydrophone using the methodology developed by Heinzel et al. (2002).

First, the data from the sensors are padded with zeros to the next power of two, resulting in N data points. Then, the Fast Fourier transform (FFT) is applied to each data string, which converts the vector of N complex numbers x[k], k=0, ..., N−1, into a vector of N complex numbers y[m], m=0, ..., N−1. The resulting data in the frequency domain is normalized by dividing by the number of data points N.

The frequency range of interest extends from 0 to the Nyquist frequency, f_{Ny}, which is half the sample frequency, at which the signal is mirrored. The frequency resolution, f_{res}, is calculated by dividing the sample frequency by the length of the data string. The data in the frequency domain can be compared using the linear spectrum (LS), which is expressed in the same units as the original time-domain data. The LS is the square root of the power spectrum (PS), which is the data in the frequency domain squared and multiplied by two, to keep the same energy.

By using these methods, researchers can evaluate the transmission losses in the frequency domain and assess the effectiveness of new noise mitigation techniques for reducing low-frequency noise peaks.

The formula to procure the LS for the accelerometer in three directions; for the data from the strain gauges; and for the sound pressure waves measured by the hydrophone can be calculated via the equation:

$$LS[m] = \sqrt{2} \left| \frac{1}{N} \sum_{k=0}^{N-1} x[k] e^{-i2\pi \frac{mk}{N}} \right|, \qquad (A.8)$$

for m = 0, ..., N/2.

The LS for the sound pressure, the Sound Pressure Spectrum (SPS) measured by the hydrophone, can be used to calculate the peak SPL in the frequency domain using:

$$SPL_{peak}(f) = 20 \log^{10} \frac{SPS[f, r, z]}{p_{ref}}, \qquad (A.9)$$

where the SPL is expressed in Decibel [dB], and the p_{ref} is 1 μPa for water.

A.3. Methods and materials

The small-scale impact pile driving test was conducted at the lab facilities of Huisman Equipment B.V.. Sound-absorbing foam was attached to the tank walls using double-sided tape and glue to minimize the wall effect. The tank was filled with regular filling sand to a height of 280 mm with a deviation of 20 mm, and the water level for the test setup was set to 950 mm.

The test setup included a MP, with a Conventional Cushion on top of the MP, placed in the middle of the tank on top of a damping plate consisting of 20 mm of SRB tile installed to separate the MP from the tank bottom. The MP was kept in a vertical position by a small-scaled gripper installed just below the sensors on the MP. An impact hammer was used to generate a transient force, causing a compression wave in the pile, which was measured by an accelerometer and strain gauges.

The test was executed with a hydrophone at nine different locations, repeated three times, resulting in 54 tests. The impact hammer was manually lifted to the desired height above the cushion with an electrical winch, and the height was indicated by the position sensor next to the hammer rail. The lifting tolerance was set at 1 mm around the desired lifting height, and the hammer was released using a quick release connector.

The eigenfrequency of the test tank was tested to asses the attenuation of the precautionary damping measurements. The eigenfrequency prediction of the MP was validated by the data from the sensors on the pile wall and the hydrophone. The repeatability of the test setup was assessed by comparing the data from the sensors to determine the scattering.

A.4. Results and discussion

The eigen frequencies of the MP and the test tank were determined using a hydrophone prior to the small-scale impact test. The attenuation of the eigenfrequencies of the test tank using damping precautions were assessed by a test with the hydrophone placed at a depth of 500 mm and 1000 mm from the pile wall. The test tank was struck on different places of the tank wall while the hydrophone measured peaks in the sound pressure waves caused by the eigen frequencies of the tank. The data from the hydrophone was normalized to eliminate the variation in hammer impact, after which the SPS was calculated.

The average SPS of the test tank is shown by the black dashed curve in figure A.2. The curve shows a peak SPS around 780 Hz, which is very close to the numerically determined $f_{0,2,0}$ of 757 Hz. The eigen frequencies for the tank should be avoided when designing or testing a mitigation technique for a transmission loss at a certain frequency.

The eigen frequencies of the MP were extracted using the hydrophone, placed at the same location as previous tests. The pile was struck by a synthetic hammer, while the sensors on the pile wall and the hydrophone in the test tank measured the impact results. The data from the strain gauges and hydrophone were first normalized, after which the normalized LS and SPS were calculated.

The second and fifth eigen frequencies were expected to show the highest peaks, as shown in figure A.1. The numerical second eigen frequency, 595 Hz, of the MP was exactly where it was predicted, shown in the first peak in the graph in figure A.2. The highest peak caused by the MP was also a peak in the plot from the test tank around 915 Hz. As the MP was already in the tank during the eigen frequency determination of the test tank, it is not clear if the peak is caused by the eigen frequency of the MP or by the eigen frequency of the test tank. A third option is also possible: The hammer used in the test also causes a peak. Impulse hammers with built-in frequency determination sensors should be used in future research.

When tests to determine the eigenfrequencies of the tank were performed, the accelerometer measured the movement of the pile. These vibrations of the pile wall can also be used to determine the radial eigen frequencies of the MP causing the sound pressure peaks. The peak vibrations in the radial direction of the pile wall occurred at the frequencies: 195 Hz; 235 Hz ;265 Hz; 330 Hz; 450 Hz; 860 Hz; and 950 Hz.

It can therefore be concluded that the SPS peaks at 860 Hz and 950 Hz are caused by the eigen frequencies of the MP. The eigen frequency of the tank around 790 Hz was detected by the accelerometer in the axial direction of the pile, the movement in the axial direction may be caused by the vibrations of the bottom of the tank, showing the eigen frequencies of the tank. For future research, the MP should be removed from the tank when determining the eigen frequencies of the test tank.

The test setup should be able to asses the noise reduction of a mitigation technique in the frequency

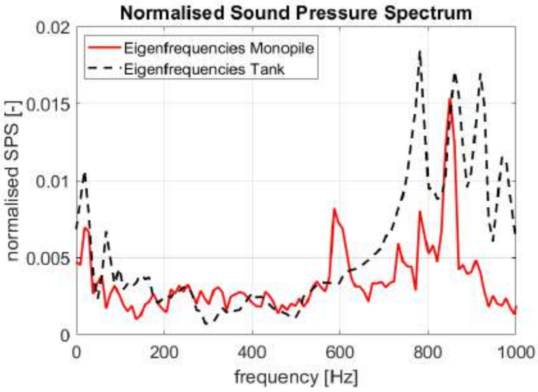

Figure A.2: Normalised SPS for the eigenfrequency determination of the test tank plot by a red solid curve and of the MP plot by a black dashed curve

domain. First the SEL_{ss} and the $SPL_{z,p}$ in the time domain should be determined for the zero measurement to compare with the mitigation technique. The SEL_{ss} was 206 dB (re 1 $\mu Pa^2 s$) and the $SPL_{z,p}$ was 183 dB (re 1 μPa).

The repeatability of the test setup was assessed by comparing the data from the strain gauges and hydrophone to determine the degree of scattering. The findings revealed that the variation in the LS of the strain gauges between repeated tests was less than 10%, as demonstrated in figure A.3. This indicates that the test setup was reliable, and the obtained results can be used to effectively evaluate the ability of noise reduction techniques.

The impact of the pile generated sound pressure waves, which were detected by the hydrophone. The SPL was calculated from the hydrophone data and are shown in figure A.4. The SPL can be used to evaluate the effectiveness of noise reduction techniques. It is crucial to measure the SPL of the pile before and after the application of noise reduction measures.

The results indicate that TLs can be measured using both strain gauges and hydrophones in the low frequency spectrum. As an example, the transmission loss detected by the strain gauges around the frequency of 220 Hz is illustrated in figure A.5, where the outcomes from the conventional cushion showed a peak value, while the mitigation cushion displayed a trough.

A.5. Conclusion

This experiment investigated the design of a small-scale pile driving test to assess the ability to filter unwanted sound pressure peaks in the frequency spectrum. The research questions were formulated to address the fundamentals of the test, the methodology used for evaluating a mitigation technique,

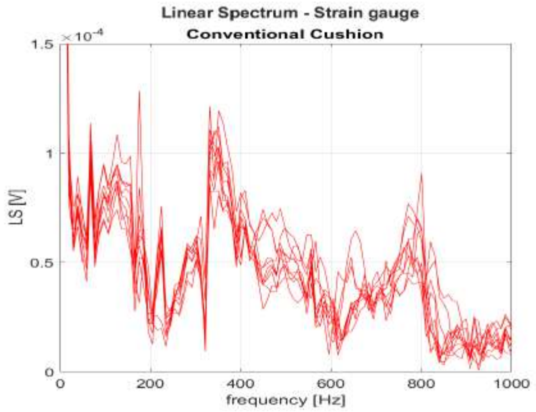

Figure A.3: LS of strain gauges from the small-scale impact tests on a conventional cushion to asses the repeatability of the test setup

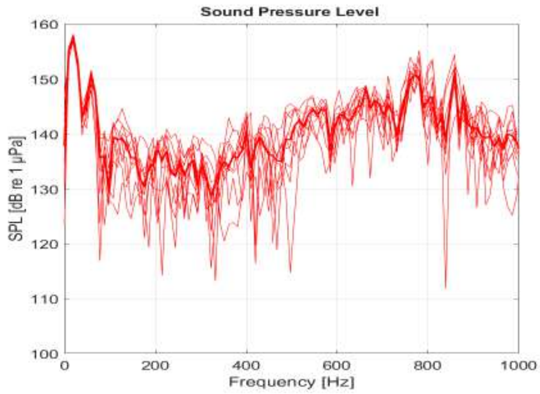

Figure A.4: Sound Pressure Level from the small-scale impact tests on a conventional cushion to asses the repeatability of the test setup

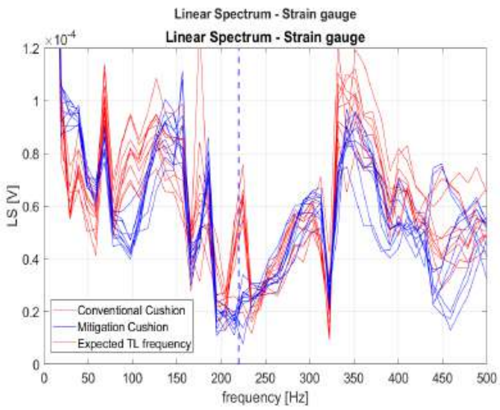

Figure A.5: Example of a TL detected by the strain gauge by comparing the data from the conventional cushion with a mitigation cushion designed at a frequency of 220 Hz

and the extent to which the test setup can evaluate noise reduction.

Based on the results of the experiment, it can be concluded that a small-scale impact test can be used to assess the effectiveness of noise reduction techniques in the frequency spectrum. The test setup was shown to be reliable and repeatable, as demonstrated by the low scattering of the strain gauge data.

The methodology used for the small-scale impact test involved the use of strain gauges and hydrophones to measure the sound pressure waves generated by the impact of the pile. The TL was calculated from the data obtained by these sensors, and the results showed that TLs can be measured using both sensors in the low frequency spectrum.

The experiment also showed that the small-scale test setup can effectively evaluate noise reduction techniques. The results obtained from the conventional cushion and the mitigation cushion showed significant differences in TL, indicating that the mitigation cushion was able to filter unwanted sound pressure peaks in the frequency spectrum.

Overall, this experiment provides valuable insights into the design of a small-scale pile driving test for evaluating noise reduction techniques in the frequency spectrum. The methodology used and the results obtained can be used to further develop and optimize the test setup, and to guide the design of future experiments in this field.